



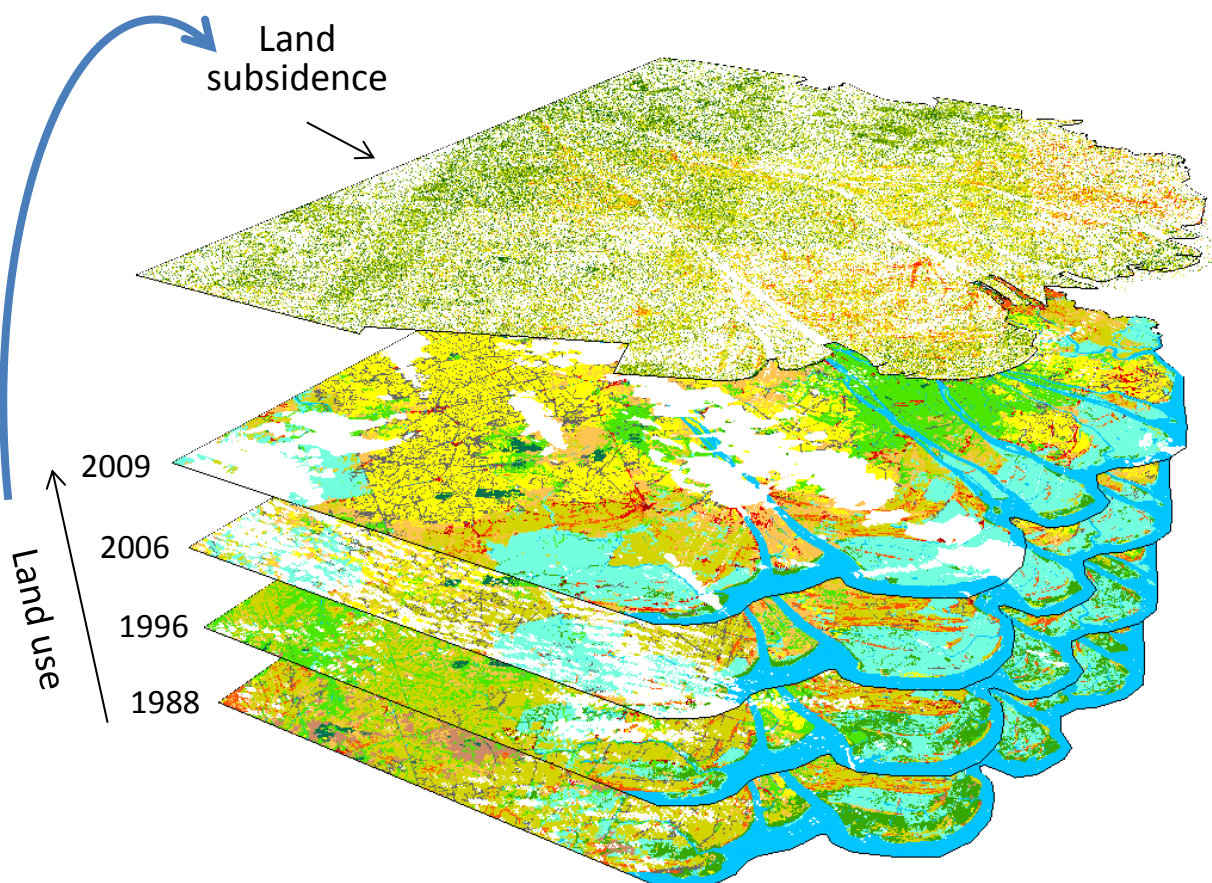
Universiteit Utrecht
Faculty of Geosciences

MSc. Thesis

Relating Land Subsidence to Land Use through Machine Learning using Remote-Sensing Derived Data

A case study in the Mekong Delta, Vietnam

Laura Coumou



Final version

Utrecht, 03-07-2017

Relating Land Subsidence to Land Use through
Machine Learning using Remote-Sensing Derived Data

– A case study in the Mekong Delta, Vietnam –

Author:

Laura Coumou

Student number:

3963942

Supervisors:

Dr. E. Stouthamer

Dr. E.A. Addink

P.S.J. Minderhoud MSc.

This thesis is part of the curriculum of the programme 'Earth Surface and Water' of the
Master of Science 'Earth Sciences'

Utrecht University

Faculty of Geosciences

Department of Physical Geography

Final version, July 3, 2017

Summary

Land subsidence poses millions of people at risk in deltas. Ongoing research focuses generally on subsidence processes and drivers, and urban areas rather than rural areas. An overview on the magnitude of and differences in subsidence coupled to land use (LU) at a delta scale is lacking. Though, this would be a comprehensible way to create awareness among a wide audience and to make quick predictions of the impact of (future) LU changes. Besides, the influence of past LU on the current subsidence rate through time-dependent effects is still unclear. Therefore, this study aimed to 1) quantify and compare land-subsidence rates for different LU types and LU changes, 2) determine the importance of time-dependent effects related to LU history on land-subsidence rates, and 3) determine to which extent LU history can predict land-subsidence rates. A data-mining approach was applied for the Vietnamese Mekong Delta (VMD) with the InSAR-based subsidence-rate dataset of Erban et al. (2014) for the period 2006-2010 as reference. LU maps of the same period and the two decades before were used for coupling with the subsidence rates.

A consistent, digital LU map series of the VMD was not available. So, as first step, LU was classified for 1988, 1996, 2006 and 2009 using a single dry-season Landsat 5 image. Hereto, an object-based approach and the random forest algorithm were used. The maps confirm the expansion and intensification of agri- and aquaculture, and urbanization in the delta. The overall accuracy ranged between at 77% and 94% based on validation samples of all 16 classes.

Subsequently, the mean subsidence rate was determined for all 12 relevant LU classes for areas where the LU did not change since 1988. Urban areas subsided fastest, followed by agricultural areas with non-rice crops. Wasteland/marsh areas subsided slowest, followed by fresh-water melaleuca forests and irrigated double or triple rice cropping fields. Urbanization and a change to orchards probably increased the subsidence rate, while the intensification of agriculture (rain-fed to irrigated rice) may have reduced subsidence rates. No conclusions could be drawn about aquaculture and mangrove due to inaccuracies in the InSAR-dataset. It can be concluded that time-dependent effects related to the LU history are important based on the comparison of the subsidence rates for areas with different LU histories.

As final step, the LU changes over all combinations of LU maps were used to predict the subsidence rate for 2006-2010 using a random forest regression. The spatial patterns in the predicted rates are similar to those in the InSAR-based subsidence dataset. More than one sixth (>17%) of the variance in the observed rates could be explained by the predictions (root-mean-squared deviation = 0.6 cm/yr). This percentage is relatively high considering the variation in subsidence rates within the LU classes. The random forest is promising, because it has no bias and is consistent. The unexplained variance can be related to the quality and type of input data as well as the type of model. Although LU history can predict a relatively large part of the subsidence signal, more factors should be included to predict the entire signal. If only one LU map was used for the predictions, less variation in the original data could be explained. This supports the conclusion that time-dependent effects related to the LU history are important. Hence, past LU should be taken into account when coupling land subsidence to LU.

Key points for this case study in the Vietnamese Mekong Delta:

- 1) Land subsidence can be related to land-use (LU) history at a delta scale. Past LU changes should be taken into account due to time-dependent processes.
- 2) LU history can predict at least one sixth of the total variance in the observed land-subsidence rates with the random forest (RF) algorithm.
- 3) Urbanization will result in higher land-subsidence rates; conversion to orchards probably too. Intensification of agriculture (from rain-fed to irrigated rice) may result in lower subsidence rates.

Keywords: *Land subsidence, land use, land-use change, Vietnamese Mekong Delta, data mining, machine learning, random forest, remote sensing, object-based image analysis (OBIA).*

Content

List of figures	V
List of tables	VII
List of acronyms.....	IX
Acknowledgements	XI
1. Introduction.....	1
2. Literature review	3
2.1. Land subsidence	3
2.2. Land use in the Vietnamese Mekong Delta over the past decades	11
2.3. The connection between land use and land subsidence	16
3. Methodology and data	19
3.1. Overview.....	19
3.2. Study area.....	20
3.3. Data	21
3.4. The random forest algorithm	24
3.5. Land-use classification and change detection.....	26
3.6. Relation land subsidence and land use	33
3.7. Prediction of land subsidence based on land use and land-use changes	35
4. Results	38
4.1. Land use and land-use changes.....	38
4.2. Relation land subsidence and land use	43
4.3. Prediction of land subsidence based on land use	46
5. Discussion	51
5.1. Land-use classification.....	51
5.2. InSAR-based subsidence rates.....	53
5.3. Relation land subsidence and land use (change)	54
5.4. Predicting land subsidence based on land use.....	56
5.5. Implications and suggestions for future research.....	57
6. Conclusion	60
List of references	62
Appendix 1 Overview of pre-existing land-use/cover maps	A.1
Appendix 2 Land-use classification: segmentation settings.....	A.9
Appendix 3 Land-use type code per land-use class.....	A.10
Appendix 4 Spectral and spatial characteristics of all LU classes	A.11
Appendix 5 Spectral and spatial segment features used for land use classification.....	A.16
Appendix 6 Land-use classification maps	A.17
A6.1. Land-use map of 1988.....	A.17

A6.2.	Land-use map of 1996	A.18
A6.3.	Land-use map of 2006	A.19
A6.4.	Land-use map of 2009	A.20
Appendix 7	Areal statistics of the land-use classification maps.....	A.21
Appendix 8	Confusion matrices land-use maps based on validation segments	A.22
A8.1.	Confusion matrices land-use classification 1988	A.22
A8.2.	Confusion matrices land-use classification 1996	A.25
A8.3.	Confusion matrices land-use classification 2006	A.28
A8.4.	Confusion matrices land-use classification 2009	A.31
Appendix 9	Land-use changes	A.34
Appendix 10	Land-subsidence rate per land-use class.....	A.38
Appendix 11	Impact of past land-use changes on subsidence rates.....	A.39
A11.1.	Impact land-use change on subsidence based on all InSAR-tiles.....	A.39
A11.2.	Impact land-use change on subsidence based on the Tra Vinh InSAR-tile	A.40
Appendix 12	Importance of the different LU periods for predicting land-subsidence rates	A.41

List of figures

Figure 1	Elevation of the Vietnamese Mekong Delta above mean sea level.....	2
Figure 2	Schematic overview of main drivers and processes of subsidence.....	4
Figure 3	Example of the relationship between fluid reservoir size and the magnitude of the land-subsidence rate due to reservoir compaction.....	5
Figure 4	Decrease in relative subsidence (consolidation) rate over time in a case of a constant weight of the overburden.....	7
Figure 5	Cumulative subsidence history for six locations around the world.....	8
Figure 6	Yearly land-use maps of the VMD for 2000 up to 2007 focused on aquaculture and rice cropping system, based on MODIS time-series analysis.....	11
Figure 7	Overview of the methodology.....	19
Figure 8	Overview map of the Vietnamese Mekong Delta.....	20
Figure 9	Annual averaged InSAR-based land-subsidence rates for the period 2006-2010 and error estimates for InSAR stacks superimposed on land subsidence map.....	22
Figure 10	Simplified example of a random forest.....	24
Figure 11	Overview of all steps to create a land-use map from a Landsat 5 satellite image, including pre- and post-processing steps.....	26
Figure 12	Examples of spectral profiles of all land-use classes used for classification based on the Landsat 5 TM image of 2009.....	29
Figure 13	Stacked bar plot of the area of each land-use class for each classified image, including the area of clouds and cloud shadows.....	38
Figure 14	Land-use maps for 1988, 1996, 2006 and 2009.....	39
Figure 15	Mean InSAR-based land-subsidence rates for the period 2006-2010 per land-use (LU) class for all pixels where the LU was constant between 1988 and 2009.....	43
Figure 16	Notched boxplots of the land-subsidence rates for the period 2006-2010 per land-use (LU) class based on all points in all tiles for which the LU did not change between 1988 and 2006/2009.....	44
Figure 17	Impact of past land-use changes on the mean land-subsidence rate for the period 2006-2010 based on all tiles.....	45
Figure 18	Density scatter plot and linear regression of observed InSAR-based land-subsidence rates versus predicted land-subsidence rates for the period 2006-2010 for all tiles (run 1 in Table 9) and the Tra Vinh tile (run 6 in Table 9).....	47
Figure 19	Map of predicted land-subsidence rates and observed InSAR-based land-subsidence rates for the period 2006-2010 based on all tiles and based on the Tra Vinh tile.....	49
Figure 20	Reflectance signatures of rice plants at different growth stages.....	A.11
Figure 21	Smoothened EVI (Enhanced Vegetation Index) profiles for single-cropped rain-fed rice, double-cropped irrigated rice, double-cropped rain-fed rice and triple-cropped irrigated rice.....	A.12
Figure 22	Spectral signature of two mangrove species, measured using a with spectrometer in the province Ca Mau in the VMD in January 2010.....	A.14
Figure 23	Visualization of which combination of mean or median land-subsidence rates per LU class are significantly different from each other at the 95% confidence level based on boxplot notches and/or multiple comparison.....	A.38
Figure 24	Impact of land-use changes on the mean land-subsidence rate for the period 2006-2010 based on the Tra Vinh tile only.....	A.40

List of tables

Table 1	Examples of measurement techniques to determine the land-subsidence rate with their characteristics and whether they are available in the Vietnamese Mekong Delta	9
Table 2	Landsat 5 TM surface reflectance images used	21
Table 3	Spectral band designations Landsat 5 TM	21
Table 4	Land-use classes used for the classification	28
Table 5	Overview number of sample segments for the random forest land-use classification per LU class and year	30
Table 6	Land-use changes for which the impact on the subsidence rate was assessed	33
Table 7	Validation statistics for all four land-use maps.....	41
Table 8	Comparison of the area (km ²) of aquaculture, forest and dry-season rice per province in the random forest classification of this study and the statistics of the General Statistics Office of Vietnam.....	42
Table 9	Evaluation of predicted land subsidence for the period 2006-2010 for all tiles together and the Tra Vinh tile with random forest regression using all four land-use change maps.	46
Table 10	Results of prediction land subsidence for all tiles and the Tra Vinh tile with random forest regression using different single land-use change maps	50
Table 11	Multiresolution segmentation settings for each classification of clouds	A.9
Table 12	Segmentation settings for each land-use classification.....	A.9
Table 13	Land-use (LU) classes used in for classification including LU type code.	A.10
Table 14	Rice-cropping seasons and systems.....	A.13
Table 15	Areal statistics of the classified land-use maps.....	A.21
Table 16	Confusion matrix of the land-use map of 1988 based on the out-of-bag segments in the random forest classification.	A.22
Table 17	Confusion matrix of the land-use map of 1988 based on the separate validation segments.....	A.23
Table 18	Confusion matrix of the land-use map of 1988 based on the separate validation segments, corrected for the segment area.....	A.24
Table 19	Confusion matrix of the land-use map of 1996 based on the out-of-bag segments in the random forest classification.	A.25
Table 20	Confusion matrix of the land-use map of 1996 based on the separate validation segments.....	A.26
Table 21	Confusion matrix of the land-use map of 1996 based on the separate validation segments, corrected for the segment area.....	A.27
Table 22	Confusion matrix of the land-use map of 2006 based on the out-of-bag segments in the random forest classification.	A.28
Table 23	Confusion matrix of the land-use map of 2006 based on the separate validation segments.....	A.29
Table 24	Confusion matrix of the land-use map of 2006 based on the separate validation segments, corrected for the segment area.....	A.30
Table 25	Confusion matrix of the land-use map of 2009 based on the out-of-bag segments in the random forest classification.	A.31
Table 26	Confusion matrix of the land-use map of 2009 based on the separate validation segments.....	A.32
Table 27	Confusion matrix of the land-use map of 2009 based on the separate validation segments, corrected for the segment area.....	A.33
Table 28	Area of land-use changes between 1988 and 1996 in km ²	A.34
Table 29	Area of land-use changes between 1988 and 2006 in km ²	A.35
Table 30	Area of land-use changes between 1996 and 2006 in km ²	A.36

Table 31	Area of land-use changes between 2006 and 2009 in km ²	A.37
Table 32	InSAR-based land-subsidence rate statistics per land-use (LU) class based on respectively all points in all tiles and in the Tra Vinh tile for which the LU did not change between 1988 and 2006/2009.	A.38
Table 33	Impact of past land-use changes on the average land-subsidence rate based on all InSAR-tiles.	A.39
Table 34	Impact of past land-use changes on the average land-subsidence rate based on the Tra Vinh InSAR-tile only.....	A.40
Table 35	Importance of the different land-use periods for predicting land-subsidence rates for all tiles and for the Tra Vinh tile based on the increase in mean square error importance measure of the random forest regression	A.41
Table 36	Importance of the different land-use periods for predicting land-subsidence rates for all tiles and for the Tra Vinh tile based on the increase in node-purity importance measure of the random forest regression.	A.41

List of acronyms

ASAR	Advanced Synthetic Aperture Radar
DN	Digital number
DWRPIS	Division for Water Resources Planning and Investigation for the South of Vietnam
ENVISAT	Environmental Satellite; has an ASAR sensor aboard
GSO	General Statistics Office (of Vietnam)
InSAR	Interferometric Synthetic Aperture Radar
ISODATA	Iterative Self-Organizing Data Analysis Technique: a RS LU classification method
(Landsat) ETM	(Landsat) Enhanced thematic mapper
(Landsat) MSS	(Landsat) Multispectral scanner system
(Landsat) TM	(Landsat) Thematic mapper
LIDAR	Light detection and ranging
LU	Land use
OBIA	Object-based image analysis
RF	Random forest
RS	Remote sensing
(R)SLR	(Relative) sea level rise
SPOT	Satellite Pour l'Observation de la Terre
TOA	Top of atmosphere
TWOPAC	Twinned object and pixel-based automated classification chain
USGS	United States Geological Survey
VMD	Vietnamese Mekong Delta
WRS	Worldwide Reference System: a global notation system used to catalog Landsat data WRS-1 is used for Landsat 1 to 3, WRS-2 is used for Landsat 4 to 8.

Acknowledgements

Of course, this thesis could not have been finished successfully without support from others during the process. At first, this thesis could not even have started without my three supervisors – Esther, Elisabeth and Philip – accepting the challenge to help building bridges between the ‘remote-sensing world’ and the ‘land-subsidence world’. As is the case for most pioneering projects, several pathways have been explored before this study got its final shape. I appreciated the useful input and encouraging feedback of all my supervisors and the space they gave me to explore the options I wanted to. Moreover, I am grateful to my boyfriend (Sake) for proofreading the final version of my thesis. Next, I am happy that I could always share and discuss everything whenever I needed to with Sake and my friends (Bente, Steven, Lianne, Erik and others). Besides, they provided regular and welcome distraction and breaks. The same holds for all other people I shared the room with for several months. Additionally, I would like to thank the GEO ICT employees (Rob Iseger, Maurits Uffing, Dennis Swanink, Gerard Dekker and Theo van Zessen) for their patience, enthusiastic help and inventive solutions for the computer related challenges I encountered during the processing phase. Last but not least, I would like to thank all people who provided data for this study, or helped in the preparation (e.g. Pepijn for georectifying the InSAR tiles). Especially without the processed InSAR-data of the research group of Dr. Laura Erban this study could not have come about.

1. Introduction

During the last decades, attention has been paid to the effects of anthropogenic climate change, such as absolute sea-level rise (e.g. IPCC, 2014; Vellinga & Leatherman, 1989). However, in especially low-lying deltas, *relative* sea-level rise (RSLR) is of prime interest for cases like salt-water intrusion and increased flooding risk from the sea. RSLR includes the contribution of land subsidence, which can be several orders of magnitude larger than the contribution of absolute SLR (Syvitski et al., 2009). Many delta areas are prone to subsidence, because their subsurface is not yet fully compacted and because of extraction of groundwater and hydrocarbons, drainage and loading.

In order to mitigate the consequences of subsidence, the first step is to quantify past and current subsidence rates. However, subsidence rates can vary strongly over space and there is no universal method to easily measure subsidence at high spatial, temporal and vertical resolution. For large, inaccessible and/or data-poor delta areas, remote sensing (RS) is a very important data source to assess recent subsidence rates for larger areas. A more and more commonly used RS technique is Interferometric Synthetic Aperture Radar (InSAR) (e.g. Smith, 2002). Satellite InSAR availability improves with more satellites becoming available, but extracting accurate subsidence rates from the data especially for delta areas remains challenging.

The next step is to predict future subsidence rates to determine effective measures to mitigate the impact on society as quickly as possible. Extrapolation of InSAR-derived subsidence rates over time is not directly possible. Conventional predictions require information on the complex processes involved, which are part of ongoing research. These processes are still difficult to be combined into a comprehensive, physics- or process-based model to predict subsidence rates. Even if such a model exists, the problem of lacking complete, accurate input datasets – for example on subsurface composition – remains.

A complementary approach which depends less on thorough knowledge of processes of subsidence and subsurface data can be useful to provide policy makers more rapidly with estimates of current and future subsidence rates. Land use (LU) may be a suitable key for estimating subsidence rates. Firstly, because LU data are more widely and freely available than subsurface data: it can be derived from globally available remote-sensing products. Secondly, because LU is related to many land-subsidence drivers. Differences in subsidence rates between different LU classes may be caused by differences in natural and anthropogenic loading (subsidence due to compression), the amount of groundwater extraction (subsidence due to consolidation) and the managed depth of the groundwater table (subsidence due to oxidation, ripening and compaction). In addition, quantifying land subsidence in relation to LU is a comprehensible way to create awareness among a wide audience and to provide a base for policy changes.

However, research on the relation between different LU types and subsidence at delta scale is very limited. Most studies focus on subsidence in urban areas; studies on rural areas are strongly underrepresented. No study has been found that quantifies and compares land subsidence per LU type and looks at the impact of LU changes on subsidence at delta scale. Besides, time-dependent effects on land-subsidence rates related to current and past LU (hereafter LU history) are still unclear. These effects include 1) changes in subsidence rates over time while the LU remains the same, and 2) time lags between LU changes and changes in subsidence rates. If time-dependent effects have a significant impact on subsidence rates, past LU should be taken into account when coupling subsidence rates to different LU types.

Therefore, this study aims to:

- 1) quantify and compare land-subsidence rates for different LU types and LU changes;
- 2) determine the importance of time-dependent effects related to LU history on land-subsidence rates;
- 3) determine to which extent LU history can predict land-subsidence rates.

The Vietnamese Mekong Delta (VMD) is used as case study to achieve these three aims. This delta was chosen because it is very prone to land subsidence and associated problems, as it largely lies less than 1 m above mean sea level (Syvitski et al., 2009) (Figure 1). In the last 25 years, subsidence rates increased significantly due to the strong increase in groundwater extractions (Minderhoud et al., 2017). This threatens all 18 million inhabitants and all people depending on the large rice production in the delta. In the same period, significant LU changes took place (e.g. Tran et al., 2015), which are probably related to the changes in subsidence rates. At last, the VMD is a good example of a data-poor environment for which a complementary, data-mining approach appears to be useful.

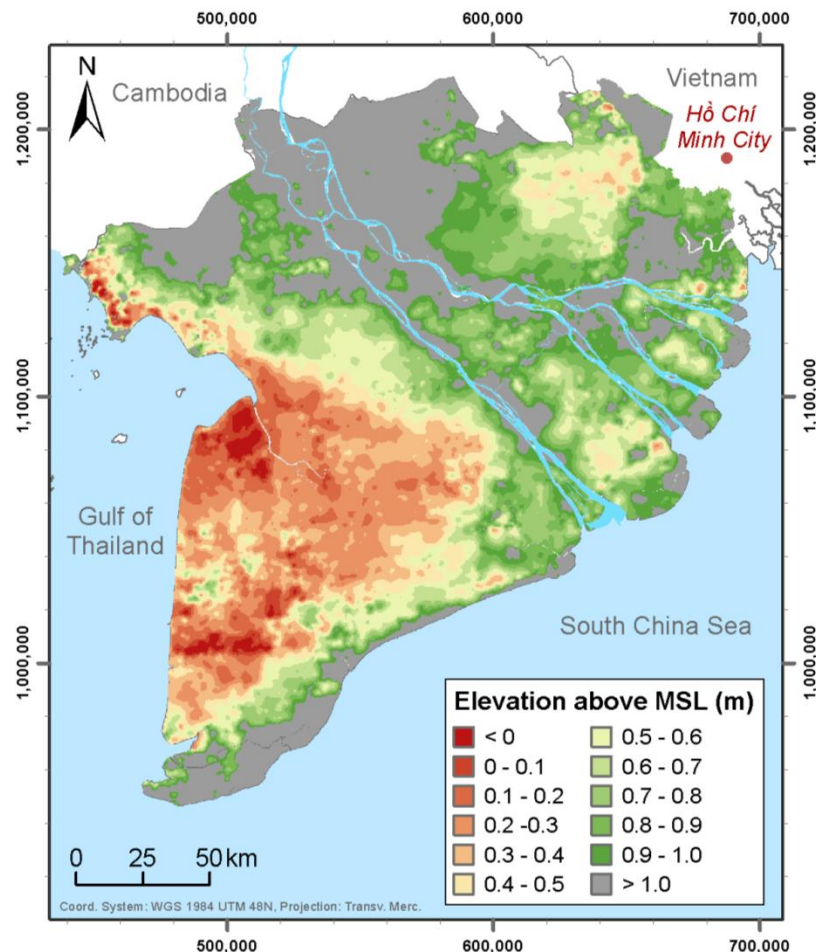


Figure 1 Elevation of the Vietnamese Mekong Delta above mean sea level (MSL).
After Coumou (2016).

This report starts with a review on the current knowledge on land subsidence, LU in the Vietnamese Mekong Delta and the relation between land subsidence and LU. Subsequently, the methodology and data used is given, including some background on the study area. The methodology, results and discussion each have three main parts: the classification of LU, direct coupling of LU to the existing subsidence dataset and the prediction of subsidence rates based on LU. The last part of the discussion indicates implications of this study for society and provides suggestions for future research. This will be followed by the conclusions. The appendices provide additional information on parts of the method and results.

2. Literature review

2.1. Land subsidence

For many deltas, land-subsidence rates exceed absolute sea-level rise and hence should not be neglected. This is also the case for the VMD (Erban et al., 2014). However, actual subsidence rates are often unknown – especially in rural areas (Higgins et al., 2013) – and the contribution of different drivers and processes to subsidence are not yet fully understood. This section will introduce some main definitions and discuss the current knowledge on the causes of subsidence in general and in the VMD and on land subsidence measuring methods.

Total versus net subsidence rate

Land subsidence is the downward movement of the land surface. A subsidence rate can represent a total subsidence rate as well as a net subsidence rate. The total subsidence rate exclusively represents the downward movement of the land surface. The net subsidence rate is the total subsidence rate minus the upward movement rate. Upward movements include accumulation of clastic and organic material and in some cases upward directed effects of redistribution of the Earth's masses. Upward movements are no driver of subsidence, but they are important to include if the actual change in surface elevation is of interest. If no upward movement takes place, the total and net subsidence rate are equal. Depending on the focus of the study and the measurement technique used, the subsidence rate refers to (a specific part of) the total or net subsidence rate. This difference should be taken into account when comparing different studies.

Causes of subsidence: drivers and processes

There are two main approaches of analyzing the determinants of land subsidence: analyzing the drivers or the processes. The drivers can be split in natural and anthropogenic drivers (e.g. Tosi et al., 2009). Anthropogenic drivers can result in several orders of magnitude larger subsidence rates than natural drivers (Erkens et al., 2015). The processes can be subdivided based on the physical depth at which they play a role (e.g. Higgins, 2015). Since the drivers and processes are linked, they can be combined into one overview: Figure 2. LU has the most direct link with the (anthropogenic) drivers. Therefore, the driver approach will be used below to give an overview of the main causes of land subsidence.

The total subsidence rate S_{tot} can be expressed as the sum of the impact of all main drivers: loading (L), fluid (and gas) extraction (F), lowering of the groundwater table (GW) and redistribution of the Earth's masses (e.g. tectonics and isostasy) (M). Together with the accumulation rate, this gives the net subsidence rate S_{net} :

$$S_{net} = \underbrace{L + F + GW + M}_{S_{tot}} - A \quad \text{Eq. 1}$$

M in Eq. 1 can be both positive and negative. In the VMD, the total subsidence rate based on an InSAR analysis is approximately 1 to 4 cm/yr averaged over nearly the entire delta (Erban et al., 2014).

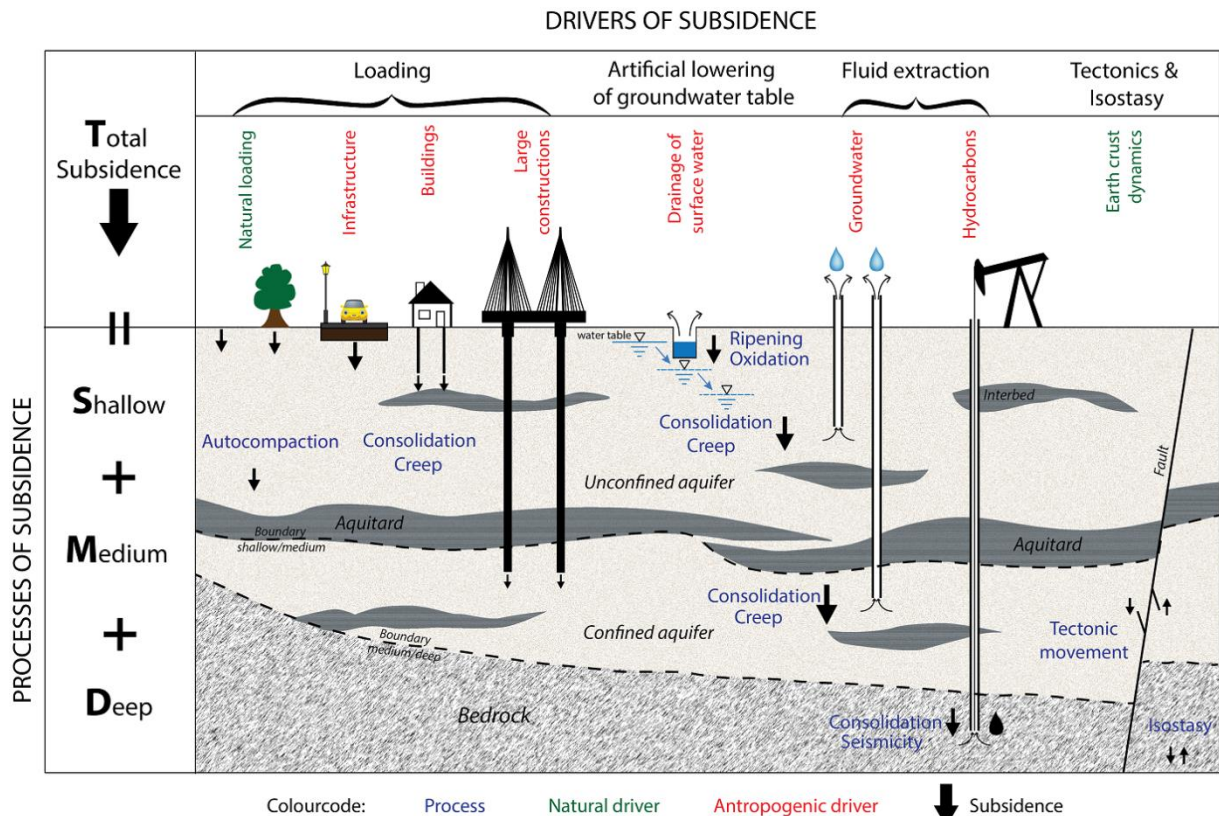


Figure 2 Schematic overview of main drivers and processes of subsidence. The shallowest aquitard is the boundary between the shallow (unconfined) and deep (confined) subsurface. Adopted from Minderhoud et al. (2015).

The first driver – loading – includes natural loading mainly induced by water bodies and sediment overburden (i.e. all overlying sediment), and anthropogenic loading by infrastructure, buildings and other constructions. This can result in differential subsidence between urban and rural areas, as is observed in the InSAR-based subsidence data of Erban et al. (2014). The terminology of the processes behind loading differ. In this review, ‘compression’ is used as an overarching term. Compression can be divided into compaction and consolidation. Compaction is the reduction in pore volume due to the reduction in air volume and thus it occurs in the very shallow, unsaturated subsurface (Higgins, 2015). Consolidation consists of primary and secondary consolidation. Primary consolidation is the reduction in pore volume related to expulsion of water from the sediment and takes place in the saturated layers. Water expulsion reduces the internal pore pressure. Once the pore pressure becomes smaller than the overburden pressure, the pores collapse (Yuill et al., 2009). Secondary consolidation or creep is related to the slow, gradual, steady and largely irreversible reorientation of sediment grains into a more tightly packed alignment (Yuill et al., 2009). Creep may continue even after hydraulic heads increase again (Erkens et al., 2015). The consolidation rate depends on the sediment grain properties (e.g. permeability), the volume of water in the sediment and the overburden pressure (Yuill et al., 2009). Natural peat compression due to overburden under saturated conditions can be much slower than oxidation as a result of lowering of the groundwater table (Higgins, 2015).

The second driver – extraction of resources such as water, oil and gas from the subsurface – reduces the pore pressure and results in additional consolidation of the sediment layer and in turn subsidence of the land surface (Erban et al., 2014; Yuill et al., 2009). The magnitude of subsidence depends among others on the magnitude and rate of fluid extraction, and the depth and size of the reservoir (Figure 3) (Yuill et al., 2009). At larger depth, the subsidence potential is smaller, because the larger overburden pressure has already consolidated the sediment to a larger extent. The subsidence rates decline with distance to the pumping well (Figure 3) (Yuill et al., 2009). Especially clays are susceptible for pumping-induced consolidation; sands are much less compressible (Erban et

al., 2013). Groundwater and hydrocarbon extraction dominate the human-induced accelerated subsidence in many areas, especially in (large) delta cities such as Ho Chi Minh City – just northeast of the VMD (Figure 1) –, Bangkok, Jakarta and Tokyo (Erban et al., 2014; Erkens et al., 2015; Higgins, 2015). The demand for groundwater is increasing in deltas due to rapid urbanization, population growth, industrialization and pollution of surface water. Often, this groundwater is extracted from intermediate to deep confined aquifers (e.g. Erkens et al. (2015) for New Orleans, Minderhoud et al. (2017) for the VMD).

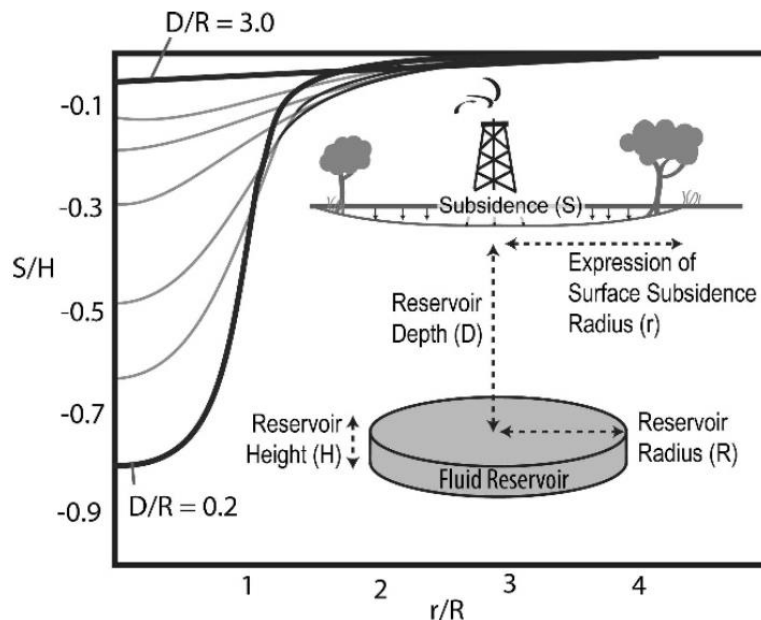


Figure 3 Example of the relationship between fluid reservoir size and the magnitude of the land-subsidence rate due to reservoir compaction. The curved lines represent the predicted ratio between the subsidence rate and the reservoir height (S/H) as function of the ratio between the radius of the expression of the surface subsidence and the reservoir radius (r/R) for different measured ratios between the reservoir depth and the reservoir radius (D/R) between 0.2 and 3.0. A deeper reservoir results in smaller surface subsidence rates over a larger area. Adopted from Yuill et al. (2009).

Groundwater extraction is a main driver of subsidence, not only in the mega city of Ho Chi Minh City (~ 4 cm/yr based on InSAR), but also in the VMD (Erban et al., 2014, 2013; Minderhoud et al., 2017). Groundwater extraction in the VMD could explain between $\sim 50\%$ and $\sim 95\%$ of the observed, InSAR-based subsidence rates (Minderhoud et al., 2017). Since the early 1900s pumping wells have been active, but since the early 1980s the use intensified (Erban et al., 2013). Based on a survey in 2007, at least 465,230 wells were active in the VMD which extracted in total over 1.2 million m^3/day (Deltares et al., 2011). By 2015, the extraction rate had increased to about 2.5 million m^3/day (Minderhoud et al., 2017). The water is used for agricultural, aquacultural, domestic as well as industrial purposes (Erban et al., 2013; Renaud & Kuenzer, 2012; Wagner et al., 2012). Hydraulic heads have been declining due to groundwater extraction over the last decades (Minderhoud et al., 2017). In Ca Mau (southwest VMD) the hydraulic head dropped more than 15 m since the mid-90s. Current decline rates range from 9 to 78 cm/yr with an average of 26 cm/yr in the VMD (Erban et al., 2014). Groundwater is extracted from a large range of depths (Nesbitt, 2005). Most water is extracted from the deep ($\approx 170 - 500$ m) aquifers, because of polluted surface and shallow groundwater (Erban et al., 2013). However, this old groundwater could not be recharged from local rainfall. By 2005, shallow aquifers were exhausted and some medium depth aquifers were no longer artesian (Nesbitt, 2005), while they were in 1991 (Minderhoud et al., 2017).

Based on 1D compression calculations, these groundwater extractions result in subsidence rates of on average 1.6 cm/yr [0.28 to 3.1 cm/yr] in the VMD (Erban et al., 2014). A transient 3D aquifer simulation suggested subsidence rates of 1.1 to 2.4 cm/yr and a total subsidence of 27 cm since 1988

for the central part of the VMD (western part or Tien Giang province). The high groundwater extraction rates in Ho Chi Minh City are not responsible for subsidence in at least that part of the VMD (Erban et al., 2013). Besides, InSAR-based subsidence patterns correspond with the variations in decline in hydraulic head due to pumping at different locations in the VMD (Erban et al., 2014). Erban et al. (2014) attributed the average of 1 to 4 cm/yr net subsidence in the VMD based on the InSAR data also mainly to groundwater extraction.

The third driver of subsidence is lowering of the groundwater table by for example drainage (Erkens et al., 2015; Yuill et al., 2009). As long as peat and sediments which contain organic matter are below the water table, the decay of organic matter (OM) is very limited. Once the water level is lowered, organic matter (OM) is exposed to oxygen and several biological and chemical reactions accelerate the decay of OM (Yuill et al., 2009). These processes together are often collectively called 'oxidation' and they result in subsidence (cf Higgins, 2015). Moreover, microbial decay of organic matter is increased in partially or seasonally saturated conditions instead of continuous saturation (van Asselen et al., 2009). Besides, the ripening of clayey sediments above the water table results in subsidence. At last, the replacement of water by air in the pores results in a decrease in pore pressure. Depending on the overburden pressure, this can also result in sediment compaction (Erkens et al., 2015; Yuill et al., 2009). No information is available on the absolute and relative contribution of these processes to the total subsidence rate in the VMD, but in general, mean subsidence rates due to drainage of the shallow subsurface are in the order of 0.1 to 1 mm/yr (Yuill et al., 2009).

The last drivers of subsidence are earth crust dynamics, or the redistribution of Earth's masses. Deltas are generally located in subsiding basins in which accommodation space is created because of basin and local tectonics. At the moment, tectonics can result in subsidence at various spatial and temporal scales and with different magnitudes (Higgins, 2015). In addition, the crust responds to changes in the weight of the overlying materials such as sediment, water and ice (Erkens et al., 2015; Higgins, 2015; Yuill et al., 2009). This is called isostatic adjustment. The magnitude of vertical elevation change can be several centimeters. Glacial isostatic adjustment as a result of the melting of glaciers and ice sheets at the end of the last glacial period still results in vertical elevation changes due to upbouncing and in some areas due to forebulge collapse (Higgins, 2015; Yuill et al., 2009). The crust can also deform elastically at shorter, annual time scales as a consequence of annual loading and unloading of groundwater and surface water (Higgins, 2015). Erban et al. (2014) indicate that natural subsidence related to crustal loading and oxidation of organic matter (together generally < 0.5 cm/yr) probably also plays a role in the VMD. Though, its role is minor. Little is known about the actual contribution of these processes on the total subsidence rate in the VMD.

Next to the drivers of subsidence, accumulation completes the balance to determine the net subsidence rate. Accumulation rates of clastic sediment that settles during river floods and after large events such as storm surges are generally in the order of mm/yr or cm/yr, with large variations within and between deltas (Higgins, 2015). Human induced soil erosion – e.g. as a consequence of poor agricultural practices and deforestation – increase the sediment input to rivers and hence potential aggradation in a delta. However, flooding and hence sediment deposition is prevented due to human constructions such as dams and dikes and reductions in flow velocities upstream (Higgins, 2015). Currently, (controlled) flooding occurs mainly in the upstream part of the VMD (Tri, 2012), resulting in an accumulation rate of about 6 mm/yr (Hung et al., 2014).

Accumulation rates of organic material are related to deposition of organic detritus by vegetation and the expansion of the root network in for example mangrove forests. Peat can accumulate with several centimeters per year. In the VMD, mean accretion rates of 42.7 mm/yr, 36.8 mm/yr and 67.8 mm/yr were measured in different mangrove areas along the coast (Lovelock et al., 2015), which probably is a combined effect of accumulation of organic and clastic materials.

At last, it should be noted that the spatial patterns and magnitude of subsidence is not only determined by the drivers, but also by the composition of the subsurface (Erkens et al., 2015). Sand and gravel are nearly incompressible and barely loose volume after deposition. The compressibility of silt and especially clay is larger. However, the lower hydraulic conductivity of clay results in slower compression than that of silt. Thus, it takes longer for clay to become denser than silt. The most compressible soil type is peat, which can compact very fast (Higgins, 2015). The shallow subsurface of the VMD mainly consists of fine grained sediments: clay and silt. Organic matter and some peat layers are also present in the VMD, mainly in the upstream marshy plains (Nguyen et al., 2000). Hence, the VMD is susceptible to many subsidence processes.

So, in short, three drivers of subsidence dominate the subsidence rate in the VMD: loading, groundwater extraction and lowering of the groundwater table. Groundwater extraction is the most important of these drivers. Besides, the fourth driver – earth crust dynamics – only plays a minor role. Moreover, subsidence can partly be compensated by accumulation of clastic and organic matter especially in floodplains and swampy areas.

Time-dependent effects on land-subsidence rates

Subsidence rates do not only vary over space, but also over time. Shallow subsidence rates due to decomposition of organic matter decrease over time after initial dewatering because of organic matter depletion (Yuill et al., 2009). Subsidence rates related to primary consolidation also decrease over time until an equilibrium between pore pressure and overburden pressure is reached. Secondary consolidation continues even after primary consolidation ends until the grains can no longer be reorganized to a significantly tighter packing (Figure 4) (Yuill et al., 2009). The time needed to reach an equilibrium – the hydrodynamic period in case of primary consolidation – depends among others on the sediment characteristics. This period is longest for fine-grained sediments such as peat and clay due to their low permeability (van Asselen et al., 2009). Changes in the boundary conditions such as extraction of water or increased loading alter the equilibrium situation and will result in further consolidation (Yuill et al., 2009). At last, the subsidence potential of a sediment layer decreases if the sediment gets more and more compacted. This also results in a decrease in subsidence rates over time. This is most important for shallow subsidence which have a shorter subsidence history. The subsidence potential of the shallow surface in the VMD is still large and it will take relatively long before a decrease in subsidence potential will be noticeable in the subsidence rates over time.

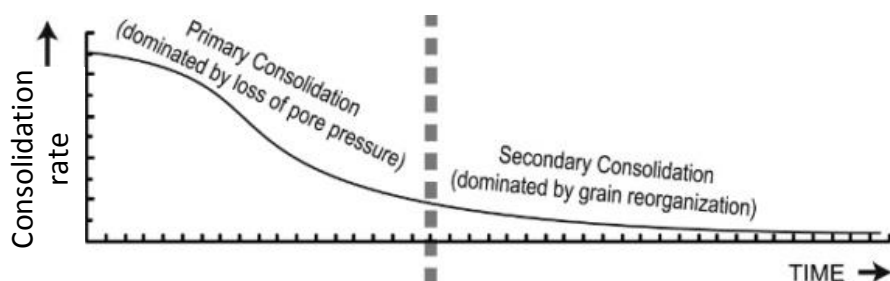


Figure 4 Decrease in relative subsidence (consolidation) rate over time in a case of a constant weight of the overburden. Adapted version of fig. 8 in Yuill et al. (2009).

Next to gradual changes over time, time-lag effects can also play a role. These are a consequence of a delayed response of the system to a change in the subsidence drivers. This is observed as a reaction to changes in groundwater extraction. A sandy aquifer from which water is extracted is recharged quickly after extraction stops. Consolidation occurs mainly in the clayey aquitards with low permeability. In these layers, the hydraulic head can still decrease while it already increases in the sandy aquifer. Hence, primary consolidation can continue for a few months to years after extraction stopped (Isotton et al., 2015). An example of time-lag effects due to among others secondary consolidation is observed in Tokyo. The city of Tokyo stopped intensive groundwater pumping in the early 1960s, but the strong decrease in subsidence rates is only observed several years later (Figure 5) (Erkens et al., 2015).

Thus, two time-dependent effects can influence the subsidence rates. Firstly, 'time effects' correspond to processes which result in a (gradual) change in subsidence rates over time without changing the boundary conditions. Secondly, 'time-lag effects' correspond to the delayed response of a system to a change in subsidence drivers.

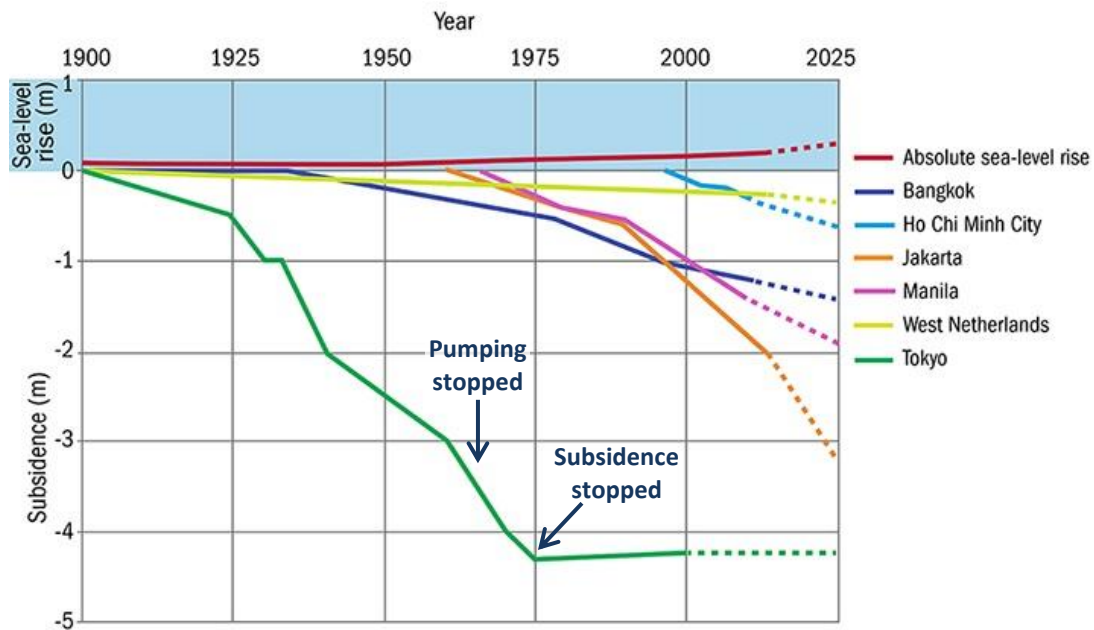


Figure 5 Cumulative subsidence history for six locations around the world. Absolute or eustatic sea-level rise is given as reference. Subsidence rates can vary significantly within a region: the values represent averages for local subsidence hotspots. In Tokyo, groundwater pumping stopped in the early 1960s, but the subsidence stopped only several years later. Adjusted from Erkens et al. (2015).

Methods to measure land-subsidence rates

No measuring technique can resolve every process at all relevant temporal and spatial scales. Each technique has its own advantages and disadvantages (Table 1), which will be discussed in this section. Techniques have to be combined to form a complete picture (Higgins, 2015).

Spirit leveling, a dGPS, an extensometer and a Rod Surface Elevation Table (SET) can be used for point measurements (Galloway & Sneed, 2013; Higgins, 2015). Additionally, net subsidence rates can indirectly be derived from analyzing surface-water level trends. Based on such an analysis, the VMD subsided on average 6 mm/yr in the period 1987-2006 (Fujihara et al., 2016). Similarly, an average rate of 17.1 mm/yr for the period 1993-2013 is found for the city of Can Tho in the middle of the VMD (Takagi et al., 2016). Spirit leveling and a dGPS can be used to determine a subsidence rate of the subsurface below the anchor point of a benchmark. Benchmarks anchored at different depths reveal variations in subsidence over depth, which helps in identifying the causes of subsidence (Higgins, 2015). Depth-specific subsidence rates can also be measured with an extensometer which could be anchored at different depths up to several hundreds of meters deep at one location (Galloway & Sneed, 2013). A Rod SET is a portable mechanical leveling device that measures elevation changes of the shallow subsurface up to the bottom depth of the benchmark rod (generally max. 25m). In combination with a marker horizon (MH) it accurately gives the total shallow subsidence rate, especially in wetlands (Cahoon et al., 2002). In the VMD, several (Rod) SET-MH are in operation, though limited data has been published. Based on the available data, the total shallow subsidence rate is 25.3 mm/yr, 31.6 mm/yr and 41.0 mm/yr for the period 2010-2014 for different mangroves or similar environments in the VMD (Lovelock et al., 2015). Due to high accretion rates, nearly all locations showed a net elevation increase (average of 11.6 mm/yr, 36.2 mm/yr and 1.8 mm/yr respectively).

Table 1 Examples of measurement techniques to determine the land-subsidence rate with their characteristics and whether they are available in the Vietnamese Mekong Delta (VMD). dGPS = differential Global Positioning System, Rod SET-MH = Rod Surface Elevation Table – Marker Horizon, other acronyms: see list of acronyms.

Technique	Coverage	Subsidence rate type	Advantages	Disadvantages	Available in the VMD?
dGPS elevation measurements	Points	Net	- Relatively easy ³	- Often unavailable ¹	No
Spirit leveling	Points	Net	- Accurate	- Small areas	No
Rod SET-MH	Points	Shallow (& accretion)	- Accurate ²	- Limited availability ²	Yes, but limited data published
Extensometer	Point	Total per depth interval	- Vertical variation in subsidence ^{1,3,4} - Accurate ³	- Often unavailable - Expensive	Under construction
InSAR	Spatial	Total or net	- High resolution ¹ - Large coverage ¹ - Signal of permanent reflectors reflects total subsidence ¹	- Required permanent (corner) reflectors scarce in deltas ^{1,4} - Difficult to process	Yes, 2006-2010
LIDAR	Spatial	Net	- Highest resolution ¹ - Large coverage ¹ - Performs better in rural and vegetated areas than InSAR ¹	- Expensive ^{1,3} - Often unavailable ¹	No, maybe in future

¹ (Higgins, 2015) ² (Lovelock et al., 2015) ³ (Galloway & Sneed, 2013) ⁴ (Erkens et al., 2015)

Subsidence rates can vary significantly over space, for example due to variations in sediment grain size, time since deposition and thickness of overburden (Higgins, 2015). Hence, though point measurements can provide accurate subsidence rates, their lack of spatial coverage is a disadvantage. InSAR (Interferometric Synthetic Aperture Radar) and LiDAR (Light Detection and Ranging) techniques overcome this disadvantage (Erkens et al., 2015; Higgins, 2015). Especially InSAR is often used for subsidence studies (e.g. Amelung et al., 1999; Chen et al., 2014; Higgins et al., 2013; Lu & Liao, 2008; Osmanoglu et al., 2011). The spatial patterns revealed by these techniques can be used to determine which drivers or processes are dominant.

Synthetic Aperture Radar (SAR) instruments are active microwave systems which can also be used at night and with clouds (Lillesand et al., 2008). They send out a radar (radio detection and ranging) pulse and measure the amplitude and phase of the returned signal (Smith, 2002). This returned signal is strongly influenced by the surface roughness of the objects and wetness. A specular reflector such as a flat, flooded surface returns no signal. A corner reflector such as the base of a building can return the entire signal. Diffuse reflectors return a part of the signal (Lillesand et al., 2008). For InSAR, generally the L-band (wavelength = 23 cm) is used as emitted pulse, because this long wavelength penetrates through vegetation and returns a signal from the surface. An interferogram is an image of the difference in phase between two images taken at approximately the same location at different times (repeat-pass method) or at the same time at different locations (single-pass method) (Lillesand et al., 2008; Smith, 2002). The phase difference over time can be converted to elevation change. This method only works accurately for objects which reflect a clear signal to the sensor (ideally a corner reflector) at both times (Erkens et al., 2015). Preferably, the reflectors remain exactly the same. However, the reflector will change in case of erosion and aggradation or it will remain at the same elevation. Hence, erosion and aggradation cannot be resolved (Higgins, 2015). Thus, the elevation change will reflect more likely the total than the net subsidence rate.

The LiDAR technique uses an airborne and sometimes ground-based sensor to measure the surface elevation of an area with a very high resolution and 15-30 cm accuracy. Just like InSAR, lidar sensors are active systems, but in this case laser light pulses are used instead of microwave energy (Lillesand et al., 2008). These laser pulses also penetrate through vegetation. The time each pulse needs to return to the sensor can be converted to an elevation. To obtain subsidence rates, the measurements have to be repeated to compare the elevations. Since LiDAR has not the limitation of requiring permanent reflectors, it also works for rural and vegetated areas. Besides, the elevation change includes the effect of aggradation and erosion. Hence, this technique always gives the net subsidence rate (Higgins, 2015).

Overall, several techniques exist with large differences in the temporal and spatial coverage, vertical accuracy, depth(s) for which they measure subsidence rates and whether net or total subsidence is measured. For areas such as the VMD, the amount of measurements is limited (Table 1). Our study is at a delta scale, hence, the InSAR dataset is most suited to be used. However, other measurements would be useful as validation and to complement information which cannot be resolved with InSAR.

2.2. Land use in the Vietnamese Mekong Delta over the past decades

The current LU situation in the VMD is characterized by aquaculture areas behind small mangrove strips along the coast, extensive agricultural areas with mainly rice and orchards close to the main rivers. However, LU changed rapidly and at large scale over the last few decades in Southeast Asia, with the Mekong standing out as a change hotspot (Giri et al., 2003). The VMD follows the general trends in riverine and coastal environments: deforestation occurred and simultaneously the area of urban areas and aquaculture increased (Tran et al., 2015). Moreover, rice cropping intensified strongly over the past decades (Figure 6).

Below, the current situation followed by the main past changes will be described per LU type.

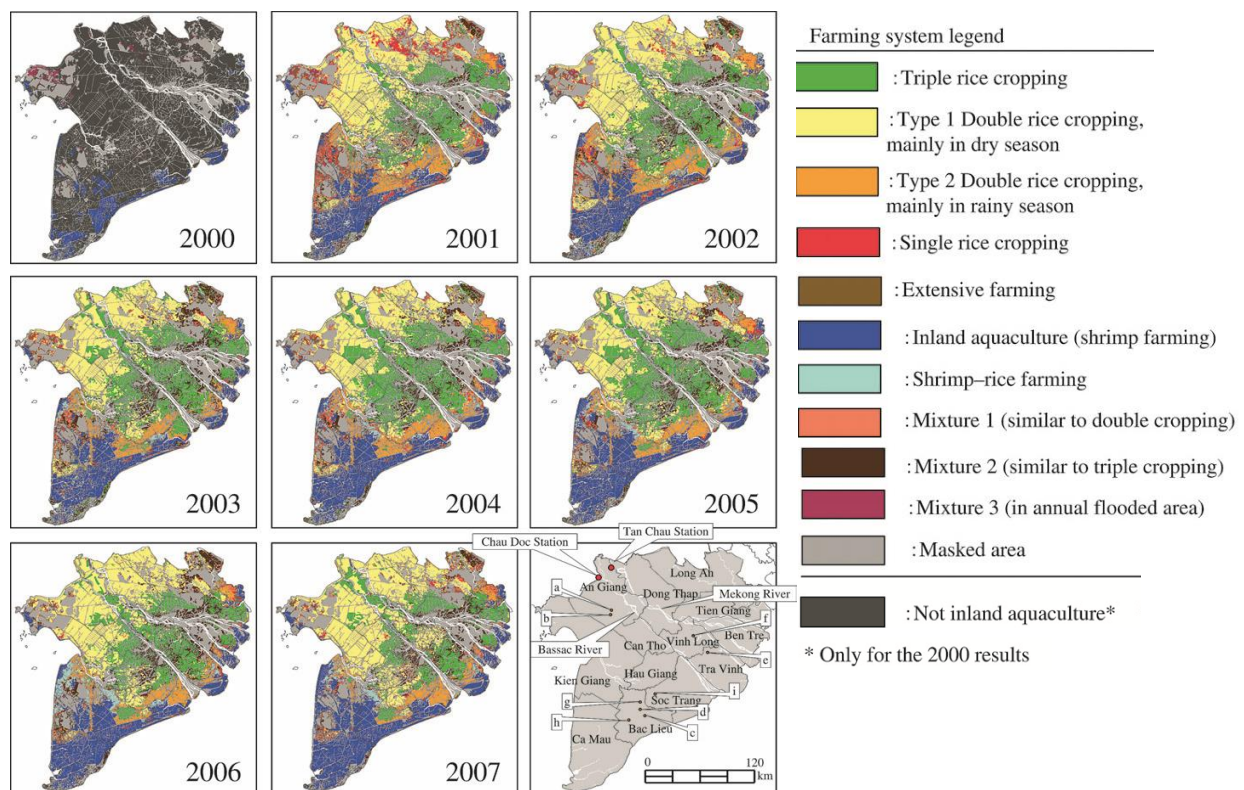


Figure 6 Yearly land-use maps of the VMD for 2000 up to 2007 focused on aquaculture and rice cropping system, based on MODIS time-series analysis. The masked area is based on the Sub-NIAPP land use map of 2002 in Sakamoto et al. (2006) and includes orchards, unused land and forests. Adopted from Sakamoto et al. (2009a).

Agriculture

Cultivated land covered and covers the largest part of the VMD and is dominated by rice. Currently, the number and timing of the rice-cropping cycles varies over the VMD. Besides, sometimes rice is alternated with other crops or even aquaculture within the same year (e.g. Nguyen-Thanh et al., 2014; Sakamoto et al., 2006; Sakamoto et al., 2009a). The upper part of the VMD is mainly dominated by irrigated double rice cropping during the dry season. During the wet season large water depths related to yearly floods inhibit rice cropping in this area. The coastal area is generally characterized by rain-fed double rice cropping during the wet season. This is because during the dry season, the higher salinity of the irrigation water inhibits rice cropping. The area in between is dominated by triple rice cropping at the moment, as it is limited to a lesser extent by flooding and salinization and has enough irrigation water available due to the proximity of the rivers. Some

scattered areas in especially the coastal region suffer from poor soils and are characterized by single-cropped rain-fed rice in the rainy season. Next to rice, some areas are used for other crops: upland or perennial crops, such as onions, watercress, ladyfingers, chili and shallots. If rice and crops are alternated, sweet potato, onions and spinach can be found (Binh et al., 2005). Their extent is limited to the higher, more fertile, well-drained soil types during the wet season or are fully irrigated during the dry season (Nesbitt, 2005). This agricultural pattern has gradually developed over time.

Trends in LU change differ over the delta (Sakamoto et al. 2009b). Large inland areas of the Mekong delta were covered with natural wetlands or wasteland around the end of the Vietnam war in 1975 (old LU maps (Appendix 1); Nguyen & Viet, 2013; Tanaka, 1995). The doi moi policy initiated in 1986 in combination with a new Land Law in 1993, which designated wetlands – defined as ‘unused land’ – to be converted to economically more valuable LU such as agriculture, aquaculture and forest plantations, led to the strong reduction in wetland, despite wetland protection initiatives (Funkenberg et al., 2014). The total area of upland crops showed a slight increase in area between 1990 and 2004 (Nhan et al., 2007). The total area of rice showed an increase of 1255 km² (> 3% of the delta area) between 2001 and 2012 (Nguyen-Thanh et al., 2014). Locally, the area of rice cropping increased from less than 50% of the area before the eighties to about 90% in 2005 (Nguyen & Viet, 2013). In the coastal areas, agricultural fields are converted to aquaculture and urban areas (e.g. Binh et al., 2005; Karila et al. , 2014; Tran et al., 2015).

Next to the extent of agriculture, the number, kind and timing of (rice) harvests over the year changed (Giri et al., 2003). The temperature in the VMD allows year-round production of rice, but water availability and quality is a limiting factor which cannot be overcome in all regions (Sakamoto et al., 2009b). Originally, one traditional rice crop with a long growing period (180-210 days) was grown from May to December or January (Binh et al., 2005). Since about the 1990's, a vegetable crop (e.g. onions, sweet potato or spinach) was grown after the rice harvest from February to April (Binh et al., 2005). Besides, the popularity of growing two rice crops per year increased with two short-duration, high-yield crops, or a long and short rice crop (Binh et al., 2005). However, the double cropped rain-fed rice in the coastal area partly decreased due to conversion to single cropped rain-fed rice or combined shrimp-rice farming between 2001 and 2008 (Nguyen-Thanh et al., 2014).

After double rice cropping became standard, triple rice cropping increased in popularity in the VMD over the last few decades (Nguyen-Thanh et al., 2014). One of the required boundary conditions for this change was the improvement of the dike system after a severe flood in 2000, which ensured better control of water levels in the paddies (Bouvet & Le Toan, 2011). The expansion of triple rice cropping was at the expense of especially the double cropped irrigated rice more upstream (Nguyen-Thanh et al., 2014), although double rice cropping remained dominant in the upper part of the VMD over the period 2000-2007 (Figure 6) (Sakamoto et al., 2009a). In 2001, using an additional rice crop in the dry season was already common in the Hau Giang province and the northern part of the Soc Trang province (for the locations of all provinces in the VMD, see Figure 8) (Sakamoto et al., 2009b). This conversion even occurred slowly in the coastal area after 2001 (Sakamoto et al., 2009a). The increase in triple rice was rapid up to 2005, but subsequently dropped due to environmental concerns and disappointing yields (Nguyen-Thanh et al., 2014; Sakamoto et al., 2009a). This resulted in an increase in double-rice cropping again.

Aquaculture

Currently, aquaculture covers relatively large areas bordering the coast in the VMD. In addition, some aquaculture is found more inland. Shrimp farming is the main type of aquaculture (Wilder & Phuong, 2002). However, this situation has only recently developed. Roughly a century ago, the first Vietnamese extensive shrimp farms were created (Binh et al., 2005). The income per ha for shrimps is about 160 times larger than for rice (Binh et al., 2005). Up to the seventies, aquaculture was very limited, but as soon as the government allowed aquaculture expansion in the eighties, the extent and intensity of aquaculture quickly expanded (Binh et al., 2005; Sakamoto et al., 2009b; Tran et al.,

2015). In the first decade of the 21st century, aquaculture was performed in most coastal provinces (Figure 6) (Karila et al., 2014; Sakamoto et al., 2009a). The main increase in area of shrimp farms was between 1995 and 2004/2005 (Sakamoto et al., 2009b; Tran et al., 2015) with the sharpest increase between 1999 and 2000 (Binh et al., 2005) or 2001 to 2003 (Sakamoto et al., 2009b). This was a consequence of several new policy resolutions and institutions stimulating aquaculture. Between 2000 and 2001, the area of shrimp farming increased by 42.6% in Vietnam (Binh et al., 2005). This happened at the expense of forest and rice fields (Binh et al., 2005; Sakamoto et al., 2009b; Tran et al., 2015).

Many shrimp ponds are only used temporarily and are then abandoned, at least between 1995 and 2001. New ponds are created at the expense of mangroves elsewhere (Thu & Populus, 2007). Abandoned ponds are generally too polluted and salinized to be used for e.g. agriculture (Tho et al., 2008). Meanwhile, there is a continuous competition for the 'correct' salinity of the irrigation canals between shrimp farms – which require brackish water – and rice fields – which require fresh water – (Nhan et al., 2007). Sluices are used to supply rice fields with fresh water, impeding aquaculture (Sakamoto et al., 2009b; Tuong et al., 2003). Vice versa, a rice field enclosed by aquacultural ponds may get too saline for rice crops, forcing the farmer to shift to aquaculture too (Binh et al., 2005). This results in sharp transitions between larger regions of aquaculture and rice, with the borders existing of mainly canals and rivers (Sakamoto et al., 2009b).

Urban areas

Currently, the VMD is relatively densely populated with over 17 million inhabitants. However, before the Vietnam war, most parts of the swampy backlands of the main rivers in the VMD were not inhabited or cultivated. After the war, many migrants were sent to these areas to reclaim the land (Tanaka, 1995). The urban area increased significantly over the last decades, because the population density increased and the infrastructure improved (Binh et al., 2005; Giri et al., 2003; Tran et al., 2015). The main increase in urban area in a part of the province Ca Mau is observed between 1995 and 2004 (Tran et al., 2015). The settlements expanded along the canals, rivers and main roads since the end of the sixties (Binh et al., 2005). Some of these settlements had formed small villages by the start of the 21th century, as observed in old LU maps (Appendix 1).

Forests and orchards

Forest areas are not widely spread in the VMD nowadays. Only small strips of mangrove (salt-water forest) are present along the coast, and some fresh water, melaleuca forests more inland in low-elevated parts. This situation changed considerably over the last decades. Before the Vietnam War (1961-1971), extensive mangrove forest bordered the coast and large inland areas were covered with fresh-water forests and other vegetation (Tanaka, 1995). During the Vietnam War, large areas of salty, brackish and fresh water forest in the VMD were deliberately destroyed by herbicides (Giri et al., 2003; Nguyen et al., 2011; Thu, 2006). Until about 1979, parts of these bare areas recovered (Nguyen et al., 2011).

In the meanwhile, from at least the 1960's or 1970's to the end of the 2000's, the conversion of mangrove and melaleuca forest increased. At first, these lands were converted to cultivated (rice) lands (Tanaka, 1995) and in coastal areas later on to aquaculture (Binh et al., 2005; Nguyen et al., 2011; Thu, 2006; Tran et al., 2015). In the period 2001-2005, 65% of the forested area of an upstream part of the VMD was lost and mainly converted to irrigated rice fields, followed by conversion to shrimp farms (Son & Tu, 2008). In the south of the VMD, a decrease of 75% in forested area and a strong reduction in the diversity of the forest types were observed in the period 1968-1992 (Binh et al., 2005). Some rice fields in the inland areas were converted back to melaleuca forest due to problems in cropping rice (Tanaka, 1995). In 1991 and 1998 laws were implemented to prevent

further deforestation. Although still a net reduction occurred, some reforestation took place (Thu, 2006), and some protected parks were created. Between 2004/2005 and 2009/2010, a slight increase in melaleuca forest is observed in several provinces in the VMD. This is generally related to a conversion from grassland to melaleuca plantations (Space Technology Institute, 2011).

Next to forests, orchards are nowadays also important in the VMD. Orchards are located along the rivers in the VMD in areas where many people live. Between 1968 and 1992, the area of settlements with fruit gardens increased considerably in a part of the province Ca Mau, but decreased slowly afterwards (Binh et al., 2005). In recent years, there has been a sharp increase in fruit trees in the coastal province Ben Tre (Karila et al., 2014). The area of fruit trees in the VMD has expanded from 175,000 ha in 1995 to almost 300,000 ha in 2002. A further increase to over 500,000 ha after 2005 is expected (Nesbitt, 2005).

Taking all LU developments in the VMD together, it can be concluded that LU changed significantly over the last decades. Along the coast, mangroves were converted to aquaculture. More inland, wasteland was reclaimed to create agricultural areas mainly for rice cropping. Besides, rice cropping intensified by growing more crops a year. Moreover, urbanization took place. This resulted in the growth of settlements and an extensive network of roads, dikes and canals along which people live.

Land-use maps of the Vietnamese Mekong Delta

The trends in LU described in the previous sections are based on written sources and LU maps. LU maps for the end of the 19th century are scarce, while a wide variety of maps exists for the 20th century. This is a direct consequence of the large amount of available remote sensing products. Remote sensing is an effective tool for land-use/cover mapping, because a large area can be analyzed at once for different moments in time in a cost-effective way. In fact, remote sensing is used to reveal the land cover, which can be converted to LU using the context. E.g. an area with rice can be interpreted as agriculture, and patchy water ponds as aquaculture. However, different LU classes can correspond to the same land cover class and vice versa, which complicates the conversion.

An overview of LU maps covering at maximum the entire VMD together with their characteristics is given in Appendix 1. These maps are generally difficult to be compared, because of differences in:

1) *The focus of the study*

Many studies focus on especially rice cropping systems over time (e.g. Bouvet & Le Toan, 2011; Karila et al., 2014; Kono, 2001), followed by studies focusing on the expansion of shrimp farms and the related reduction in forested area (e.g. Giang & Hoa, 2013; Tong et al., 2004; Vo et al., 2013).

2) *The extent of the maps*

The extent of the land-use/cover maps varies from local studies on district level to LU studies/maps for several countries or even the entire world. Examples at regional/provincial scale are published by Chen et al. (2012) and Sakamoto et al. (2009b). Examples for the entire VMD or even a larger area are published by Chen et al. (2011), Sakamoto et al. (2006 and 2009a), Son et al. (2014) and Xiao et al. (2006). The larger the extent, the lower the resolution of the map generally is.

3) *The land-use/cover classes and their definitions*

The classes and corresponding criteria used for LU/cover maps differ per study in order to have a representative, classifiable set of classes for the specific study area which is sufficient to answer the research questions (Kuenzer et al., 2011). Hence, similar class names in different studies can have different definitions.

4) *The data source (spatial, temporal and spectral resolution)*

Many satellite products with different characteristics – such as timing of imaging, temporal resolution, data availability, covered area, ground resolution, price, spectral characteristics – exist. For a review on products which can be used for LU mapping, see Kuenzer et al. (2011) and Kuenzer & Knauer (2013). For mapping the number and type of crops one or more years, low-resolution, multi-temporal MODIS (EVI (Enhanced Vegetation Index)) images are mostly used which cover relatively large areas (Kuenzer & Knauer, 2013), but also the NDVI (Normalized Difference Vegetation Index) of multi-temporal SPOT Vegetation images have been used (e.g. Nguyen et al., 2012). A single image cannot easily reveal different cropping systems (e.g. Karila et al., 2014; Leinenkugel et al., 2013; Liew et al., 1998).

Especially if low-resolution images are used, problems with mixels (pixels which represent multiple land cover/uses) occur and small rice fields and shrimp farms are easily misclassified (Kuenzer & Knauer, 2013). Hence, for LU studies considering more than rice only, higher-resolution images are preferred, such as Landsat images (e.g. Funkenberg et al., 2014; Son & Tu, 2008), or for smaller areas high resolution SPOT images (e.g. Giang & Hoa, 2013; Karila et al., 2014; Thu, 2006; Vo et al., 2013) or Rapid Eye (e.g. Huth et al., 2012). Landsat images are available for a long time span.

5) *The method used to classify the images*

A wide range of classification methods exists. For a review of methods with their advantages and disadvantages for mangrove and rice mapping, see respectively Kuenzer et al. (2011) and Kuenzer & Knauer (2013). These reviews are representative for LU mapping in the VMD in general. Classification methods of remote sensing products used for the LU maps of the VMD include both pixel-based and object-based classifications, unsupervised and supervised classifications, decision tree classifications and hybrid classifications such as TWOPAC (Huth et al., 2012), as indicated in the appendix. Band ratios or indices such as the NDVI, EVI and Land Surface and Water Index (LSWI) are often used to aid the classification (e.g. Xiao et al., 2006).

Object-based image analysis (OBIA) means that the images are firstly segmented: pixels are grouped according to for example some specified criteria about e.g. shape and spectral resemblance (multi-resolution segmentation). Subsequently, these segments or objects are classified using the characteristics of the segments, including information about neighboring objects, shape and texture (Kuenzer et al., 2011). Generally, OBIA performs better than pixel-based approaches especially with high-resolution imagery (Vo et al., 2013). Though, the number of land-use/cover classifications in the VMD which use OBIA is very limited.

6) *The accuracy of the maps*

If the accuracy of the maps is given, they are generally above 75%. However, due to the large variety in quantity and quality of the ground truth data and differences in the method of the accuracy assessment, accuracies in different studies cannot always directly be compared or even trusted. In some cases the accuracy is not given at all.

As a consequence of all these differences, no single study or combination of studies was found which mapped LU changes at a useful resolution over the last few decades with a regular time interval, covering the largest part of the VMD and using similar LU classes. The LU maps produced by the Vietnamese government each five years (Dijk et al., 2013; Phuong & Catacutan, 2014) satisfy most conditions, but are not accessible and no further metadata on the precise data and methods used and the accuracy have been found. However, such a time series of maps is needed to be able to couple land-subsidence rates to LU.

2.3. The connection between land use and land subsidence

No studies were found which directly couple multiple LU types with differential land subsidence. However, combining the knowledge on the drivers of subsidence and LU in the VMD gives insight in this relation. In general, LU can be coupled to the drivers loading, fluid extraction and lowering of the groundwater table. Below, the most important drivers will be discussed for the main LU types in the VMD, followed by the expected relative differences in subsidence rates between the LU types and time-dependent effects on subsidence.

Agriculture

Agricultural areas are especially vulnerable to subsidence, but remain largely out of scope in previous studies (Higgins, 2015). In these areas, subsidence is dominated by groundwater table control measures and groundwater extraction. Accumulation during floods partly compensates subsidence.

During the periods that the groundwater table is below the surface, oxidation, compaction and especially ripening of the mostly clayey soil can take place. This is the case for most crops year-round. For soils with a high organic matter content in the Sacramento-San Joaquin delta (Northern California), different crops could not be related to differences in subsidence rates (Rojstaczer & Deverel, 1995). These different crops all have groundwater levels below the surface. However, rice is grown under inundated conditions (Bouman, 2009), inhibiting oxidation, ripening and compaction. Therefore, rice might have lower subsidence rates than other crops. The rice cropping phenology (the timing and number of crops a year) and related periods of inundation and dry land determine the period during which oxidation and ripening take place.

The subsidence rate of (especially irrigated) crops is expected to be dominated by groundwater extraction. The strong impact of groundwater extraction for irrigation on subsidence rates is for example observed in the Quetta Valley in western Pakistan. Here, amplification of groundwater extraction related to the expansion of agriculture resulted in a strong increase in subsidence rates (Khan et al., 2013). However, environmental conditions in this area are very different from the VMD and the crops grown do not contain rice or other crops which require inundation. In the VMD, especially areas with dry-season rice crops require irrigation (Nhan et al., 2007). Rice requires most irrigation water (0.8 l/s/ha), followed by upland crops (0.6 l/s/ha) and perennial crops (0.4 l/s/ha) (Nesbitt, 2005). Irrigation water can be derived from rivers and/or groundwater. The water availability, quality and timing of water supplied via the canal network generally deteriorate downstream (Nhan et al., 2007). During the dry season, river water shortages may occur (Nesbitt, 2005), which could result in more groundwater extraction. Besides, more irrigation water is needed in upstream provinces as consequence of deep groundwater-table levels (Nhan et al., 2007). This irrigation water for rice is mainly supplied by pumping (Nhan et al., 2007). Hence, it is expected that subsidence due to groundwater extraction for irrigation increases with the distance to the rivers, and is large in the upstream provinces as well as in coastal areas with surface water salinization problems. This is in contrast to the statement of Nesbitt (2005) that only the areas between and along the Bassac and Mekong rivers in the VMD use groundwater for agricultural production. Another effect which plays a role is that during the wet season, the river flood water recharges part of the shallow aquifers. This can partly prevent subsidence related to groundwater extraction (Liu et al., 2010; Wen, 1995).

In sum, many aspects play a role in the proportion of the subsidence rate which is related to groundwater extraction for irrigation. Assuming that the amount of irrigation water needed is the best indication of the subsidence rate for agricultural areas, rice cropping systems with a dry-season crop are expected to have largest subsidence rates. This is followed by other rice cropping systems and non-rice crops.

Aquaculture

In aquaculture areas, oxidation, ripening and compaction can only occur when aquaculture ponds are drained to be cleaned. Local subsidence due to groundwater extraction will be dominant, as fresh pumping water can be used to dilute the salty sea water to grow brackish water species such as shrimps (Higgins et al., 2013). Strong local subsidence up to 25 cm/yr is observed for aquaculture ponds in the Yellow River delta (China) with similar subsurface composition (Higgins et al., 2013). These subsidence rates are equally high as in cities (Higgins et al., 2013).

Urban areas

Urban areas often experience high subsidence rates. A main driver is the heavy anthropogenic loading by all buildings and infrastructural constructions. In the Beijing plain (Chen et al., 2014) and in Shanghai (Yan et al., 2002), a positive correlation between construction density and land subsidence is found, which probably also applies to the VMD. Besides, groundwater extraction in or bordering urban areas is an important driver (Minderhoud et al., 2017). Groundwater is extracted in the urban areas of the VMD for drinking water (Buschmann et al., 2008), industry and in rural or open urban areas for washing, bathing and watering vegetables (Tran et al., 2010).

Forests and orchards

The subsidence rate for forests and orchards probably differs per subclass. At first, a natural mangrove forest is not expected to subside, but rather to rise with the sea level due to net accumulation of clastic sediment and organic material. This is in agreement with the net accumulation rates of 4 to 7 cm/yr in the VMD (Lovelock et al., 2015).

Freshwater forests with mainly melaleuca trees and forestry areas are expected to show only slight subsidence rates. The ground water level is expected to be mainly below the surface without human intervention, creating potential for oxidation, ripening and compaction. These processes may be compensated by accumulation of organic matter.

Orchards are mainly found close to the river branches in the VMD, which is probably related to the slightly higher elevation and coarser sediment at and close to the levees. Orchard areas also seem to have a relatively dense but scattered human population. For this type of LU, it is difficult to say which driver of subsidence will dominate. Anthropogenic as well as natural loading probably differ strongly over space and the contribution of oxidation and ripening depends on the presence of clay and organic matter in the subsurface. The groundwater usage will depend on the irrigation needs of the specific trees and the type of irrigation. Some fruit trees are occasionally irrigated using a permanently flooded ditch and dyke system, but also irrigation by canal and ditches, by pump and hose or via trickle irrigation techniques can be applied (Nesbitt, 2005). Deep-rooted trees can lower the water table and extract water from the shallow aquifer. This increases the need for irrigation – potentially using deeper groundwater – for surrounding shallow-rooted crops (Nesbitt, 2005).

Wasteland/marshes

Wasteland and/or marshes which were omnipresent in the past are expected to have relatively low or even negative subsidence rates. Groundwater extraction, antropogenic loading and manually lowering of the groundwater level do not play an important role. Some peat consolidation could result in subsidence, while peat oxidation is expected to be limited because of the wet conditions. Accumulation of peat and clastic river sediment supplied during the yearly floods might compensate or even exceed the subsidence rate.

Relative differences in subsidence rate per land-use class

The previous five paragraphs showed how different LU types can be coupled to subsidence. The main drivers of subsidence and the resulting subsidence rate vary between the LU types. Taking all these relations together, it is expected that urban areas will subside most rapidly due to strong loading in combination with groundwater extraction. This LU type is probably followed by other types which extract much groundwater: areas with an irrigated/dry-season rice crop and aquaculture. The other agricultural classes may have slightly lower subsidence rates as they require less irrigation water. Orchards probably require even less pumping water and subside even slower. Forests with fresh water trees such as melaleuca and natural wasteland/marsh are expected to experience very limited subsidence or slight accumulation. At last, mangrove is expected to aggrade.

Time-dependent effects in subsidence rates in relation to land use

As explained in section 2.2., subsidence rates can change over time in two ways: they can gradually change over time ('time effect'), and they can experience time-lag effects. This should be taken into account when relating subsidence rates to LU, assuming that different types of LU indeed result in different subsidence rates related to different drivers and processes.

Considering the time effects, the subsidence rate may decrease over time for a certain LU type which is already present for a long time, if 1) the system could slowly reach a hydrodynamic equilibrium, 2) organic matter is being depleted, or 3) the subsidence potential decreases as the sediment gets more and more compacted. On the other hand, the subsidence rate related to continued and especially intensified groundwater extraction can increase over time while the same LU class is present. This is, because the system gets more and more out of equilibrium. These time effects differ between LU classes due to differences in drivers and processes underlying the relation between LU and land subsidence. Besides, the speed of the change in subsidence rate will differ between LU changes. For example, the change in subsidence rates is expected to be quick if the subsidence rate of a certain LU class is dominated by oxidation as consequence of groundwater table lowering, or consolidation and compaction due to loading. As a consequence of all these time effects, the time span during which a specific present and previous LU type has already been present can influence the land-subsidence rate.

Considering the time-lag effects, especially the relation of the LU classes with groundwater extraction should be taken into account. In case of groundwater extraction, the hydrological system needs time to change the situation in the clayey aquitards. Such delayed effects imply that the past LU should be coupled with the subsidence rates rather than the contemporary LU.

Altogether, the relation between land subsidence and LU is complex. At first, the link between LU and land subsidence via the dominant drivers is not yet completely understood. Nevertheless, the current knowledge gives a first indication of the relative differences in subsidence rates between different LU types. Secondly, ascribing a certain subsidence rate over a period to the respective LU (change) class in the same period is only justified if time-dependent effects have a minor impact on the subsidence rate. Otherwise, the subsidence rates should be coupled to LU history. These time-dependent effects can also differ between LU types, because they depend on the dominant subsidence drivers and processes.

3. Methodology and data

3.1. Overview

This chapter is divided in six parts. First, a background on the study area is given. This is followed by an overview of all data used in this study. Subsequently, the random forest algorithm is introduced, which will be used in the methods to fulfill the main aims (Figure 7). These methods are elaborated in the last three parts.

In order to couple the subsidence rates to LU and LU change, a continuous, consistent LU map series for the VMD over the last decades was needed. As indicated in the literature review, no single study or combination of studies exists which provides such a series. Therefore, the first step was to create a new LU maps set using optical remote sensing products (Figure 7). The LU in the VMD has been classified based on an optical remote sensing image of 1988, 1996, 2006 and 2009. The images were classified using an object-based approach and the machine-learning algorithm ‘random forest’.

The second step considered the relation between subsidence rates and LU. The land subsidence per LU type was quantified by calculating standard statistics based on the InSAR-based subsidence-rates dataset for each LU class that did not change from 1988 up until 2009. The impact of past LU changes on the subsidence rates has been studied by comparing the subsidence rates of areas with a constant LU over time with the subsidence rate of areas where a certain LU change took place.

The third and last step was to predict the subsidence rates for the period 2006-2010 based on LU and LU history from 1988 up to 2009 (Figure 7). Hereto, a random forest regression has been used. The quality of all predictions was tested by a validation subset of the InSAR-based subsidence rates. The results of using all LU change maps together to predict the subsidence rates has been compared with the results of a prediction based on each LU change map separately. This was used to determine which period predicts the subsidence rates best and whether using multiple LU periods improves the prediction.

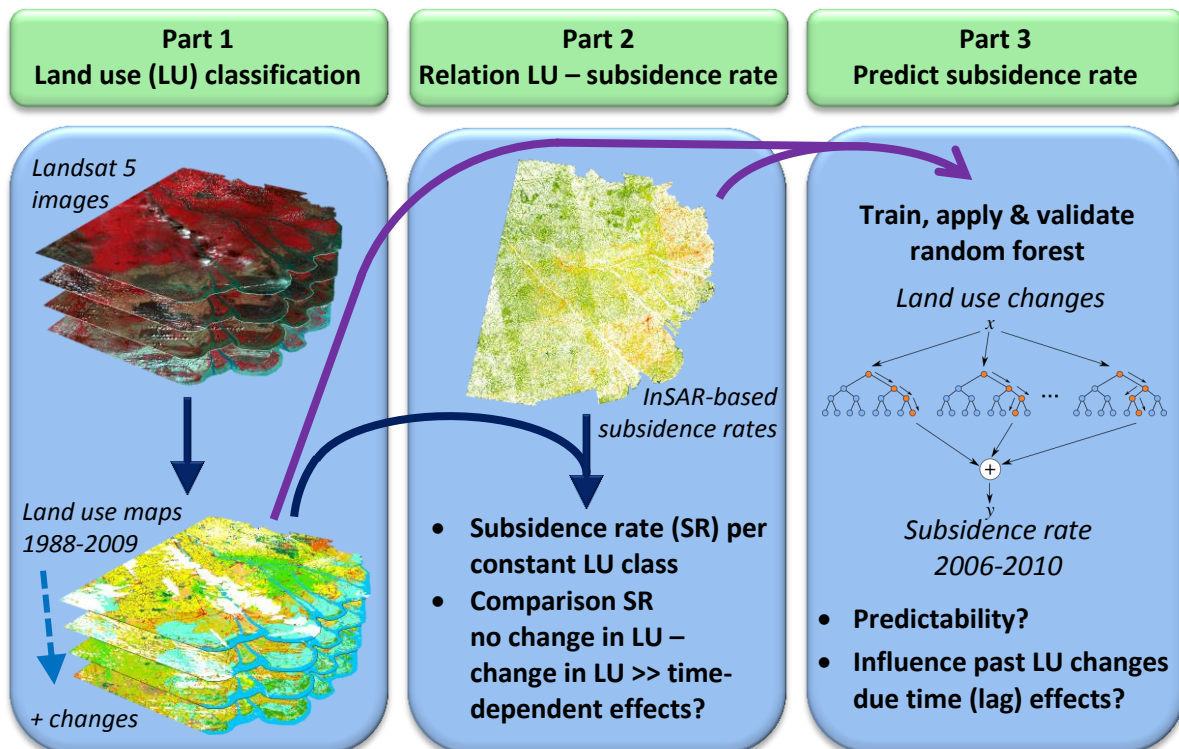


Figure 7 Overview of the methodology.

3.2. Study area

The Vietnamese Mekong Delta is located in the south of Vietnam, Southeast Asia (Figure 8). The VMD had 17.5 million inhabitants in 2014 and covers about 40 000 km², both comparable to the Netherlands. The delta largely lies below 1 m above mean sea level (Coumou, 2016). The Mekong River splits in multiple branches in the VMD (Tri, 2012). The largest city of Vietnam – Ho Chi Minh City – is located just northeast of the VMD. Can Tho is the largest city in the delta.

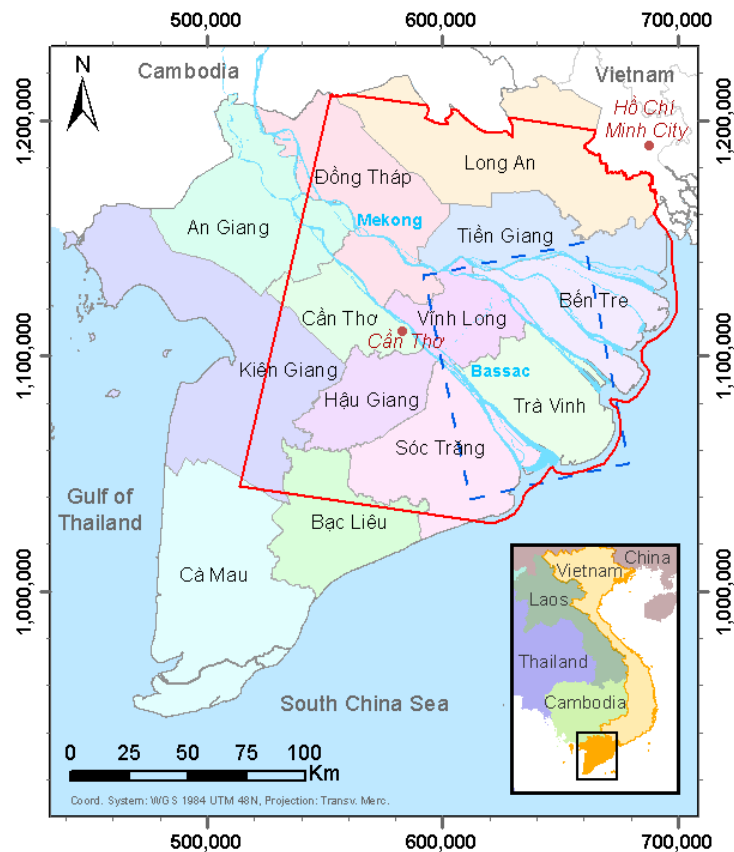


Figure 8 Overview map of the Vietnamese Mekong Delta (VMD). The red line indicates the extent of the land use maps which were classified, the blue dashed line indicates the extent of the ‘Tra Vinh InSAR-tile’. The 13 black names are province names.

The climate is moist tropical with a short dry season from January to March and a rainy season from April-May to November-December (Tong et al., 2004). Especially the Plain of Reeds (including Dong Thap, Tien Giang and Long An) and the Long Xuyen Quadrangle (An Giang and the northern part of Kien Giang) are flooded during the wet season for about 6 months (Tri, 2012).

The VMD is called the ‘rice bowl’, because its large rice cropping area makes a major contribution to the global rice production (Renaud & Kuenzer, 2012; Tri, 2012). In order to increase the yields, many canals have been dredged and dikes and sluices have been built in the delta (Renaud & Kuenzer, 2012). Currently, over 10,000 km of irrigation canals support the water distribution and transportation in the VMD (Son et al., 2014). Next to agriculture, aquaculture is of increasing importance along the coast of the VMD (Binh et al., 2005). Furthermore, the production of fruits and vegetables is an important source of income (Renaud & Kuenzer, 2012; Warner et al., 2009).

3.3. Data

Satellite imagery for land-use classification

Images of the Landsat Thematic Mapper (TM) sensor aboard the satellite Landsat 5 were used for LU classification, because 1) one tile covers a large part of the VMD, 2) the images of the same sensor are available with a high 16-days repeat interval over a long period (1984-2013), 3) the images have a wide range of available spectral bands (Table 3), 4) the ground resolution of the images is sufficiently high to classify LU (Table 3) and 5) the images are freely available. Images from other satellites are not used to limit differences between the LU maps due to differences in extent, ground resolution and available spectral bands.

Four Landsat 5 TM images have been selected (Table 2). The selection is based on the acquisition date and limited cloud cover. The cloud conditions are best during the dry season. Besides, the LU during this period is expected to be most relevant for subsidence. This is because in this period it is visible which agriculture areas apply dry-season irrigation, and this generally means that more crops are grown per year. Hence, each LU map is based on a single satellite image taken during the dry season. Images from about February were preferred, because the various dry-season rice varieties have their growth peak in about this month based on the rice cropping schemes (e.g. Figure 21 in Appendix 4). Since the reference InSAR subsidence rates correspond to the period 2006 up to 2010, one LU map has been created for the beginning of this period, and one for the end. Additionally, two maps have been created to reflect the main trends in LU change over the last decades. This is also corresponds to the period with a strong increase in subsidence rates (Minderhoud et al., 2017). Therefore, the images in Table 2 were selected.

Table 2 Landsat 5 TM surface reflectance images used (WRS path 134, row 053). The images were selected via the online LandsatLook Viewer (USGS, 2016b) and the Earth Explorer application (USGS, 2016c) and downloaded with a bulk order (USGS, 2010).

Date (yyyy-mm-dd)	Julian day	Landsat scene identifier
1988-01-30	030	LT51250531988030
1996-02-21	052	LT51250531996052
2006-03-04	063	LT51250532006063
2009-02-08	039	LT51250532009039

Each image includes the surface reflectance of seven spectral bands (Table 3) in digital numbers and three spectral indices based on the surface reflectance bands: the Normalized Difference Vegetation Index (NDVI), the Enhanced Vegetation Index (EVI) and the Normalized Difference Moisture Index (NDMI) (USGS, 2017). The preprocessed surface reflectance bands were generated from the Landsat Ecosystem Disturbance Adaptive Processing System (LEDAPS) (USGS, 2012).

Table 3 Spectral band designations Landsat 5 TM (USGS, 2016a).

Spectral band	Wavelength (μm)	Resolution (m)
1 - Blue	0.45-0.52	30
2 - Green	0.52-0.60	30
3 - Red	0.63-0.69	30
4 - Near Infrared (NIR)	0.76-0.90	30
5 - Shortwave Infrared (SWIR) 1	1.55-1.75	30
6 - Thermal Infrared (TIR)	10.40-12.50	120, resampled to 30
7 - Shortwave Infrared (SWIR) 2	2.08-2.35	30

Supporting data for land-use classification

LU maps as well as statistics were used as reference for and validation of the new LU maps. The existing wide variety of LU maps of (parts of) the VMD are summarized in Appendix 1. Provincial LU statistics of the VMD provided by the general statistics office of Vietnam are freely available at gso.gov.vn. These statistics are aggregations of largely sampled data at the district, commune or even lower level. This induces a certain error which limits the accuracy at provincial level (Bouvet & Le Toan, 2011). The following statistics are used:

- 'Area of water surface for the aquaculture by province' Year: 1996, 2006, 2009
- 'Planted area of spring paddy by province' Year: 1996, 2006, 2009
- 'Area of forest as of 31 December by province' Year: 2009

Besides, shapefiles of the ocean ('Ocean area around the Mekong Delta') and of the main river branches ('Main Mekong River Course Lower Mekong Basin') have been used in the LU classification (WISDOM, 2014).

InSAR subsidence data

InSAR (Interferometric Synthetic Aperture Radar) based subsidence rates of the VMD for the period 2006-2010 have been used in this study (Figure 9) (provided by Erban et al., 2014). This extensive raster dataset with a ground resolution of approximately 57x57 m contains the firstly available measured subsidence rates in the VMD (Erban et al., 2013). The subsidence rates are given up to a tenth mm/yr, while the estimated error is 0.5 to 1.0 cm/yr (Erban et al., 2014). Details on this dataset are given in Erban et al. (2014, 2013) and the supplementary materials of these papers.

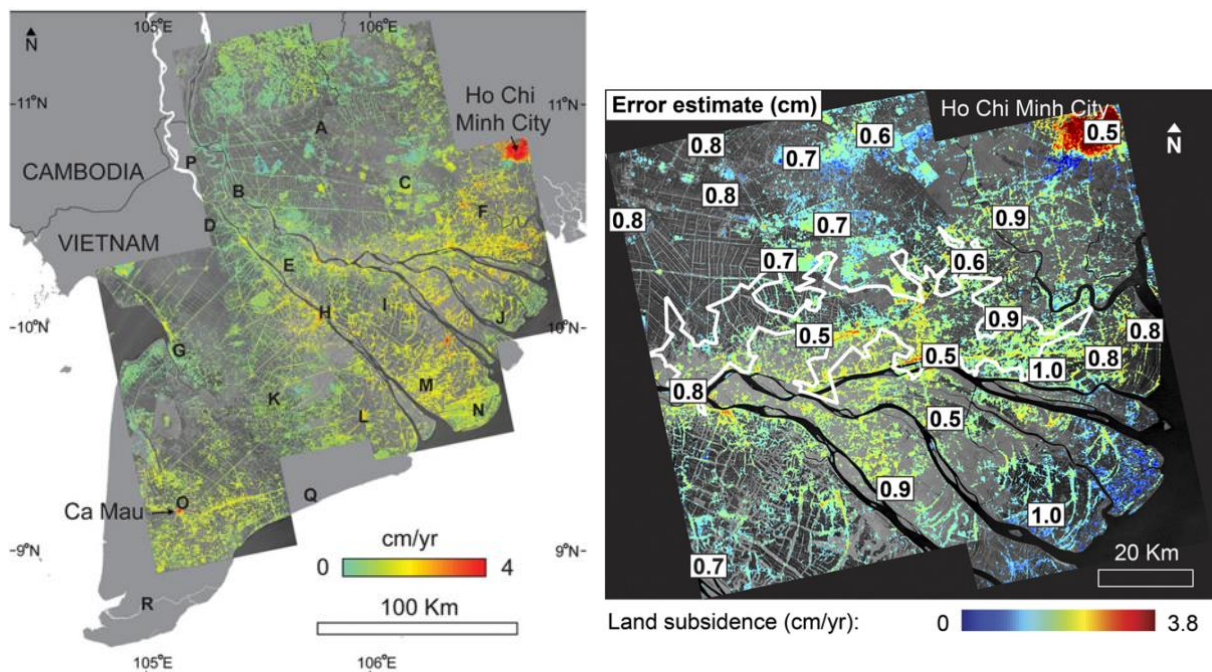


Figure 9 Left: Annual averaged InSAR-based land-subsidence rates for the period 2006-2010 (adopted from Erban et al. (2014)). Right: Error estimates for InSAR stacks superimposed on land subsidence map (adopted from supporting information of Erban et al. (2013)). The label values are the standard deviation of the stacked interferometric phase in 400-pixel windows.

Erban et al. (2014, 2013) used 121 scenes from 2007 to 2010 of the PALSAR instrument aboard the ALOS-1. Herewith, they created 5 to 12 one-year interferograms for the nine tiles covering the VMD. Correction for topology and orbital ramps was applied. Atmospheric errors were reduced by averaging the interferograms over the entire period (stacking) and by spatial averaging (multi-looking). These corrected images were converted to subsidence rates, assuming that the land-subsidence rates did not vary within the period 2007-2010. The rates are relative to a coherent reference area with limited groundwater extraction near the Cambodian border. Next, all pixels with an average correlation ≤ 0.15 within a 25-pixels window were discarded.

The spatio-temporal variability in surface scattering properties can result in errors in the range 0.5 – 1.0 cm/yr (Erban et al., 2014). Highly urbanized areas have the smallest errors (Figure 9). Flooding and the presence of wet rice paddies impede reliable InSAR results. However, the associated extensive network of levees and irrigation canals provided stable surfaces for relatively reliable InSAR subsidence rates. Due to the generally higher elevation of this network, the subsidence rates will not be affected by accumulation (Erban et al., 2014). Besides, human modifications may locally affect the subsidence rate, but at regional scale this effect will be insignificant. A source of inaccuracy which is not mentioned by Erban et al. (2014) are the relatively large errors in the SRTM digital elevation model (DEM) (Coumou, 2016), while this DEM is used for topographic correction of the images.

We received the nine subsidence rate tiles and corresponding radar amplitude tiles. We georectified the subsidence rate images using the amplitude tiles as spatial reference. Subsequently, the images were mosaicked. Overlapping tile parts show differences in subsidence rates of several millimeters up to a few centimeters in extreme cases. Most offsets are within the error range.

3.4. The random forest algorithm

In this study, the random forest (RF) algorithm has been used to classify the LU as well as to predict the subsidence rates based on LU changes. A RF is a data-mining or machine-learning technique that uses an ensemble of decision trees to predict Y using multiple X -variables (Breiman & Cutler, 2003; Breiman, 2001). Random forests can be used to perform a classification (thematic output), or a regression (continuous output). The algorithm is called 'forest', because it is an ensemble of decision trees (Figure 10). Decision trees are relatively robust, insensitive to noisy input data, and make no assumptions about the frequency distribution of training samples (Funkenberg et al., 2014). A major advantage of using a RF is the correction for the potential overfitting of a single decision tree (Breiman, 2001). For LU classification, the RF algorithm is not often used, even though it can give high classification accuracies (Gislason et al., 2006; Rodriguez-Galiano et al., 2012). The application to land-subsidence prediction is new.

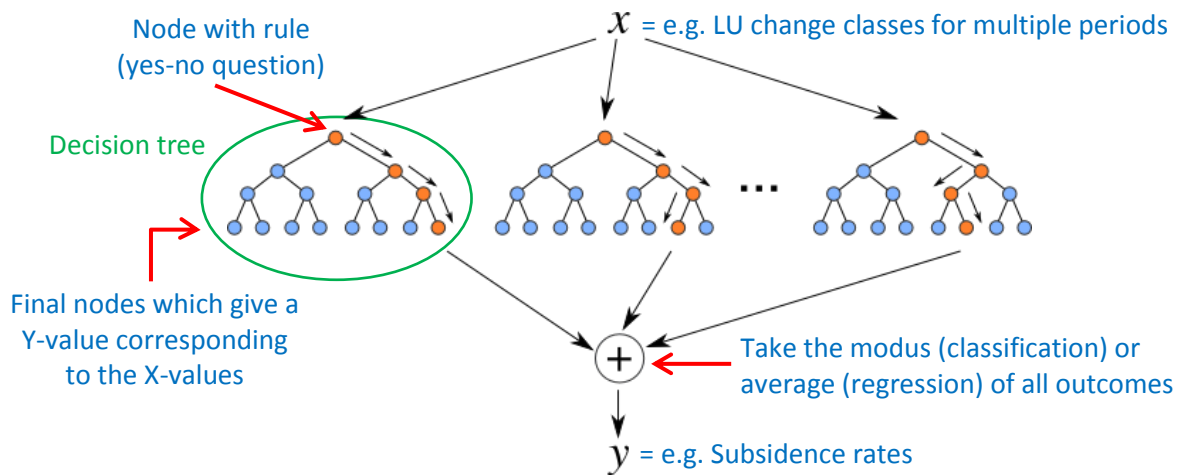


Figure 10 Simplified example of a random forest. Modified after kgpdag.wordpress.com.

Using the RF algorithm requires two steps. At first, the RF has to be created using a training dataset which contains values for the x -variables and the corresponding y -values. Each decision tree is automatically built using a random subset of the training data (hence, *random* forest). The training data which is not used for a decision tree are called the out-of-bag (OOB) samples. The decision tree is built by repeatedly splitting the training data based on the best threshold of one of the X -variables. The best splitting rule at each decision tree node is determined by the algorithm using a random sample of the X -variables (Breiman & Cutler, 2003; Liaw & Wiener, 2002). In case of a classification, the best split is based on the largest decrease in the Gini impurity criterion; in case of regression, by minimizing the sum of the squared error of the y -values in both branches. The splitting continues until the variation of the Y -values at a node is small enough: the (average of the) Y -value is assigned to this final node.

The second step is to apply the RF. All non-training data points for which the X -values are known are put into all trees (Breiman & Cutler, 2003). They follow a path determined by their X -values and the rules. Each final node they end up in gives a y -value. The y -value which is assigned to each point is the modus (in case of classification) or the average (in case of regression) of all the outcomes of the trees.

The RF algorithm gives an indication of its error using the out-of-bag (OOB) samples (Breiman & Cutler, 2003). These samples are put into all trees. Each outcome is compared with the known Y-value, giving an error rate (classification) or mean squared error (MSE) (regression) per tree. The average error rate is an estimate of the overall error rate. Besides, in case of classification, the OOB samples are used to determine the classification accuracy per class and create a corresponding confusion matrix.

The OOB samples are also used to determine the importance of the X-variables (Breiman & Cutler, 2003; Liaw & Wiener, 2002). The values of one X-variable in the OOB samples is randomly permuted. Then, the OOB samples are put into the tree again. Subsequently, the importance of a X-variable is determined in two ways. In the first case, the increase in the prediction error of all OOB-samples averaged over all trees is used: the decrease in accuracy for classification and the decrease in MSE for regression. Secondly, the total decrease in node impurities from splitting on the variable, averaged over all trees, is used. The node impurity is measured by the Gini index for classification and by the residual sum of squares for regression.

For further explanation on the random forest algorithm, see Breiman (2001), Breiman and Cutler (2003), Liaw and Wiener (2002) and the help function in the R randomForest package.

3.5. Land-use classification and change detection

A new, consistent LU map time series has been created by classifying the satellite images of 1988, 1996, 2006 and 2009. The main steps for the pre-processing, classification and post-processing are shown in Figure 11 and will be elaborated in the next subsections.

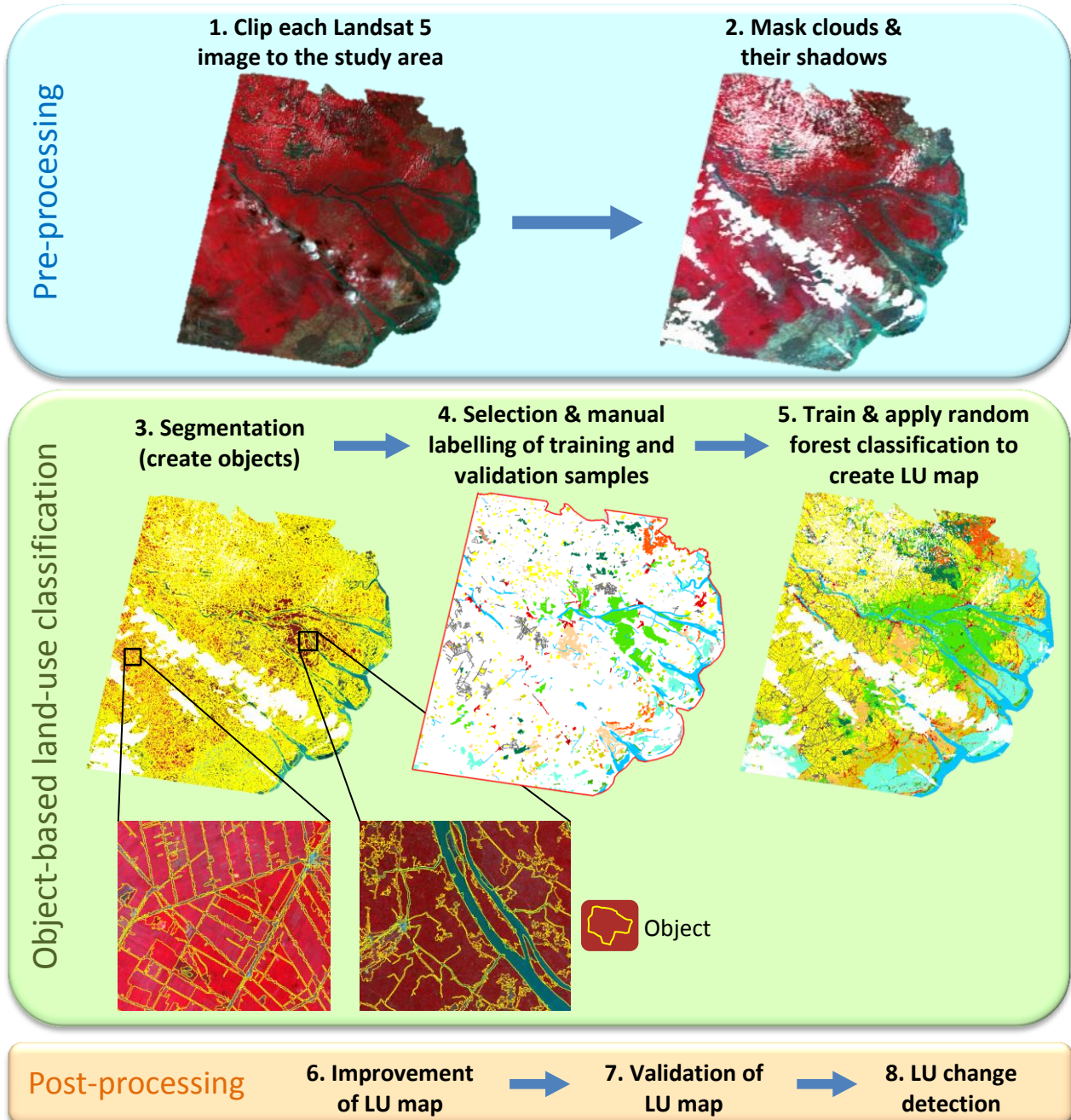


Figure 11 Overview of all steps to create a land use (LU) map from a Landsat 5 satellite image, including pre- and post-processing steps. Step 1: the satellite image was reduced to the extent of the study area (Figure 8). Step 2: the clouds and their shadows were classified and removed from the image. Step 3: the pixels were grouped into objects based on similarity in spectral characteristics; the yellow lines represent object borders. These objects were subsequently classified: an object-based classification was performed. Step 4: a largely random selection of the objects was manually labelled/classified to be used as training and validation samples; the colored lines represent the samples of different LU classes. Step 5: the random forest (RF) classification algorithm was trained with the training samples: the object spectral and spatial characteristics were used as input variables. The RF is applied to all objects to get a LU map. Step 6: the LU map is improved based on the other classified LU maps and by merging some classes. Step 7: the LU map was validated with the validation samples, and by comparison of provincial statistics with statistics of the general statistics office of Vietnam. Step 8: LU changes were detected and mapped by comparing the LU map with the other classified LU maps. RGB = NIR-Red-Green in all satellite images (false color).

Object-based image classification

An object-based image-analysis (OBIA) approach has been used to classify LU. At first, neighboring pixels in an image were grouped together into objects or segments. In this study, this segmentation was based on similar spectral characteristics of the pixels (see Appendix 2 for more information on segmentation). Areas with little spectral variation result in larger segments. Subsequently, the objects were classified based on the characteristics of the objects. The large advantage of this method over pixel-based classification is that not only spectral, but also spatial characteristics can be used for the classification. For example, characteristics related to the shape of the objects, the object size, the orientation of the object and the difference in a spectral feature with neighboring objects can be used. For the distinction of LU rather than land cover only, this information is expected to be essential for the classification success. For example, aquaculture and a river both have the spectral characteristics of water, but the shape of the objects related to these classes makes distinction possible. Besides, the object-based classification results are generally less speckled than pixel-based classification results. At last, an object-based approach is expected to result in a LU map which represents the dominant LU class in an area, which is desired for the coupling with land subsidence. A minor disadvantage of an object-based approach is that it is almost inevitable that some segments include multiple LU classes, herewith reducing the accuracy. Moreover, the boundary of segments is generally slightly different for different years, which can result in undesired sliver change classes.

Step 1 & 2. Clip and mask clouds and their shadows

The Landsat 5 TM surface reflectance images were ready to use, except for their slightly different extent. Besides, they still include clouds and their shadows. The images were clipped to the same study area extent (Figure 8). Subsequently, the clouds and their shadows have been removed from each image before LU classification, because especially the cloud shadows were easily confused with LU classes of interest, herewith lowering the classification accuracy.

The clouds were classified using object-based image analysis (see Appendix 2 for segmentation settings). A manually built decision tree has been used for classification instead of a random forest classification, because this makes it possible to 1) have more direct control on the classification, 2) classify at different segmentation levels at the same time, and 3) use features based on the spatial relation to already classified segments (e.g. relative border to the class 'cloud'). The rules corresponding to each node in the manually built decision tree are based on 1) the high reflection of clouds in (especially) the optical bands compared to the land surface, 2) the shape and size of the clouds, and 3) the low cloud temperature. After classification, a 60 m buffer around the clouds was applied. The buffered clouds were manually shifted to the cloud shadows. Some clouds and respective shadows which were missed were manually added; misclassified clouds were removed from the mask. The final shapefile of the clouds and cloud shadows together has been used to set these areas to no data in each corresponding image.

Step 3. Segmentation: create objects

Next, a segmentation is applied to each image separately: objects are created. The optimal segmentation settings for the LU classes (see Appendix 2) were determined by trial and error such that each object represented a continuous area of a single land-use class which is as large as possible. For example, an object comprises an individual field or group of fields with the same crop or a (large part of a) road, river or channel. The final segments were exported with the values for 55 selected spectral and spatial features (specified in Appendix 5) as shapefile and text file. Examples of features are the mean of red band, roundness, length divided by width and distance to ocean. The selection of useful features is based on experience with object-based classification.

Step 4. Select land-use classes and create a training and validation dataset

After segmentation, a segment dataset was created to train and validate the random forest. Hereto, at first the LU classes were chosen for the classification. These LU classes should:

- 1) be all-embracing and representative for the entire delta at all time steps under consideration;
- 2) be able to be recognized in the Landsat 5 TM images;
- 3) have an assumed link to land subsidence.

A selection of the wide variety of LU classes used in existing LU maps (Appendix 1) was used as a first set of classes. This set was subsequently tested and improved by iteratively classifying the image with a set, analyzing the accuracy and confusions between LU classes and adjusting the set. The final LU classes which were used for all classifications are shown in Table 4.

Table 4 Land-use (LU) classes used for the classification. See main text and Appendix 4 for reasoning behind the classes, and Appendix 3 for LU type codes used in the digital version of the LU maps.

LU group	LU type/subclass	Acronym
Aquaculture	Aquaculture	Aqua
Agriculture ⁴	Dry-season crop – mainly rice	Dry-S Rice
	Partly dry-season crop – mainly rice ¹	P Dry-S Rice
	Harvested dry-season crop – mainly rice ²	H Dry-S Rice
	Bare field in dry season	Bare Field
	Mixed crops – non-rice ³	Mix No Rice
Forest	Mangrove	Mangr
	Melaleuca forest ⁵	Mel For
	Orchard	Orch
Urban area	Urban dense	Urb D
	Urban open	Urb O
	Urban linear features (dikes, roads with buildings and gardens)	Urb Line
Water ⁶	Water body (river/sea)	Water
	Water: small channels	Water Ch
Other	Wasteland/marsh	Waste
	Cloud remnants ⁷	Cloud remn

¹ The classification aims at classifying LU at delta scale and therefore, relatively small scale inter-field alternations between the ‘dry-season crop’ and ‘bare field in dry season’ class are taken together as one class: ‘partly dry-season crop – mainly rice’.

² ‘Harvested dry-season crop – mainly rice’ is only used during the classification: it is taken together with ‘Dry-season crop – mainly rice’ in the final LU maps and LU-change maps and analyses. The dry-season crop accuracy is improved by separately classifying these classes due to their different spectral characteristics.

³ Mixed crops – non-rice’ is roughly similar to ‘upland crops’ in other LU studies.

⁴ Existing LU maps subdivide agriculture generally based on the type and number of crops per year. In this case, the number of crops cannot directly be determined as the classification was based on a single, dry-season image per year. Though, combining the classifications with rice crop phenology patterns (e.g. Figure 21 in Appendix 4) gives indirect information: ‘dry-season crop – mainly rice’ probably has 2 or 3 rice crops a year and ‘bare field in dry season’ probably 1 or 2 in the rainy season only. The number of crops for non-rice fields in the dry season (‘mixed crops – non-rice’) is more difficult to deduce.

⁵ Based on other LU maps, ‘Melaleuca forest’ is dominated by melaleuca trees, but other tree species may be present.

⁶ The water subclasses are only used during the classification: they are taken together in the final LU maps and LU-change maps and analyses. The water class accuracy is improved by separately classifying the subclasses due to their different spatial characteristics.

⁷ Some small clouds can be missed by the cloud mask in step 2. These cloud remnants are classified in the LU classification and are subsequently used for a second cloud mask. Hence, they are not shown in the LU and LU-change maps.

Each LU class has its own combination of spectral and spatial characteristics which were used to discriminate between the classes. A quick overview of spectral characteristics of all classes for the 2009 Landsat 5 TM image is shown in Figure 12. The variations within a class are large and some classes cannot easily be separated based on pixel spectral profiles only. Hence, characteristic spatial information on e.g. location and shape of patches of a class was also important to discriminate between the classes. In Appendix 4, both types of characteristics used for classification are elaborated per class.

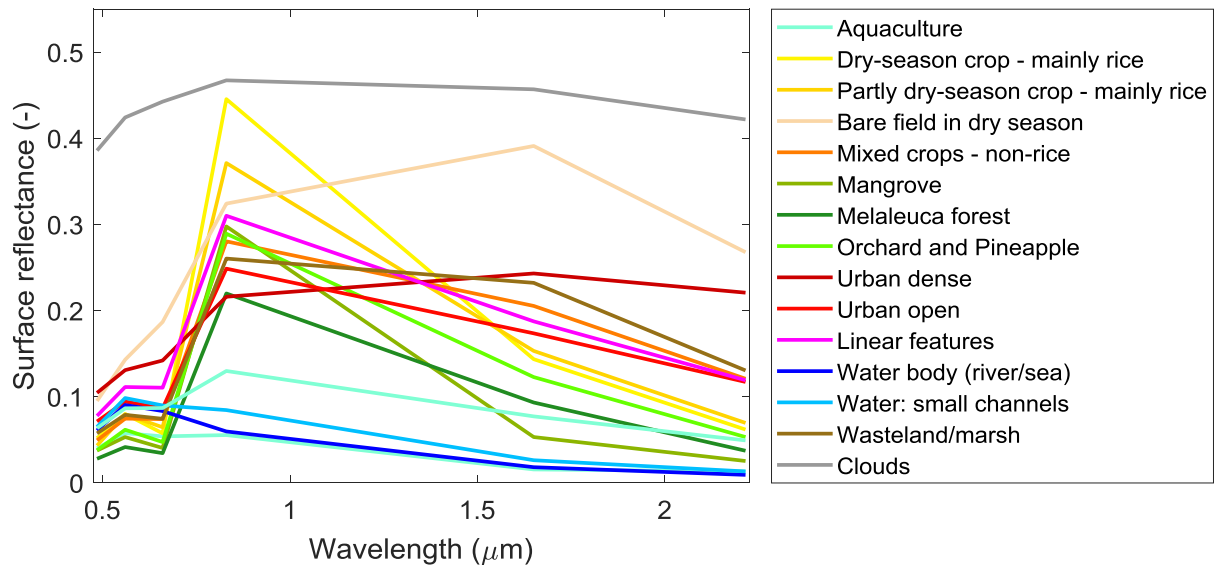


Figure 12 Examples of spectral profiles of all land-use classes used for classification (except for harvested dry-season crop) based on the Landsat 5 TM image of 2009. Profiles are based on single pixels and on the reflectance for the mean wavelength per spectral band.

After the LU classes to be classified were chosen, the training and validation set could be created. Due to differences in reflection for the same classes between the different years, a dataset – and subsequent random forest – was prepared for each year separately. A random selection of 1100 samples – about 4.5% of the total number of segments – was taken from all segments in each image. Some segments contain only one or a few pixels if they were enclosed by no-data areas due to clouds. Their shape is determined by the clouds and the spectral characteristics were often still strongly influenced by the moist air. These unrepresentative segments with an area of 2.25 ha (25 pixels) or less were removed from the selection. The remaining training segments were manually labelled or classified using the existing LU maps in Appendix 1, Google Earth and expert knowledge. A part of the randomly selected segments could not be labelled (Table 5), because the segment did not contain a single dominant LU (segmentation inaccuracy), or the reference data and expert knowledge were insufficient to determine the LU class.

The area of each LU class varies strongly. Therefore, some classes were underrepresented in the random selection of training segments. Hence, segments were added manually to the random selection (Table 5). The resulting final training segments of each year were exported together with their values of the 55 spectral and spatial characteristics as text file.

Table 5 Overview number of sample segments for the random forest land-use (LU) classification per LU class and year. Numbers in parentheses represent the random selection only; outside parentheses include manually added samples. % unknown samples = percentage of samples labelled as unknown out of all random sampled samples, % sample = percentage of total number of samples out of the total number of segments.

LU acronym	Number of sample segments			
	1988	1996	2006	2009
Aqua	67(35)	76 (49)	108 (64)	103 (71)
Ir Rice	145 (122)	272 (267)	194 (176)	332 (330)
P Ir Rice	139 (122)	101 (94)	112 (105)	88 (48)
H Ir Rice	22 (22)	27 (9)	170 (150)	28 (15)
Non Ir Rice	318 (317)	178 (168)	193 (183)	169 (120)
Non Rice	53 (29)	66 (18)	62 (20)	55 (29)
Mangr	70 (26)	76 (37)	42 (14)	40 (14)
Mel For	51 (7)	55 (31)	46 (23)	68 (27)
Orch	148 (140)	183 (172)	95 (65)	81 (54)
Urb D	24 (5)	24 (3)	35 (17)	54 (27)
Urb O	23 (4)	32 (13)	21 (15)	58 (19)
Urb Line	44 (25)	59 (28)	79 (61)	78 (47)
Water	25 (9)	39 (20)	20 (15)	43 (25)
Water Ch	79 (27)	76 (29)	52 (20)	85 (24)
Waste	107 (84)	80 (44)	13 (-)	9 (2)
Cloud remn	31 (3)	34 (2)	75 (22)	192 (34)
Unknown	111	80	56	64
Nr. of random samples	1088	1064	1011	950
% unknown samples	10.2%	7.5%	5.5%	6.7%
Total nr. of samples *	1346	1378	1317	1484
Total nr. of segments	23019	26705	28424	24016
% sample *	5.9%	5.2%	4.6%	6.2%

* *excl. unknown samples*

Step 5. Train and apply random forest classification

For LU classification, the randomForest package v. 4.6-12 in R v 3.3.2 has been used on a Windows 7 64 bit platform. The training dataset was used to train a random forest for each year with the spectral and spatial feature values as input X-variables and the LU classes as output Y-value. For LU classification, the number of trees for each forest was set to 10,000. The number of X-variables used to find the best rule at each tree node was set to the default: the square of the number of variables. A larger (or smaller) number of trees or variables did not result in an increase of the accuracy. Within the random forest algorithm, the training sample size for each tree was set to 2/3 of the samples per LU class without replacement to ensure that each class is represented in each tree and to ensure a proper randomness of the trees. The out-of-bag (OOB) samples can be used for internal accuracy assessment, but a fully independent accuracy assessment is preferred. Therefore, 1/3 of all created samples has been used for this assessment and the other 2/3 has been used for creating the random forest.

Once the random forest had been trained using the training dataset, all segments in the image were classified based on their spectral and spatial characteristics. The output text file with the class codes for each segment has been joined with the shapefile of all segments in order to get a LU map.

Step 6. Improve the land-use maps

After the classification, the number of classes has been reduced to 13: two water classes were merged to one water class, the 'harvested dry-season crop – mainly rice' class was merged with 'dry-season crop – mainly rice' and the cloud remnants were set to no data. Besides, some adjustments were performed on the LU maps based on expert knowledge in order to limit LU changes which were likely to be a result of classification inaccuracies. At first, an area which is used for aquaculture will generally not be used for fresh water crops such as rice later on. Hence, pixels classified as aquaculture in 1988 or 1996 which were covered by a rice class or 'bare field in the wet season' in 2006 or 2009 have been reclassified as 'bare field in the wet season'. Secondly, areas which were classified as water in 1996, but have an identical non-water class in 1988 and 2006, have been classified as that non-water class in 1996. A similar reclassification has been performed for 2006 based on 1996 and 2009.

Step 7. Validate the land-use maps

The accuracy of each LU map has been assessed in three ways: based on the success of the labelling of the training and validation segments, based on the classification of the validation objects and based on the comparison of the classifications with provincial LU statistics of the GSO of Vietnam. The first two validation methods were performed on the classified objects directly after the classification and before the relatively small improvements made in step 6. The third method is applied to the final LU maps, after step 6. Actual ground truth data is very limited and could not be used. The existing LU maps in Appendix 1 could not be used in an independent validation. This is because 1) they were used as reference for the classification or 2) their extent, timing and/or classes used were too different from this study.

The first validation method used the percentage of the randomly selected training and validation samples of which the LU class could successfully be determined. This gives an indication of the highest possible overall accuracy that the classification could reach.

The second validation method used the validation segments to calculate the overall accuracy, Kappa statistic, reliability per LU class (user's accuracy), accuracy per LU class (producer's accuracy) and a confusion matrix, which shows which classes are confused with each other. The Kappa statistic is an index which corrects the accuracy for the chance that a class is correctly classified: a value of 0 indicates that a random classification is as good as the performed classification, while a value of 1 indicates that the classification is perfect (Lillesand et al., 2008). These calculations were performed internally in the training of the random forest algorithm using the OOB samples, and more importantly, after the training phase using the independent validation segments. In both cases, the calculations were based on the number of (in)correctly classified samples. Additionally, the same calculations were performed using the area of the independent validation segments. This gives a more representative accuracy estimate for the individual pixels in the LU maps. Hence, the latter method was used for the results section; the results of the other methods are given in an appendix. Note that all these accuracies did not take the unknown samples into account and hence give an optimistic estimate of the accuracy.

In the third validation method, the area of three LU classes – aquaculture, forest and dry-season rice – has been compared to provincial LU statistics of the general statistics office (GSO) of Vietnam for all years for which GSO statistics are available. The definition of aquaculture is similar in both cases (Socialist Republic of Vietnam General Statistics Office, 2015). The definition of forest of the GSO is less clear and is assumed to correspond to the sum of melaleuca forest and mangrove in this study. The GSO uses another categorization for agriculture, so their class 'spring paddy (Lúa đông xuân)' was compared to the sum of 'dry-season crop – mainly rice', 'partly dry-season crop – mainly rice' and 'harvested dry-season crop – mainly rice'. The accuracy of the GSO statistics and the method used to derive the statistics could not be found in English. Besides, the GSO statistics are

representative for each entire province, while the new LU maps contain no data areas due to clouds and do not cover all provinces entirely. This resulted in smaller areas for the new maps compared to the GSO statistics. Altogether, this comparison only gave an indication of the accuracy of our classification. No hard conclusions could be drawn.

Step 8. Land-use change detection

LU change maps were created using post-classification change detection. A change map has been created for all six combinations of two LU maps. Each pixel in a change map contains a class code in which the first two digits represent the class in the oldest map and the second two digits the youngest map.

3.6. Relation land subsidence and land use

The land subsidence per LU type has been quantified by calculating the average, standard deviation (in case of an approximately normal distribution), median and quartiles (visualized in boxplots) of the land-subsidence rate based on the InSAR-dataset for all areas of each LU class that did not change from 1988 up until 2009. A constant LU ensures that potential delayed responses to past LU changes do not influence the land-subsidence rates. Gradual changes in subsidence rates over time could not be incorporated and hence extrapolation of the rates over time and space should be done with caution. The relative differences in subsidence rates between different LU classes give an indication of the potential change in subsidence rate in case of a certain LU change.

Secondly, the impact of past LU changes on the subsidence rates has been studied by comparing the subsidence rates of areas with a constant LU over time with the subsidence rate of areas where a certain LU change took place. For example, the rate for no change in aquaculture was compared to 1) the rate for areas with mangrove in 1988 and aquaculture in 1996 and 2006/2009 and 2) the rate for areas with mangrove in 1988 and 1996 and aquaculture in 2006/2009. If direct responses of subsidence rates to LU are dominant, those rates are expected to be similar: only the LU in 2006/2009 matters for the subsidence rate. If delayed responses are dominant, the rates will be different. The magnitude of the difference is expected to be related to the difference in the subsidence rate between the two respective LU classes in case of constant LU. The impact of only a selection of all possible LU changes has been studied (Table 6). This selection is based on their relevance and/or occurrence based on the literature review, the accuracy of the LU (change) classes and the magnitude of the difference between the average constant LU subsidence rate of the LU classes under consideration.

Table 6 Land-use changes for which the impact on the subsidence rate was assessed

Category	LU change	
	From ...	To ...
Change to aquaculture	Mangrove	Aquaculture
Urbanization	Dry-season crop - mainly rice	Urban dense
	Bare field in dry season	Urban dense
	Orchard	Urban dense
	Wasteland/marsh	Urban linear features
Change to and intensification of agriculture	Bare field in dry season	Dry-season crop - mainly rice
	Wasteland/marsh	Dry-season crop - mainly rice
	Wasteland/marsh	Bare field in dry season
Change to orchards	Dry-season crop - mainly rice	Orchard
	Wasteland/marsh	Orchard

All analyses between LU and land subsidence were performed for two extents. At first, the mosaic of all tiles of the InSAR-based subsidence rate dataset have been used, because this dataset represents almost the entire VMD. However, the offsets between the tiles could influence the outcome. In order to determine the impact of these offsets on especially relative differences in subsidence rates between LU classes, the same analyses were performed for a single tile too: the tile covering the Tra Vinh province and surroundings ('Tra Vinh tile' hereafter) (Figure 8). This tile does not cover the upstream area which is frequently flooded: accumulation of river sediment is negligible. Besides, the Tra Vinh tile shows clear patterns in land-subsidence rates and covers a part of the study area in which the different LU classes are best represented. However, the tile cannot replace the mosaic, because several LU (change) classes are not present or underrepresented. Moreover, the tile has a

smaller variation in subsidence rates than the mosaic: a standard deviation of 0.61 cm/yr compared to respectively 0.68 cm/yr. The average subsidence rate of the Tra Vinh tile is higher than that of the mosaic: respectively 1.1 cm/yr and 1.4 cm/yr.

In order to perform the calculations, the subsidence raster dataset was converted to a points dataset with a point at the center of each raster cell. The LU class in each year at each point and the respective LU changes were added to the points. Only points for which a LU class is available for each year were used for analysis: the clouds for all years together were masked.

For the analyses, the LU map for 2006 was used as representative for the period 2006-2009. This is at first because the cloud cover in 2009 is very extensive, which resulted in a strong reduction in the number of points which could be used for the analyses. Besides, the areas without cloud cover are still strongly influenced by the high air water content, resulting in a less reliable classification and herewith analyses. Moreover, the LU changes in this period are limited.

For the analysis of the subsidence rate per LU class, and the effect of past LU changes on subsidence rates, the significance of potential differences has been tested in two ways. At first, the boxplot notches were used to test the null hypothesis that two *medians* truly differ at the 0.05 level. The notches around the median represent the 95% confidence interval of the median. If they do not overlap, the null hypothesis can be rejected and the medians differ significantly (Chambers et al., 1983). The advantage of this method is that boxplots do not require the assumption of a certain statistical distribution.

Secondly, if the probability density of the land-subsidence rate for each LU class were approximately normally distributed, a one-way analysis of variance (ANOVA) has been applied to the dataset to statistically determine whether one or more *mean* values of the LU classes differ significantly from the others at the 95% confidence level. If there was a significant difference, multiple comparison using the Tukey-Kramer method (Toothaker, 1993) has been applied to determine which combinations of LU classes are significantly different.

Note that if a difference in subsidence rate between two LU classes is significant, this does not directly mean that the difference is relevant, for example if the difference is a fraction of a mm/yr.

3.7. Prediction of land subsidence based on land use and land-use changes

At last, it has been tested to which extent the LU and LU changes can predict the land-subsidence rate for the period 2006-2010 using a random forest regression. The random forest used different LU change periods as input variables to predict the land-subsidence rates. It was decided to use the LU change map of the periods '88-'96, '88-'06, '96-'06 and '06-'09. Using these separate LU change periods made it possible to get insight in which periods are most important for the subsidence signal. Besides, more different LU histories over the entire period can be analyzed than present in the training dataset. The explicit links between the different periods is lost, but if certain combinations of LU types in different periods are important, this data-mining technique is expected to use this indirectly while looking for the best way to split the data.

Again, the LU map of 2006 has been used as representative for the period 2006-2009. Remember that LU change classes include no-change classes too. Only areas for which the LU was known for all LU maps under consideration were used: all pixels which are clouded in any image were excluded. Moreover, no reliable radar signals return from water surfaces. So, all pixels in areas which were classified as water in 2006 have been excluded: this year is used for the calculation of the InSAR-based land-subsidence rates.

In order to determine whether time-dependent effects are important, the results of using all LU change maps together to predict the subsidence rates have been compared with the results of a prediction based on each LU map separately. To determine whether the predictions for all tiles together do not suffer from the differences between the mosaicked tiles, the results have been compared with the results for the same cases based on the Tra Vinh tile only.

In contrast to the LU classification, the input variables are thematic (LU changes) and the output values are continuous (subsidence rates). Hence, a regression rather than a classification is performed by the random forest (for explanation on differences: see Appendix 6). The randomForest package 4.6-12 in R v. 3.2.2. has been used on a 64 bit Linux platform with 128Gb RAM to provide the required computational power. The random forest has been trained using a random selection of the point dataset with InSAR-based subsidence rates. These points also contain the corresponding LU change classes for the four periods, which were also used to study the relation between land subsidence and LU. Preferably, the ratio between points used for training the random forest versus validation points is $2/3 : 1/3$, but due to limitations in computational power and the randomForest package in R, the proportion of training points was smaller: 45,396 points. This corresponds to 21% of the points of the Tra Vinh tile after classes have been selected (selection explained below). The random forest contains 1000 trees and the ratio training samples to out-of-bag (OOB) samples within the algorithm has been set to $2/3 : 1/3$. The default number of X-variables has been used to determine the best node split; the number of samples divided by three. The internal and external validation samples were selected randomly. The creation of the random forests has been repeated a few times with different random samples (seed of 10, 100, 1000 or 10000) to determine its sensitivity to this selection. The training of a random forest requires multiple X-variables. In case of using a single LU change map for the random forest, each LU change class has been transformed to a separate one-hot encoded X-variable (1 if the sample corresponds to the class, 0 if not).

It is preferred to use all LU classes to create the random forest. Only then the subsidence rate can be predicted for all other points of which the LU changes are known. The random forest algorithm in R is limited to a maximum of 53 classes per X-variable, while a LU change map can contain up to 169 classes. Hence only a selection could be used, which has been based on the LU classification accuracy, the relevance for land subsidence and the relative area covered by the LU change class. For each LU change map, the 53 classes were selected following these steps:

- 1) Merge the LU change classes 'urban open to urban dense', 'urban dense to urban open', 'no change urban open' and 'no change urban dense' to one LU change class 'no change urban' and include this class;
- 2) Exclude the LU change class if one or two of the respective LU classes has a reliability below 50%;
- 3) Exclude the LU change class if the area of confusion between the respective LU classes is larger than 5% of the total area of one (or both) of the respective classes;
- 4) Exclude the LU change class if one or two of the respective LU classes is/are water;
- 5) Exclude the LU change class if one of the respective LU classes is urban dense or urban open;
- 6) Include all no-change classes if they are not yet excluded;
- 7) Add LU change classes with the highest frequencies until the selection contains 53 LU change classes.

After the training phase of the random forest, the subsidence rate has been predicted for the large amount of independent validation points (170,773 for Tra Vinh tile; 1,672,460 points for all tiles). The observed subsidence rates – directly from the InSAR-based dataset – have been compared with the predicted rates according to the goodness-of-fit evaluation recommended by Piñeiro et al. (2008). A linear regression was applied to the observed versus predicted values. The regression equation was compared to the 1:1 line to determine whether there is a bias (intercept $\neq 0$) and whether the predictions are consistent (slope = 1). The relative contribution of different 'errors' has been quantitatively determined by decomposing the variation of the observed values (*obs*) which is not explained with the predictions (*pre*) (the squared sum of the prediction error) using Thiel's partial inequality coefficients (Paruelo et al., 1998):

$$U_{bias} + U_{slope} + U_{error} = 1$$

in which U_{bias} is the proportion associated with mean differences between observed and predicted values, a bias:

$$U_{bias} = \frac{n * (\overline{obs} - \overline{pre})^2}{\sum_n (obs_i - pre_i)^2}$$

in which \overline{obs} and \overline{pre} are respectively the average of the observed and predicted values.

U_{slope} is the proportion associated with the deviation of the slope (β) of the fitted model from the 1:1 line – the degree consistency – with n is the number of samples:

$$U_{slope} = \frac{(\beta - 1)^2 * \sum_n (pre_i - \overline{pre})^2}{\sum_n (obs_i - pre_i)^2}$$

U_{error} is the proportion associated with the unexplained variance – the degree of scatter – for which *est* are the values estimated from the fitted linear regression line:

$$U_{error} = \frac{\sum_n (est_i - obs_i)^2}{\sum_n (obs_i - pre_i)^2}$$

Additionally, the root mean squared deviation (RMSD) has been calculated: the mean deviation of predicted values with respect to the observed ones (in cm/yr). At last, the coefficient of determination (r^2) has been used as a measure of the proportion of variance in observed values explained by the predicted values. r^2 is not only calculated for the independent validation dataset, but also for the internal random forest OOB validation samples to compare the internal and external validation.

In the cases that all LU change maps were used, the two random forest importance measures (see section 3.4) have been used to determine whether one of the LU change maps is structurally more important to create the random forest than the others. This could indicate that the LU changes of the respective period have the strongest relation to the subsidence rates. In turn, this gives information on the importance of time effects and time-lag effects.

4. Results

4.1. Land use and land-use changes

Land-use changes over the period 1988-2009

The classified LU maps for 1988, 1996, 2006 and 2009 are shown in Figure 14 (all together) and Appendix 6 (large format). Statistics about the area of each LU class for each year are shown in a graph (Figure 13) and in a table (Appendix 7). Appendix 9 shows how the LU changed between the different moments for which the LU has been mapped. This includes no-changes.

For all years, about half of the area of the delta is used for agriculture. Within this main class, there is a clear shift between subclasses. Especially between 1988 and 1996, the area of 'dry-season crop – mainly rice' (hereafter: dry-season rice) expanded significantly at the expense of partly dry-season rice and bare field in the dry season. The decrease in bare fields in the dry season continued until 2009. Also the wasteland/marsh area in the north is converted to dry-season rice. These changes denote an intensification of the agriculture sector: assuming that all agricultural classes at least include a wet season crop, the number of crops per year increases. The area of mixed, non-rice crops is minor and shows only a slight increase.

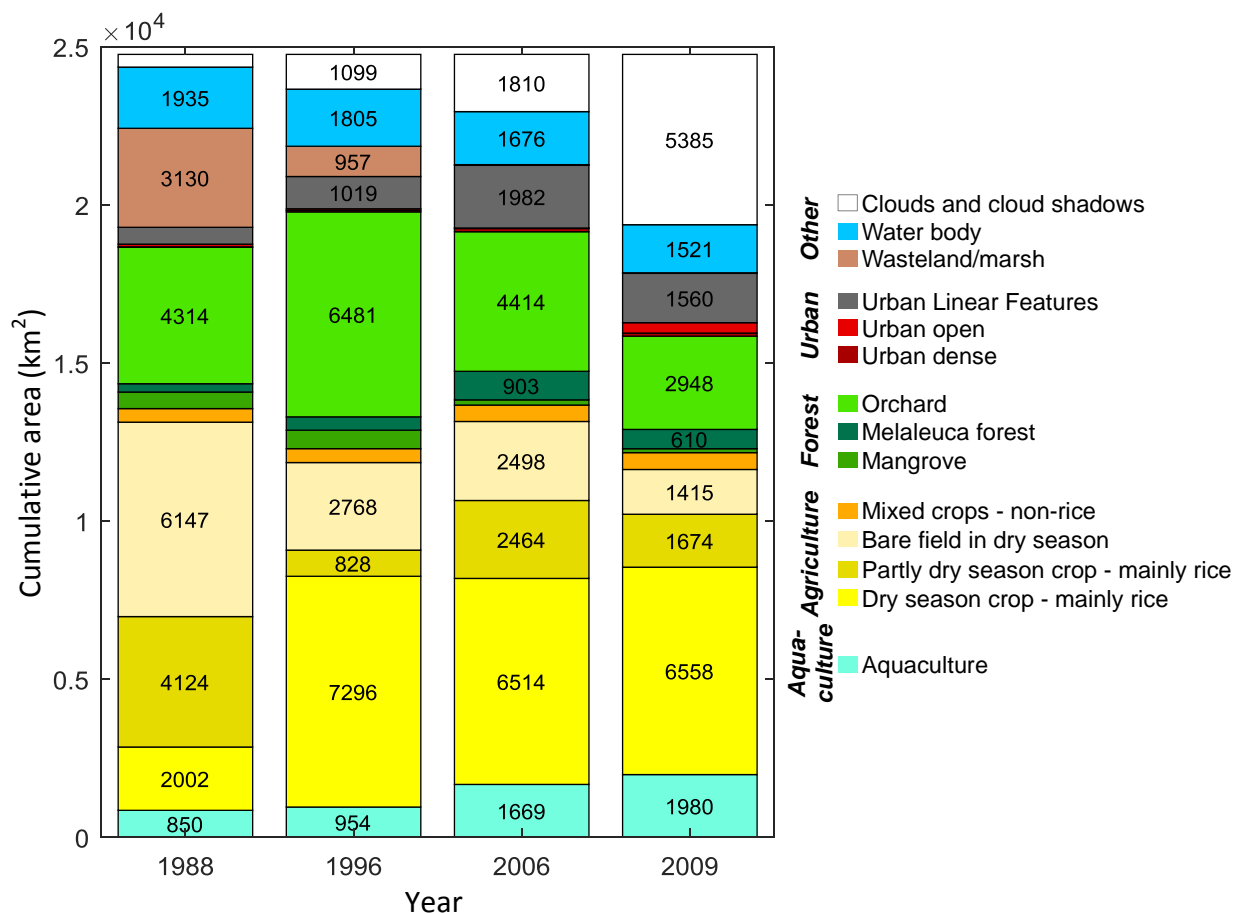


Figure 13 Stacked bar plot of the area of each land use (LU) class for each classified image, including the area of clouds and cloud shadows. Values in the bars are the area per LU class in km². Note that the clouds and cloud shadows cover different areas of each LU class in each year.

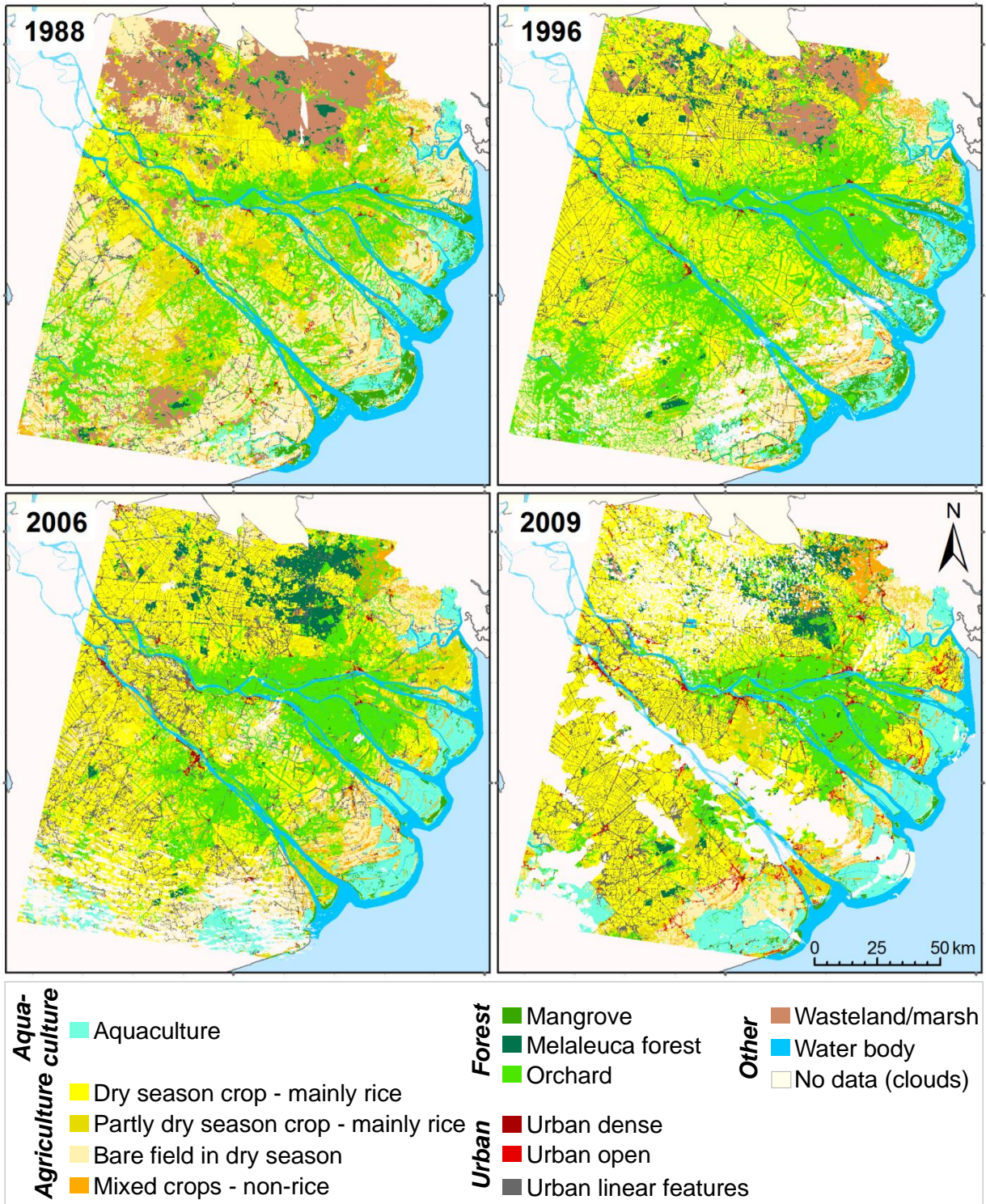


Figure 14 Land-use maps for 1988, 1996, 2006 and 2009.

The area of aquaculture along the coast increases strongly over all years. This area also expanded further away from the coast in the southwestern corner of the study area. Aquaculture mainly expanded at the cost of mangroves. The most significant increase in aquaculture occurred between 1996 and 2006. In this period, more than 320 km² of the about 540 km² of mangrove in the study area was converted to aquaculture (Table 30 in Appendix 9). Only very small strips of mangrove were left along the coast in 2006 and 2009.

The total area of the main class 'forest' fluctuated around 20-25%. The fluctuation is related to actual changes in the subclasses, but also to the cloud cover. The orchard subclass rapidly expanded between 1988 and 1996 along the main river branches and in the southwestern corner of the study area. Afterwards, it decreased again mainly in the southwestern corner. The conversion of agricultural fields to orchards along the main river branches did not reverse. The melaleuca forest expanded significantly between 1996 and 2006 at the expense of almost the entire area of wasteland/marsh which was left. It seems that natural succession took place, and/or these areas were converted to forestry areas.

The original delta wasteland/marsh area was clearly reclaimed between 1988 and 2006. Its area decreased from 13% of the delta area to almost 0%. In first instance, this area was converted to rice cropping areas, and later on to melaleuca forest. Besides, urban linear features appeared: roads and dikes were built. Urban linear features also appeared more and more elsewhere in the delta. This is in direct relation to the population growth and urbanization in the delta: the urban dense (and open) area increases too.

Overall, the LU changed considerably between 1988 and 2009. In 2006, only 30% of the area had the same LU as in 1988. The largest area changed between 1988 and 1996: in 1996, 38% of the area had the same LU as in 1988, while in 2006, 50% of the area had the same LU as in 1996. Between 2006 and 2009 – a much shorter period – the changes were smaller: in 2009, 57% of the area was used in the same way as in 2006.

Validation of the land-use maps

Manual labelling of the training and validation samples

During the manual labelling of the training and validation samples, a class could successfully be assigned to 90%, 92%, 94% and 93% of the randomly selected samples for respectively 1988, 1996, 2006 and 2009 (Table 5). This gives an indication of the highest possible overall accuracy of the LU maps.

Generally, the assignment of a class to the training and validation data was more difficult for earlier years. This was due to a lack of reference data for earlier years in combination with smaller differences in spectral object characteristics and less pure objects. The latter was related to the larger local variation in LU. This is reflected by the larger number of unknown samples. Besides, especially for 1988 and 1996, the training data itself may be less certain. In these years, aquaculture was difficult to distinguish from wasteland, bare and harvested fields or flooded areas as consequence of limited difference in spectral and spatial characteristics. Other potential confusions in the samples of especially 1988 are between 1) 'dry-season crop – mainly rice' and 'orchards' due to smaller differences in the NDVI and related features compared to other years, 2) 'urban linear features' and 'orchards', because they are often intertwined in elongated objects, and 3) 'mangrove', 'mixed crops – non-rice' and 'orchards' close to the coast due to limited spectral difference and limited decisive spatial context. For all years, the distinction between the urban classes was difficult because no hard lines can be drawn between these classes. The distinction between 'mixed crops – non-rice' and other vegetated classes was difficult due to similar spectral characteristics and limited decisive spatial characteristics. In most cases, the spatial and temporal context was used for final distinction to be able to label enough objects for each LU class.

Classification accuracy of the validation samples

The overall accuracies based on the area of the validation segments are high. They vary between 77% and 93% and the respective κ coefficient between 0.74 and 0.93 (Table 7). These accuracies are probably slightly too high, because they are not corrected for the number of random samples which could not be labelled and hence were excluded from the validation dataset. Even though the most reference data was available for 2006 and 2009, 1996 shows a slightly higher overall accuracy and κ -coefficient. The slightly lower accuracy for 2009 is most probably related to the widely spread small clouds and related atmospheric disturbance. The overall accuracy and κ -coefficient is lowest for 1988, which can be explained by the lack of reference data for this period.

The reliability and accuracy varies strongly between and within the LU classes. Nevertheless, generally the reliability and accuracy is very high: 100% is no exception (Table 7). Some classes have a low reliability and accuracy for multiple years: ‘urban open’, ‘harvested dry-season crop – mainly rice’ and ‘partly dry-season crop – mainly rice’. These classes generally also cover a relatively small area.

Table 7 Validation statistics for all four land-use maps. Based on the independent validation segments and corrected for the area of each segment. All percentages below 50% are colored red, percentages of 95% or higher are colored green.

LU class	1988		1996		2006		2009	
	Reliability	Accuracy	Reliability	Accuracy	Reliability	Accuracy	Reliability	Accuracy
Aqua	90%	100%	93%	96%	99%	100%	99%	100%
Dry-s rice	76%	66%	99%	100%	93%	64%	92%	97%
P dry-s rich	94%	88%	44%	17%	54%	72%	72%	80%
H dry-s rice	0%	0%	52%	44%	91%	98%	82%	49%
Bare field	83%	84%	95%	95%	91%	95%	80%	79%
Mix no rice	74%	86%	97%	89%	99%	79%	82%	81%
Mangr	98%	96%	92%	74%	100%	100%	100%	72%
Mel for	74%	94%	94%	98%	97%	97%	86%	92%
Orch	69%	88%	86%	98%	56%	83%	85%	65%
Urb D	95%	49%	88%	89%	91%	95%	66%	66%
Urb O	60%	69%	77%	38%	-	0%	46%	37%
Urb Line	72%	44%	99%	99%	93%	94%	90%	97%
Water	100%	50%	93%	100%	100%	100%	96%	100%
Water ch	8%	88%	100%	94%	100%	95%	100%	100%
Waste	99%	98%	98%	96%	100%	88%	100%	100%
Cloud remn	100%	33%	67%	87%	82%	85%	93%	91%
Overall accuracy	77%		94%		92%		89%	
κ-coefficient	0.74		0.93		0.90		0.88	

Inaccuracies can be related to confusions between classes with similar spectral and/or spatial characteristics (see confusion matrices in Appendix 8). Examples of confusions related to similar spectral characteristics are between 1) classes within the same main LU group, 2) urban classes and agricultural classes with low vegetation cover (bare field in dry season, harvested and partly dry-season crop – mainly rice), and 3) orchard and agricultural classes with high vegetation cover (dry-season crop – mainly rice, mixed crops – non-rice). Examples of confusions related to similar spatial characteristics such as the object shape are between orchard and urban linear features, and small channels and urban linear features. Moreover, uncertainties can be caused by the presence of some cloud shadows which passed through the mask and influence the spectral characteristics of the objects.

Comparison of provincial statistics

The area of aquaculture is higher in the coastal provinces and lower in the inland provinces compared to the provincial statistics of the General Statistics Office (GSO) of Vietnam (Table 8). This is in contrast to its very high reliability and accuracy in Table 7. The higher values may be related to the fact that the classification does not take into account whether ponds are active, while this is potentially distinguished in the survey-based GSO statistics. Besides, unused flooded areas in the coastal areas are easily confused with aquaculture in the creation of the training and validation samples as well as the classification itself. The lower inland values may be related to more scattered aquaculture ponds which are too small to be separately classified: the ponds are included in the 'water' or the '(harvested) dry-season crop – mainly rice' class. So, in the new LU maps, the aquaculture class mainly corresponds to brackish-water aquaculture rather than including fresh-water aquaculture. This is an advantage for coupling to land subsidence, as brackish-water ponds probably need more groundwater to dilute the ponds than upstream fresh-water ponds do.

The difference between the statistics for the forest area in 2009 is not very large (Table 8). The area of dry-season rice is smaller in most provinces in especially 1996 compared to the GSO statistics. The difference in dry-season rice area in 2006 and 2009 varies between the provinces. Hereto, only provinces which were not affected by clouds and which are completely covered in the study area were analyzed. Especially the provinces with a relatively large area of 'bare field in dry season' in this study (e.g. Soc Trang) have a lower dry-season rice area than in the GSO statistics. It seems that the dry-season rice class definition of the GSO also includes part of the 'bare field in dry season' class of our study.

In all cases the deviations between the provincial statistics are relatively small. As expected, the surface area of most classes is lower than the GSO statistics in the case that the province in this study did not represent the entire province. The latter could be due to clouds and/or if a part of the province was located outside the study area.

Table 8 Comparison of the area (km²) of aquaculture, forest and dry-season rice per province in the random forest classification of this study (RF) and the statistics of the General Statistics Office (GSO) of Vietnam. Only provinces which are covered for more than 50% by our study area are included. Forest area based on the RF classification = area 'mangrove' + area 'melaleuca forest'. Dry-season rice (incl. harvested and partly dry-season rice class) is compared with the GSO category 'spring paddy (lúa đông xuân)'. In 1996, Hau Giang is still part of Can Tho. Grey values may be too low due to clouds which cover relatively large areas in the respective province and year. * GSO statistics represent the entire province, but RF does not as part of the province falls outside the study area.

		Aquaculture						Forest		Dry-season rice					
		1996		2006		2009		2009		1996		2006		2009	
		RF	GSO	RF	GSO	RF	GSO	RF	GSO	RF	GSO	RF	GSO	RF	GSO
Coastal provinces	Ben Tre	341	247	467	410	480	420	40	38	221	218	359	207	331	211
	Tra Vinh	251	250	456	413	397	340	18	72	346	391	468	528	359	561
	Soc Trang*	152	241	293	643	541	692	82	105	385	614	737	1397	1031	1386
	Long An*	107	25	140	116	165	90	352	465	1325	1816	1511	2345	998	2490
Inland provinces	Hau Giang	-	-	0	74	1	62	29	25	-	-	783	842	852	823
	Tien Giang	30	92	59	124	75	126	144	88	798	877	872	839	829	827
	Vinh Long	2	11	4	23	7	25	3	-	709	738	481	697	720	676
	Can Tho*	0	105	5	136	3	131	4	-	1429	1636	769	930	606	901
	Dong Thap*	1	12	5	45	14	50	36	84	1788	1893	1723	2056	1331	2072

4.2. Relation land subsidence and land use

Land-subsidence rate per land-use class

At first, the subsidence rate per LU class was determined. Hereto, all InSAR-based land-subsidence rates for areas with a constant LU over the period 1988-2006/2009 were used (Figure 15, Figure 16 and Appendix 10 (Table 32)). All LU classes subside on average: on average net accumulation occurred for none of the classes. Though, almost all LU classes have a part of their lower whisker in the net accumulation zone (Figure 16). Most LU classes have a rate of about 1.3 or 1.4 cm/yr. 'Urban dense' has the highest mean subsidence rate: about 2.0 cm/yr. This class is followed by 'mixed crops – non-rice' and 'urban open' with about 1.8 cm/yr. The lowest mean subsidence rates are observed for wasteland/marsh (0.6 cm/yr), melaleuca forest (0.7 cm/yr) and dry-season crop – mainly rice (0.8 cm/yr).

If only the Tra Vinh tile is used for the same analysis, the patterns in relative subsidence rates between LU classes are similar (Figure 15, Appendix 10). The main differences are: 1) higher absolute subsidence rates for all LU classes except mangrove, 2) a higher relative subsidence rate for urban linear features (similar to bare field in dry season), and 3) the absence of melaleuca forest and wasteland/marsh.

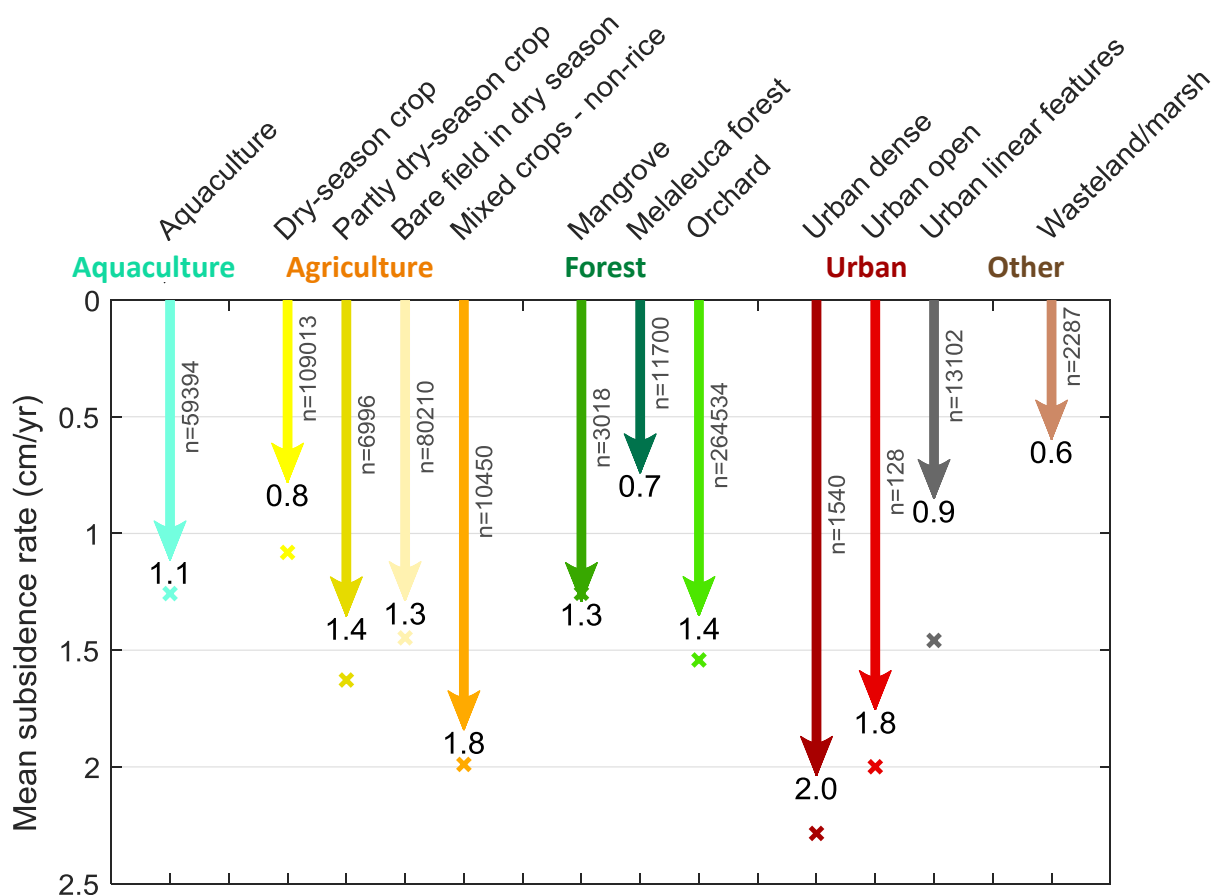


Figure 15 Mean InSAR-based land-subsidence rates for the period 2006-2010 per land-use (LU) class for all pixels where the LU was constant between 1988 and 2009. Arrows represent the land-subsidence rates for the entire area (all tiles, with value), while the crosses represent the rates for the Tra Vinh tile only. For the Tra Vinh tile, melaleuca forest and wasteland/marsh are absent. n = number of points used for calculating the mean.

The ranges of land-subsidence rates per LU class overlap, irrespective of the tile(s) used for the analysis (Figure 16, Appendix 10). The variation within each class is large: the coefficient of variation varies between 0.2 and 0.7 and the standard deviation is on average about 0.6 cm/yr. The median and mean subsidence rate of all LU classes are compared to all other classes: the 66 class combinations in the entire area are tested on their significance. The same is performed for the 45 combinations in the Tra Vinh tile. A class combination is for example the rate of aquaculture compared to that of mangrove. The significance of the differences in the median subsidence rate are based on the boxplot notches; the significance of the differences in the mean are based on one-way ANOVA and subsequent multiple comparison. Most combinations are significantly different at the 95% confidence level (Figure 23 in Appendix 10). This is partly related to the large group sizes. The median of 63 LU class combinations (i.e. 95%) for all tiles are significantly different. For the Tra Vinh tile only, this applied to 41 combinations (i.e. 91%). One-way ANOVA convincingly indicated that at least one combination was significantly different (for respectively all InSAR tiles and the Tra Vinh tile $F(11,562360) = 10455, p = 0$ and $F(9,112905) = 1043, p = 0$). Comparably to the medians, the mean of 64 class combinations (i.e. 97%) for all tiles are significantly different. For the Tra Vinh tile only, this applied to 40 combinations (i.e. 89%).

In this study, all class combinations with differences of more than a mm/year are significantly different based on both analyses for both extents (Figure 23 in Appendix 10). The only exception is urban open – urban dense in the Tra Vinh tile; two classes with relatively few points for analysis. Other combinations which could not be proven to be significantly different are combinations between mangrove, orchard, partly dry-season crop and bare field in dry season, and the combination urban open and mixed crops – non-rice. In some other cases, the outcome of both statistical analyses vary.

Overall, all classes combinations with a difference in subsidence rates that actually has a physically relevance (i.e. a difference of several mm/yr) are significantly different.

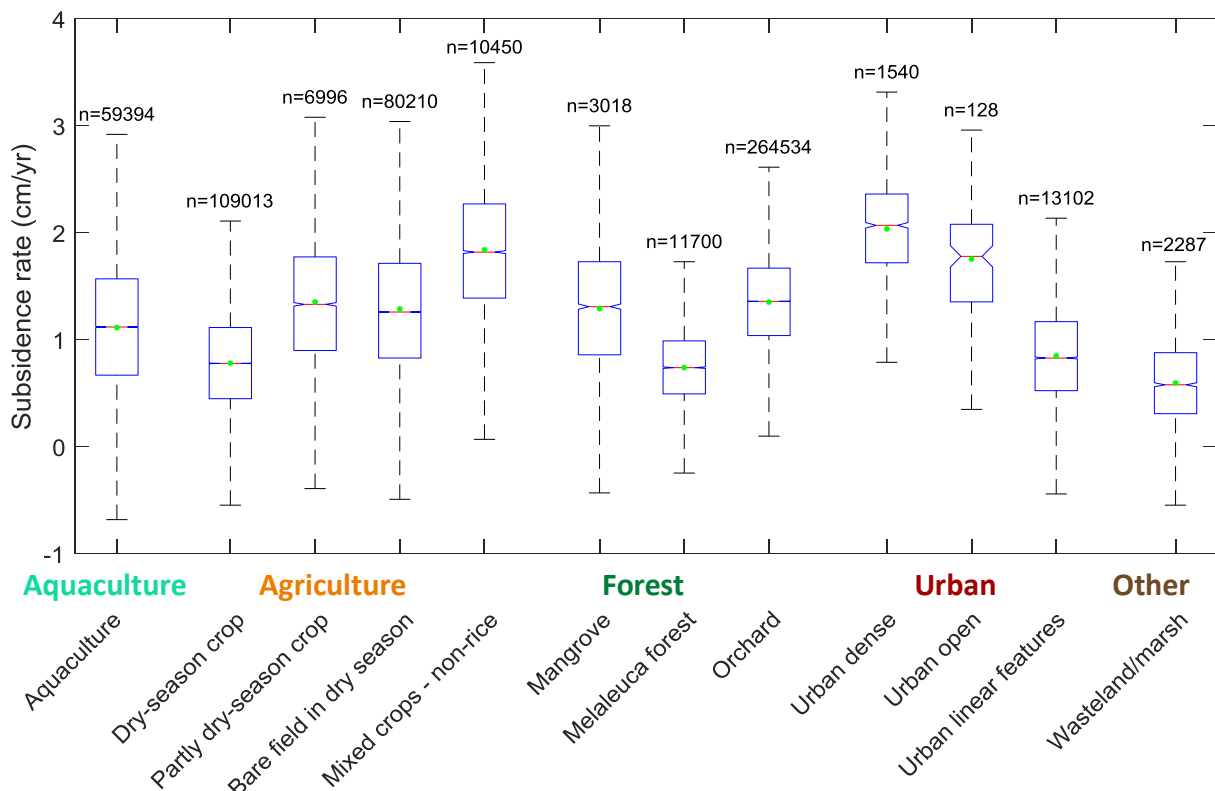


Figure 16 Notched boxplots of the land-subsidence rates for the period 2006-2010 per land-use (LU) class based on all points in all tiles for which the LU did not change between 1988 and 2006/2009. Outliers are not shown and whiskers extend up to maximal 1.5 times the interquartile range (IQR). n = number of points in the class.

Impact of past land-use changes on subsidence rates

The average land-subsidence rate for areas with different LU histories based on all InSAR-tiles are shown in Figure 17 (and Table 33 in Appendix 11). This is used to determine whether past changes in LU affects subsidence rates. The results of the same analysis for the Tra Vinh tile are shown in Appendix 11.1. Almost all differences between the average subsidence rates of a certain LU change at different moments in time are significant at the 95% confidence level (Table 33 in Appendix 11). Exceptions which do not show a significant difference based on all tiles are 1) the conversion from wasteland to dry-season rice and 2) the conversion of mangrove to aquaculture between two periods.

For most LU changes, a trend is visible (Figure 17). The average subsidence rate gradually changes from the average subsidence rate corresponding to the first LU (as shown in Figure 15) to the rate corresponding to the second LU as function of the moment of change. These trends are similar for the analysis based on all tiles together as based on the Tra Vinh tile only. No logical trend can be distinguished for the conversion from mangrove to aquaculture (Figure 17). This may partly be related to the small difference in average subsidence rates for mangrove and aquaculture in case of no change. For urbanization, the average subsidence rate generally is higher for areas where the urban LU class has already been present for a longer time. For the intensification of and change to agriculture, the trend is even clearer. For areas where wasteland is converted into agricultural land, the average subsidence rate is higher if the conversion took place earlier (Figure 17). The opposite is observed for the conversion from bare field in dry season to dry-season crop. This is because the average subsidence rate for bare field in no change areas is higher than for the dry-season crop class. For the change to orchards there is a clear increase in average subsidence rate if the conversion from wasteland or dry-season crop to orchard took place earlier.

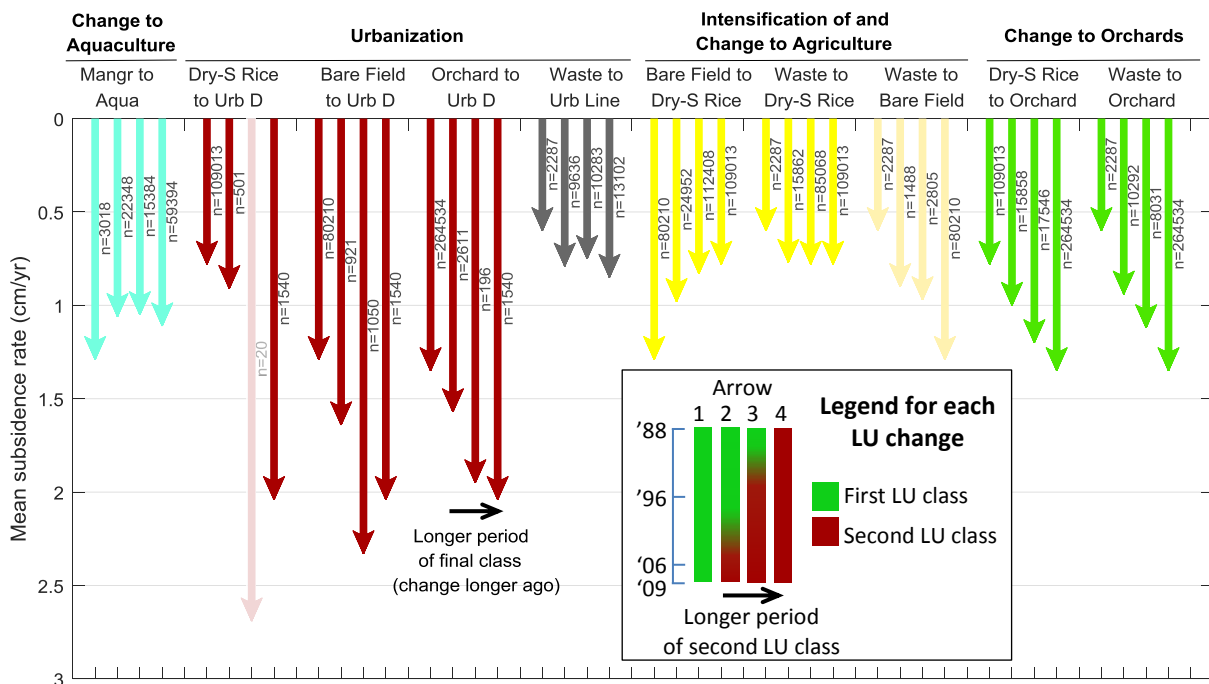


Figure 17 Impact of past land use (LU) changes on the mean land-subsidence rate for the period 2006-2010 based on all tiles. The first arrow corresponds to the area with no change in the first LU class, the second to the area with the first LU class in 1988 until 1996 and the second LU class in 2006/2009, the third to the area with the first LU class in 1988 and the second LU class in 1996 until 2006/2009 and the last to the area with no change in the second LU class. Note that the changes to orchards are the least important in the VMD over the past decades. n = number of points on which the average is based. The transparent arrow is based on less than 100 data points and is thus less representative. For values and significance of differences between arrows: see Table 33 in Appendix 9. Full LU class names of the acronyms in the LU changes: see Table 4.

4.3. Prediction of land subsidence based on land use

The previous section showed that there is a relation between LU and land subsidence. Here, the LU change maps for the period 1988-2009 were used to predict land subsidence rates for the period 2006-2010.

Prediction based on all land-use change periods

At least 17% of the total variance in the observed InSAR-based subsidence rates can be explained by the random forest prediction when all four periods of LU change were used to train the random forest for all tiles together. If the random forest is trained for the Tra Vinh tile only, this percentage is lower: 13% (Table 9). This coefficient of determination (r^2) of 17% and 13% is similar for the internal and external validation, and similar for different random samples used in the training phase of the random forest (Table 9). r^2 increases with increasingly more data used to train the random forest.

The difference between the observed and predicted subsidence rates is relatively large (Figure 18). The root mean squared deviation (RMSD) between observed and predicted rates based on the separate validation is consistently 0.56 cm/yr for the prediction based on all tiles as well as for the prediction using the Tra Vinh tile (Table 9). In contrast to the normally-distributed observed subsidence rates, the predicted subsidence rates are bimodal distributed. Both peaks can be related to the dominant LU history. For the predictions for all tiles, the peak around 0.80 cm/yr corresponds to the large area of rice fields, the second peak around 1.35 cm/yr corresponds to the orchards. For the predictions for Tra Vinh, the peak at about 1.55 cm/yr and 1.25 cm/yr correspond to respectively orchards and aquaculture. Besides, the range in predicted subsidence rates is smaller than the range in observed subsidence rates, and the predicted values are discontinuous (Figure 18).

In sum, predictions can be considered quite acceptable, even though the r^2 seems low and the RMSD high. This is, because approaching an r^2 of 1 is unrealistic due to the variation in subsidence rates within each LU class. Moreover, only LU history is used to predict the subsidence rate, while many other factors will also play a role.

Table 9 Evaluation of predicted land subsidence for the period 2006-2010 for all tiles together and the Tra Vinh tile with random forest (RF) regression using all four land-use change maps ('88-'96, '88-'06, '96-'06 and '06-'09)). Different runs are based on different random samples (different seeds). RMSD = root mean squared deviation between observed and predicted land-subsidence rate. r_{OOB}^2 and r_{val}^2 = coefficient of determination/proportion of variance in observed values explained by predicted values of respectively the out-of-bag (OOB) samples in the random forest itself and the separate validation dataset. U_{bias} , U_{slope} and U_e are Theil's partial inequality coefficients related to respectively a bias, the degree of consistency and unexplained variation. All values except for r_{OOB}^2 are based on the external/separate validation.

Tiles used	Run	RMSD (cm/yr)	r_{OOB}^2	r_{val}^2	Linear regression		U_{bias}	U_{slope}	U_e
					Slope	Intercept			
All	1	0.56	0.176	0.174	0.99	0.01	$1.7 \cdot 10^{-5}$	$4.0 \cdot 10^{-5}$	1.0
	2	0.56	0.174	0.174	0.99	0.01	$4.3 \cdot 10^{-6}$	$1.6 \cdot 10^{-5}$	1.0
	3	0.56	0.174	0.174	1.00	0.01	$4.3 \cdot 10^{-5}$	$3.1 \cdot 10^{-6}$	1.0
	4	0.56	0.173	0.174	0.98	0.02	$7.6 \cdot 10^{-7}$	$5.6 \cdot 10^{-5}$	1.0
	5	0.56	0.172	0.174	0.99	0.01	$1.0 \cdot 10^{-5}$	$1.2 \cdot 10^{-5}$	1.0
	Mean	0.56	0.174	0.174	0.99	0.01	$1.5 \cdot 10^{-5}$	$2.5 \cdot 10^{-5}$	1.0
Tra Vinh	6	0.56	0.130	0.128	0.98	0.02	$2.1 \cdot 10^{-5}$	$4.8 \cdot 10^{-5}$	1.0
	7	0.56	0.126	0.129	1.00	0.01	$3.7 \cdot 10^{-5}$	$3.0 \cdot 10^{-7}$	1.0
	8	0.56	0.131	0.127	0.97	0.04	$1.3 \cdot 10^{-6}$	$1.5 \cdot 10^{-4}$	1.0
	9	0.56	0.129	0.128	0.98	0.04	$1.1 \cdot 10^{-6}$	$9.3 \cdot 10^{-5}$	1.0
	10	0.56	0.130	0.127	0.98	0.03	$1.6 \cdot 10^{-5}$	$7.4 \cdot 10^{-5}$	1.0
	Mean	0.56	0.129	0.128	0.98	0.03	$1.5 \cdot 10^{-5}$	$7.2 \cdot 10^{-5}$	1.0

The random forest prediction is consistent and has no clear model bias. This can be derived from the fact that the linear regression line of the observed against the predicted land-subsidence rates is very close to the ideal 1:1 line (slope ≈ 1 and intercept ≈ 0). This applies to the predictions for all tiles together as well as for the Tra Vinh tile only (Figure 18, Table 9). Additionally, the consistency and absence of a bias is confirmed by Theil’s partial inequality coefficients. The proportion of variance in the predicted values which are due to a bias and inconsistency are about zero and the unexplained error proportion is one (Table 9). The unexplained error can be related to the quality and type of input data as well as the type of model.

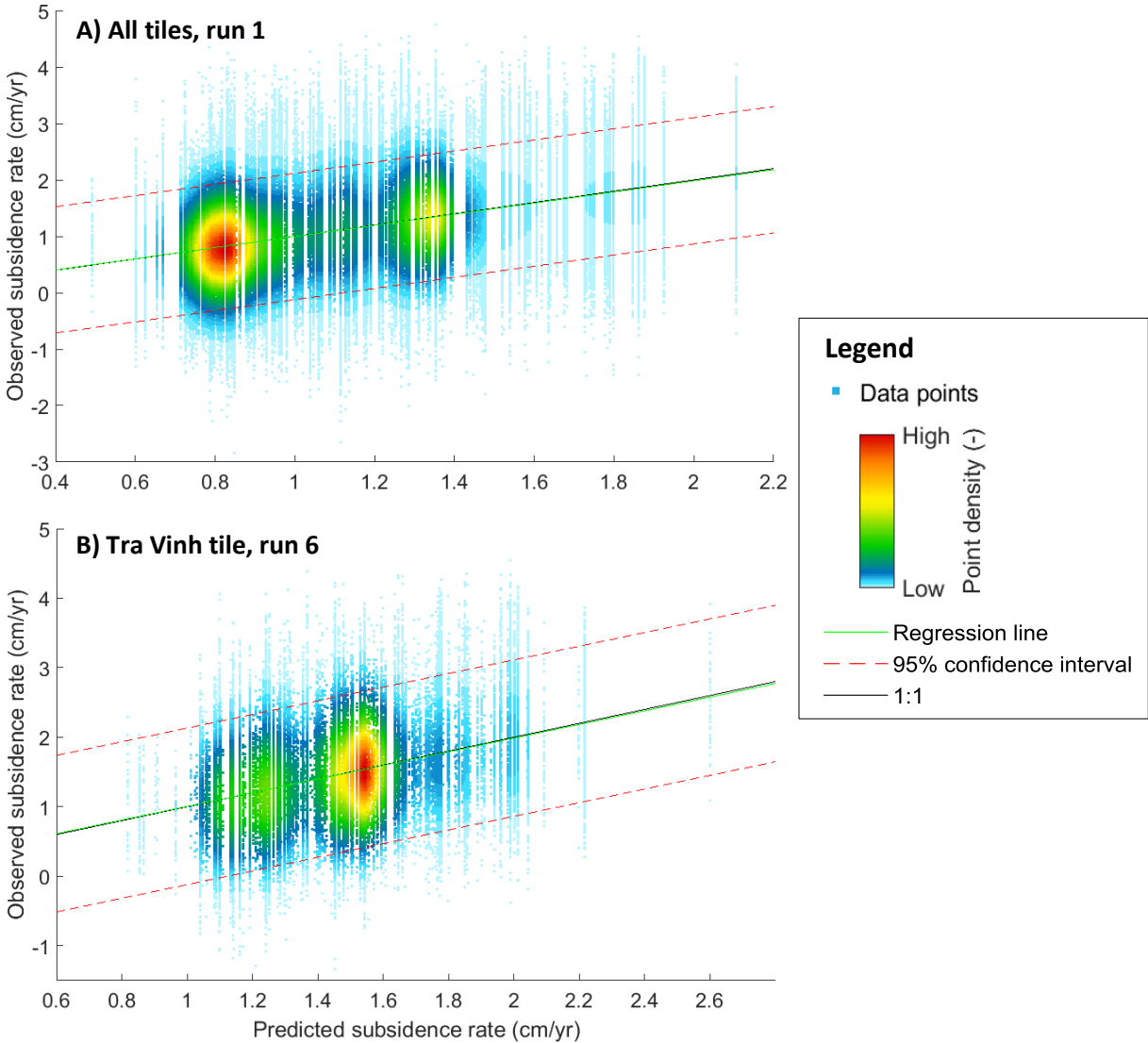


Figure 18 Density scatter plot and linear regression of observed InSAR-based land-subsidence rates versus predicted land-subsidence rates for the period 2006-2010 for A) all tiles (run 1 in Table 9) and B) the Tra Vinh tile (run 6 in Table 9). Predictions are based on all LU change periods. The regression equation is A) $obs = 0.99 \times pred + 0.01$ and B) $obs = 0.98 \times pred + 0.02$. The regression lines are very close to the ideal 1:1 line (slope = 1, intercept = 0). Other runs closely resemble these graphs. Note the different scales of the axes.

If the predicted land-subsidence rates for the separate validation points are visualized spatially, the LU patterns of the multiple LU maps are clear (Figure 19). The relative differences in subsidence rates over the VMD are largely similar to the original subsidence dataset. The main difference is that the values show less variation in space and range. The speckled pattern of the original dataset – which is related to actual local variation in subsidence as well as inaccuracies in the dataset – is removed. In the cases based on all tiles together, the offsets between the tiles are almost entirely absent. This is because the LU change classes used to predict the subsidence rate do not follow the tile borders. All these characteristics apply to all runs based on all tiles as well as based on the Tra Vinh tile only. Overall, this confirms that the predictions can be considered quite acceptable.

The two random forest importance measures are used to determine which LU change map has been structurally more important to create the random forest. This can indicate that that LU map has the strongest relation to the subsidence rates. In all cases except one, the LU map of 2006 – which represents the period 2006-2009 – was the least important for the predictions (Table 35 and Table 36 in Appendix 12). This can be derived from both importance measures for the predictions for all tiles as well as for the Tra Vinh tile only. However, this does not directly indicate that this period is least important to explain the subsidence rates, because this map has less variables – classes – to describe the same variation in the data. The map representing the entire area for the period 2006-2009 has only 11 LU change classes versus 53 LU change classes for the prior periods. For the extent of the Tra Vinh tile, this is even a class less. The other LU maps all have 53 classes which are used and can easier be compared to each other.

The relative importance of the different periods slightly varies between the cases with different random samples used for the training of the random forest (Table 35 and Table 36 in Appendix 12). Besides, the two importance measures do not give the same importance ranks. At last, the ranks differ between the predictions for all tiles and the Tra Vinh tile only. Hence, no single LU period appears to be significantly more important than the others.

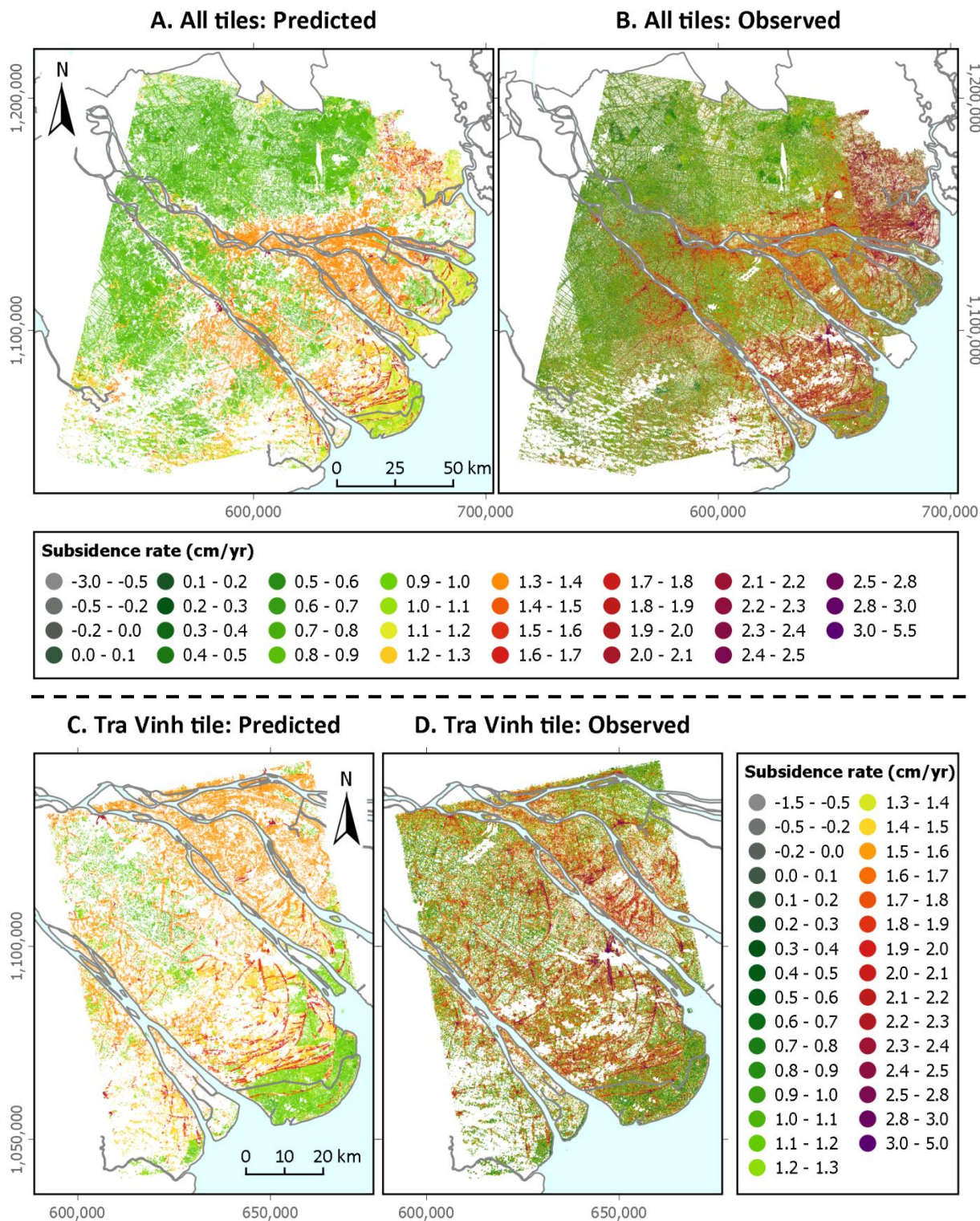


Figure 19 Map of predicted land-subsidence rates (A, C) and observed InSAR-based land-subsidence rates (B, D) for the period 2006-2010 based on all tiles (above) and based on the Tra Vinh tile (below). Only predicted values for validation points based on run 1 (all tiles) and run 6 (Tra Vinh tile) (Table 9) are shown. White no-data spaces correspond to 1) no-data areas in the input InSAR-based dataset, 2) no-data in the land-use (LU) change maps (cloud and water mask), and 3) for the prediction values also the LU change classes which could not be incorporated in the RF due to limitations in number of input classes.

Prediction based on a single land-use change period

The same analyses as in the previous section were performed using only a single LU change period as input for the random forest. For both the Tra Vinh tile as all tiles together, the RMSD is slightly larger than if all LU periods are being used. The variation in the predicted values tends to explain the linear variation in the observed values less well: 10 to 12% versus 13% for the Tra Vinh area, and 12 to 17% versus 17% for the entire area (Table 10). For both areas, the LU for the period 1996-2006 tends to give the best results, and 2006(-2009) the least. The latter is in line with the lower importance of this map for the predictions based on all LU change maps together. Again, this is partly related to the lower number of classes in this map which were used to predict the subsidence rate.

The other characteristics of all predictions are similar to the cases in which all LU change periods were used. For example, r^2 is similar if internally and externally calculated, and if different random samples are used. Moreover, the prediction is consistent without a significant model bias (Table 10). The spatial patterns are also very similar. The largest differences are observed for the case in which only the 2006 LU map is used, which is in line with the lower r^2 and RMSD.

So, overall, the prediction of land-subsidence rates based on LU improves if multiple periods are taken into account. LU during the decade prior to the prediction period seems to be slightly more important than the decade before.

Table 10 Results of prediction land subsidence for all tiles and the Tra Vinh tile with random forest (RF) regression using different single land-use (LU) change maps ('88-'96, '88-'06, '96-'06 and '06(-'09)). OOB = out-of-bag sample, r^2 = coefficient of determination/proportion of variance in observed values explained by predicted values, RMSD = root mean squared deviation. All values except r_{OOB}^2 correspond to the separate validation. Multiple runs per LU period are based on different random samples for the RF.

Tile used	LU period	Run	RMSD (cm/yr)	r_{OOB}^2	r_{val}^2	Linear regression		U_{bias}	U_{slope}	U_e
						Slope	Intercept			
All	'88-'96	11	0.56	0.159	0.159	0.99	0.00	$2.1 \cdot 10^{-5}$	$7.7 \cdot 10^{-7}$	1.0
	'88-'06	12	0.57	0.152	0.149	0.98	0.01	$2.5 \cdot 10^{-5}$	$4.6 \cdot 10^{-5}$	1.0
	'96-'06	13	0.56	0.167	0.167	0.98	0.01	$3.0 \cdot 10^{-5}$	$6.2 \cdot 10^{-5}$	1.0
	'06(-'09)	14	0.58	0.127	0.123	1.04	-0.04	$2.7 \cdot 10^{-5}$	$1.9 \cdot 10^{-4}$	1.0
Tra Vinh		15	0.57	0.109	0.109	0.99	0.01	$1.9 \cdot 10^{-5}$	$5.1 \cdot 10^{-6}$	1.0
	'88-'96	16	0.57	0.107	0.109	1.00	0.00	$2.5 \cdot 10^{-5}$	$1.3 \cdot 10^{-6}$	1.0
		17	0.57	0.106	0.109	1.00	0.00	$3.8 \cdot 10^{-7}$	$2.6 \cdot 10^{-6}$	1.0
		Mean	0.57	0.107	0.109	1.00	0.00	$1.5 \cdot 10^{-5}$	$3.0 \cdot 10^{-6}$	1.0
	'88-'06	18	0.57	0.122	0.119	0.98	0.03	$1.8 \cdot 10^{-5}$	$5.7 \cdot 10^{-5}$	1.0
		19	0.57	0.117	0.120	1.01	-0.01	$4.9 \cdot 10^{-5}$	$1.5 \cdot 10^{-5}$	1.0
		20	0.57	0.120	0.119	0.98	0.03	$6.7 \cdot 10^{-6}$	$6.1 \cdot 10^{-5}$	1.0
		Mean	0.57	0.119	0.119	0.99	0.01	$2.5 \cdot 10^{-5}$	$4.4 \cdot 10^{-5}$	1.0
	'96-'06	21	0.57	0.122	0.120	0.98	0.02	$2.0 \cdot 10^{-5}$	$3.5 \cdot 10^{-5}$	1.0
		22	0.57	0.119	0.121	1.01	0.00	$4.2 \cdot 10^{-5}$	$5.6 \cdot 10^{-6}$	1.0
23		0.57	0.120	0.120	0.99	0.02	$2.4 \cdot 10^{-7}$	$2.3 \cdot 10^{-5}$	1.0	
Mean		0.57	0.120	0.120	0.99	0.01	$2.1 \cdot 10^{-5}$	$2.1 \cdot 10^{-5}$	1.0	
'06(-'09)	24	0.57	0.101	0.099	1.04	-0.06	$2.0 \cdot 10^{-5}$	$1.4 \cdot 10^{-4}$	1.0	
	25	0.57	0.099	0.099	1.05	-0.07	$6.1 \cdot 10^{-5}$	$2.5 \cdot 10^{-4}$	1.0	
	26	0.57	0.099	0.099	1.05	-0.07	$4.1 \cdot 10^{-6}$	$2.6 \cdot 10^{-4}$	1.0	
	Mean	0.57	0.100	0.099	1.05	-0.07	$2.8 \cdot 10^{-5}$	$2.2 \cdot 10^{-4}$	1.0	

5. Discussion

5.1. Land-use classification

A new, consequent and consistent LU map series for the period of the reference subsidence data (2006-2010) and the two decades before was created at delta scale. Below, the trends are compared with the trends in the literature. Afterwards, the accuracy, method performance and consequences for coupling to land subsidence are discussed.

Trends in land use: comparison with literature

In general, the maps showed similar spatial and temporal patterns as described in the literature review: urbanization and change to or intensification of agriculture and aquaculture at the expense of wasteland/marsh and mangroves (e.g. Sakamoto et al., 2009a; Tran et al., 2015).

The timing of the main reduction in wasteland between 1988 and 1996 coincides with the economic and political reforms causing the reduction (Funkenberg et al., 2014). The corresponding expansion of dry-season rice is in accordance with the results of for example Nguyen-Thanh et al. (2014) and Binh et al. (2005). The strongest increase in aquaculture in the coastal area at the expense of agriculture and especially mangrove is observed between 1996 and 2006. This is in line with Karila et al. (2014), Sakamoto et al. (2009b), Tran et al. (2015) and Binh et al. (2005). The steady increase in urban areas along channels, dikes and roads as well as in villages observed in the new LU maps corresponds with the findings of e.g. Binh et al. (2005) and Tran et al. (2015).

The trend of mangrove being converted to aquaculture is in correspondence with literature (e.g. Tran et al., 2015). On the other hand, the conversion of fresh-water, melaleuca forest (and mangrove) to rice fields up to the end of the 2000's (e.g. the remote sensing studies of Nguyen et al., 2011; Thu, 2006) is not observed. The new LU maps show the opposite: an increase in melaleuca forest between 1988 and 2006. Maybe, the reference studies count parts of the wasteland as forest.

A limited number of studies discuss trends in orchards in the VMD. Hence, the expansion of orchards along the main river branches and the expansion and subsequent decrease in the southwestern part of the study area could not be confirmed. In general, the total area of orchards is structurally larger than the area published by Nesbitt (2005).

The spatial patterns in the number of rice crops a year as found by Nguyen-Thanh et al. (2014) and Sakamoto et al. (2009a) are compared with the spatial pattern of the 'mainly rice' classes in this study. The extent of 'dry-season crop' class largely agrees with the extent of the irrigated triple and double rice cropping areas with a dry-season crop. The extent of 'bare field in dry-season' largely agrees with the extent of rain-fed double rice cropping and single rice cropping. This relation can be used for comparison with trends found in the literature. This way, the first trend in the intensification of agriculture in especially the upstream part – from single cropping to irrigated double cropping with a dry-season crop – can be confirmed. On the other hand, the last trend in the intensification of agriculture – from irrigated double to triple rice cropping in especially the upstream part of the delta (Nguyen-Thanh et al., 2014; Sakamoto et al., 2009a) – could not clearly be observed in our LU maps.

Performance of the classification method

The accuracy based on the validation segments areas is relatively high compared to other studies and considering the number of classes: the overall accuracy is respectively 77%, 94%, 92% and 89% for the LU map of 1988, 1996, 2006 and 2009, with a κ coefficient 0.74, 0.93, 0.90 and 0.88. These values give an indication of the highest possible overall accuracy of the LU maps, as they are not corrected for the number of training and validation samples which could not be assigned to a class. Comparison

of the provincial areal statistics of the general statistics office (GSO) about agriculture, forest and dry-season rice showed that the aquaculture area in the coastal areas is slightly higher and in inland areas lower in the new maps. No consistent biases are found for the forest and dry-season rice areas.

In comparison, Son & Tu (2008) also used a Landsat ETM+ image to classify LU in a much smaller area just outside our study area. They applied a pixel-based maximum likelihood classification. This classification resulted in an overall accuracy similar to our classification of 91% and a slightly lower κ coefficient of 0.81 for the 11 classes based on reference pixels. However, their classification often confused water and shrimp farms. This confusion is limited in our study due to the object-based approach which makes discrimination based on the characteristic shape of the classes possible. Confusions which are similar in the study of Son & Tu (2008) are between winter rice, urban area and mixed forest due to low vegetation cover. Another study for comparison is that of Karila et al. (2014). In this study, a pixel-based unsupervised ISODATA LU classification is applied to Landsat images of the coastal part of the VMD. They also encountered the limitations of the persistent cloud cover and using a single image to classify LU representative for a longer period. As a result, they could only discriminate four LU classes. The extent of aquaculture in the LU maps is very wide, speckled and much further inland than expected: the LU maps of our study seem to be more reliable. A last study for comparison is that of Huth et al. (2012). They did not use Landsat images, but they did use a method similar to our study to classify LU in the VMD. They performed a hybrid, decision tree (C5.0 algorithm) classification method called TWOPAC. The object-based classification with 17 spectral classes (combined to 14 LU classes) of the central part of the VMD based on a high, 6.5 m spatial resolution Rapid Eye mosaic of 2011 resulted in a high overall accuracy of 93.7% and a κ coefficient of 0.93 based on the validation objects. The producer's and user's accuracy is at least 67% for all classes, which is higher than our classification. It is not clear whether these values correspond to the number of correctly classified objects, or the respective area. Just like in our study, class confusions are mostly related to strong spectral resemblances between classes.

The random forest algorithm gave accurate results. A main advantage of this method is that the algorithm itself determines the optimal segment variable thresholds to identify all classes. Moreover, once the right parameter settings have been determined, the training and application of the random forest classification are quick. On the other hand, a disadvantage is that the training dataset has to be manually created for each image. At last, the entire image is classified at once, so features related to the proximity of certain classes cannot be used as input segment variables. This can be used if a ruleset is being developed manually and the image is classified step by step.

Land-use classifications in relation to land subsidence

The purpose of the created LU maps is to couple LU to land subsidence. A few points should be taken into account for this coupling.

At first, the LU classes which have been chosen determine in part the success of this coupling. Classification inaccuracies could blur the expected relation between the chosen LU classes and land subsidence. For example, satellite images reveal land cover and conversion to LU requires interpretation which is not always straight forward. Therefore, the classes with low classification accuracies were excluded from the analyses to prevent error propagation. Moreover, limitations in reference data for especially 1988 and 1996 and available 'cloud-free' images required some concessions. For example, the lack of multiple images per year limits the discrimination of the exact rice cropping system and combined LU classes such as aquaculture in the dry season and rice-cropping in the summer. Even so, these classes may have different links to subsidence.

Secondly, the LU map of 2006 is taken as representative for the period 2006-2009, but 43% of the area seemed to have changed in this period. Nevertheless, this is the smallest area of change of all periods, and a part of the changes will be related to inaccuracies in especially the LU map of 2009. Not taking these apparent LU changes into account could have induced uncertainties in the coupling to land subsidence. Even so, these uncertainties are expected to be less significant than the

consequences of the data loss if the LU map of 2009 with its large data gaps due to clouds was included.

Thirdly, the LU can change quickly, especially within the agricultural classes, while this study uses only one image as representative for multiple years. Related uncertainties can be excluded by creating additional LU maps to decrease the temporal interval.

Lastly, actual boundaries between areas with a different LU are generally not as sharp as in the LU maps, especially because the maps are classified at delta scale. In other words: the maps represent the dominant LU; so a few fields with a different crop in between rice fields are for example not distinguished. On the other hand, the InSAR-based subsidence rates are given in a 67 x 67 m raster, but each raster value corresponds to the strongest reflecting *point* in the cell. These point values do not have to be representative for the larger scale LU to which they are coupled. Since many InSAR-based subsidence cells are analyzed per LU class, this issue of unrepresentative individual points is averaged out. It will only result in a larger spread of subsidence rates within a LU class. Moreover, land subsidence generally does not respect borders of LU classes, especially not if groundwater extraction – the dominant subsidence driver in the VMD – is taken into account:.

5.2. InSAR-based subsidence rates

In order to draw grounded conclusions on the relation between LU and subsidence, it is important to know the opportunities and limitations of the InSAR-based subsidence data. Erban et al. (2014, 2013) already pointed out some major issues (see Chapter 3.2.), but for this particular application, some additional points should be discussed.

At first, using InSAR in delta areas is a large challenge, especially in deltas like the VMD with significant atmospheric disturbance, and large spatial and temporal variation in surface conditions (Erban et al., 2014). The InSAR related noise in the subsidence rates is relatively large compared to the subsidence rates in the VMD. In areas with less atmospheric disturbances of the radar signals or in areas with larger subsidence rates, this problem is expected to be smaller. For example, the very high subsidence rates up to 25 cm/yr related to pumping stations at aquaculture facilities in China (Higgins et al., 2013) suffered much less from noise.

Secondly, a filter has been applied by Erban et al. (2014, 2013) to remove values which were unreliable. This filter worked fine for especially the upstream rice fields. Here, only limited values remained in the flooded paddies which return unreliable radar signals. Besides, many values remained at the dikes or levees between the paddies and buildings which return a more reliable signal. However, for other flooded ground surfaces – aquaculture ponds and mangroves – only a very limited amount of points is removed. Therefore, the subsidence rates for aquaculture and mangrove are expected to be very uncertain.

Thirdly, it is theoretically very difficult or even impossible to measure net accumulation rates with InSAR. If the radar reflector is above the surface, accumulation will not take place and hence will not be measured. If the radar reflector is located at the surface, the accumulation on top of it changes the reflector. This inhibits reliable comparison with the next moment of radar measurements. However, negative subsidence rates were observed across the delta and for most LU classes (Figure 16). Hence, these values are probably unreliable, even though net accumulation rates were expected for several classes.

Lastly, the absolute subsidence rates should be used with caution. The error estimate of 0.5 to 1.0 cm/yr (Erban et al., 2014, 2013) is based on the local variation in the dataset itself. No validation based on external subsidence rates could be performed. The offsets between the tiles of the mosaic already indicate that the error estimate should rather be seen as a relative error estimate than an absolute error estimate. This is because the estimate does not account for errors in the assumptions to set the zero-subsidence reference. Additionally, InSAR-based subsidence rates could underestimate the actual values, because regional subsidence with variation at a scale larger than an

InSAR-tile could be missed (Minderhoud et al., 2017). Nevertheless, the analysis of relative differences in subsidence rates between different larger scale units – such as LU types – seems appropriate, especially within one InSAR tile. This is because the large scale patterns in subsidence rates over the tiles are consistent. Therefore, the focus will be on the relative subsidence rates between LU classes hereafter.

5.3. Relation land subsidence and land use (change)

Land-subsidence rate per land-use class

The average land-subsidence rate per LU class based on the areas which showed a constant LU in 1988, 1996 and 2006/(2009) are largely in line with our expectations as described in section 1.4 about relative subsidence rates. It confirms that dense urban areas experience on average the highest subsidence rates, followed by open urban areas, and that wasteland/marsh experiences the lowest subsidence rates, followed by melaleuca forest. The actual subsidence rates for urban areas may even be higher than found in this study, because the rates based on the InSAR-signal correspond to the subsidence below the foundation depth of the reflecting urban constructions. Thus, part of the shallow subsidence rate may be excluded.

Other observations contradict the expectations. At first, the relatively high absolute and relative average subsidence rate for mangrove (1.3 cm/yr) and relatively low subsidence rates for aquaculture (1.1 cm/yr) are mainly attributed to the inaccuracies in the InSAR dataset as discussed in the previous section (5.2).

Three other results which deviate from the expectations are found within the agriculture category: 1) the low average subsidence rate for dry-season rice, 2) the relatively high rate for partly dry-season rice and 3) the high rate for non-rice, mixed crops. In an alluvial fan and a plain in Taiwan other crops ('upland planting') are also observed to subside more rapidly than rice fields (Liu et al., 2010). Their explanation for the relatively low rate for rice is that during the inundated periods, water is recharged to the groundwater aquifer(s), raising the groundwater table and compensating for the extracted groundwater. The potential of paddy fields to prevent subsidence due to groundwater recharge is also pointed out by Wen (1995) in general. This could also partly apply to the VMD as long as groundwater is extracted from shallow aquifers which could be recharged by surface water. However, many wells currently extract water from deeper aquifers in the VMD (Erban et al., 2013). Miyaji et al. (1995) also observed higher subsidence rates for upland crops than for paddies in peatlands in Bibai in central Hokkaido in Japan; a difference of 3 cm/yr. They ascribe this to accelerated organic material decomposition to mixing of the sublayer peat with the mineral top soil by deeper plowing and to a larger lowering of the groundwater table. Less peat is present in the VMD, but this may still play a role. Oxidation of organic matter, ripening of clay and compaction are limited for the inundated rice fields. A last option is that groundwater extractions are less pronounced in irrigated rice cropping areas than expected in advance due to a well-functioning irrigation network which supplies river water.

The subsidence rate for partly dry-season crop – mainly rice was expected to be in between bare field in dry season and dry-season crops – mainly rice, as this class is defined as an alternation of fields of those classes. This is probably an example of a significant (small) difference which is still inaccurate as a result of InSAR and/or classification inaccuracies.

The high average subsidence rate of mixed crops could partly be related to a factor which is not incorporated in the hypothesis: the subsurface composition or sedimentary environment favored by the different LU classes. The largest part of the delta has a fine-grained subsurface, but close to the coast, sandy dune ridges of a few meter thick are present (Nguyen et al., 2000). These ridges are favored to place buildings due to their higher elevation. They are also used to grow mixed, non-rice crops. The dune ridges themselves will not compact, but potentially the underlying fine grained

sediments do so because of the continuous pressure of the sand body and the additional pressure of the recently constructed buildings.

The average subsidence rate for orchards is higher than expected compared to the agricultural classes. It remains unclear whether this is related to actual subsidence processes, or to uncertainties in the mean subsidence rate. These uncertainties can be related to e.g. classification confusion between orchard and agricultural classes, or disturbed radar signals as a consequence of the high and dense vegetation.

The average subsidence rate for urban linear features – roads, dikes and direct surroundings – is considerably lower than the other urban classes. A large part of the network of urban linear features with higher subsidence rates was built after 1988 and hence is not incorporated in the analysis based on constant LU over all years. The areas which are included mainly consist of dikes with some roads between rice fields in the upstream part of the delta with low subsidence rates.

The above comparison of the observed subsidence rate per LU class with the expected rates is based on the average subsidence rate per LU class. The results showed that the within-class variation is relatively large and overlaps between classes. So, if the average of a LU class is significantly different from another class, a certain small area of those classes can still have the same subsidence rate. The within-class variation can be related to InSAR-noise and actual (local) variation. Actual (local) variation can be a consequence of unequally distributed subsidence due to processes which could still relate to LU (e.g. radial decrease in rates away from pumping wells for irrigation). It can also be related to external factors such as (local) variations in subsurface composition.

The relative differences between the average subsidence rates of multiple LU classes were used to get an indication of the impact of LU changes. For example, reclamation or exploitation of wasteland/marshes and urbanization are expected to result in most cases in a significantly higher subsidence rate. Hereto, it is assumed that a *causal* relationship between LU and subsidence exists and dominates. However, whether the relationship is causal cannot be concluded from this data-mining study. Besides, it does not have to be the case in all situations. For example, if mixed crops – non-rice is converted to another class, the effects are expected to be limited, because the high subsidence rate for this class is probably dominated by the sedimentary setting which remains unchanged. In addition, if there exists a causal relation between LU and subsidence, larger scale subsidence processes related to e.g. deep groundwater extraction do not suddenly stop at boundaries of LU classes. This blurs differences between classes.

Altogether, two main LU change trends observed in the VMD – urbanization and change to orchards – have resulted and will most probably on average result in a higher subsidence rate, while intensification of agriculture is on average related to a lower subsidence rate. For the main trend of the expansion of aquaculture at the expense of mangrove no conclusions can be drawn due to unreliable subsidence rates.

Impact of past land-use changes on subsidence rates

Next to determining the expected effect of changing LU on the subsidence rate based on the average rate per LU class, the impact of past LU changes has been assessed. This was used to determine whether time-dependent effects related to previous LU types influence the subsidence rates.

For all trends related to urbanization, change to and intensification of agriculture and change to orchards, the results suggest that the longer the ‘final’ LU class has been present, the higher the subsidence rate gets (or the lower for the conversion from bare field in the dry season to dry-season rice). The trends for the change from mangrove to aquaculture was unclear. This is in line with the conclusion that the subsidence rates for these classes are not reliable. Four of the analyzed trends were a conversion from wasteland/marsh to another class. The subsidence rates were lower for areas which had the longest period of wasteland between 1988 and 2006/2009. In 2006/2009 almost

no wasteland was left. Hence, at present, the only impact of wasteland can be that subsidence rates are lower in areas that were recently reclaimed compared to areas which were reclaimed longer ago.

Based on these results, it can be confirmed that the LU situation before 2006 has an important impact on the subsidence rates for the period 2006-2010. Thus, time lag effects and gradual changes in subsidence rates over time do play a role. The current study could not discriminate between the different time and time-lag effects. So, in general, providing an average subsidence rate for a LU class is only appropriate if past LU changes are taken into account.

The trends suggest that it takes at least about two decades before the subsidence rate depends only on the current LU. Otherwise, the mean subsidence rate for the areas with a certain LU change between 1988 and 1996 would be similar to the case with no change in the second class. For all clear trends, it seems that this takes at least two decades. However, it was expected that this period varied between different LU histories, because different LU histories are related to different processes that play a role at different time scales. The choice of the time intervals used may have influenced the apparent past LU period that influences the subsidence rate.

For the above conclusions based on the trends, two assumptions were indirectly made: 1) the subsidence processes and drivers that determine the relation between LU and land subsidence remain constant over time, and 2) no external factors play a role. The first assumption is not entirely valid, because in reality, LU practices change over time. This is for example a consequence of advances in technology. Herewith, the subsidence rate may also change. The second assumption may also be partly violated. Each mean subsidence rate per LU history is based on the data points corresponding to that specific LU history. These points correspond to different areas. Hence, differences in subsidence rates for the areas with a different LU history could also be related to other factors that result in spatial variation in land subsidence. However, these disturbing factors seem to have limited impact, because they cannot explain the clear trends in Figure 17. Moreover, the trends are very similar if only the Tra Vinh tile is used for the analysis. This also means that the offsets between the tiles do not influence the trends. So, the second assumption seems valid.

5.4. Predicting land subsidence based on land use

Quality of the predictions

The random forest regression algorithm showed to be a promising predictor of subsidence rates based on LU history. The model behaved consistent and without bias for all cases. Spatial patterns in the predicted subsidence rates agreed well with the observed rates. More than one sixth (> 17%) of the variance of the observed subsidence rates could be explained with the predicted rates. This applies to the predictions which used all four LU change periods for the entire area. The explained variance is relatively high for predictions based on LU history alone: a much higher r^2 was not expected due to the variation observed within the LU classes. In general, the unexplained variance is related to factors such as the type and quality of the input data and the type of model. Overall, the results confirm that there is a relation between LU history and subsidence, but that this relation is not sufficient to predict the entire subsidence signal. Other factors than LU are also important to predict the subsidence rates.

The root mean squared deviation (RMSD) was about 0.6 cm/yr and falls within the error range of the InSAR-based subsidence rates. The predictions for the Tra Vinh tile only could explain less of the variance compared to the predictions for the entire area: at least 12%. Apparently, the advantages related to e.g. better representation of all LU classes outweighs the disadvantage of having offsets between the tiles.

At last, the range for the predicted values is smaller than that of the observed values, and the predicted subsidence rates are discontinuous. This is partly expected based on the way the random forest applies a regression. Each end node in a regression decision tree represents the average of the

training points which ended up in the node. This evens out the predicted subsidence rates. However, if the final value assigned to a point is based on the average of all trees, a more continuous outcome is expected than observed.

Importance of including past land use

Similar to the conclusion in section 5.3, the predictions confirm that *past* LU is important for subsidence rates. Delayed (time lag effects) and slow responses (time effects) of subsidence to LU changes are important. This is based on the fact that the explained variance (r^2) is larger if all LU change periods are used rather than one of these periods only. However, the improvement of the RMSD is minimal. Note that if past LU is very important for the subsidence rates, the improvement in r^2 and RMSD is still expected to be limited. This is because a large part each LU change map is similar to the other maps. The predictions for the points corresponding to these areas are not expected to improve, which will dampen the effect of the improvement for areas which changed.

It is difficult to say whether a certain period has most influence on the subsidence rates and if yes, which one. The most recent period was expected to be most important if time-lag effects are unimportant or play a role on a shorter time span than the LU change periods. This seems to be the case: the predictions based on the period 1996-2006 resulted in the highest r^2 and lowest RMSD. So, this period seems to have the strongest relation with the subsidence rates. Though, the differences with the other periods are small. In addition, no conclusions could be drawn about which LU change period is most important for the predictions based on the random forest importance measures. This can partly be explained by the fact that the most important LU period varies per LU class, because the dominant subsidence processes and the related time scale on which they play a role differ per LU type. So, based on the current analyses, it cannot be determined whether one or more of the LU change periods can be disregarded, or whether more LU maps at a higher frequency and over a longer period are needed.

5.5. Implications and suggestions for future research

As confirmed by this study, the VMD underwent significant LU changes within a few decades. A large part of the delta was still largely uncultivated at the end of the 1980's. Based on the mean subsidence rates for the different LU types in the delta, the reclamation and urbanization of the delta resulted in an increase in subsidence rates. The consequences of this increased subsidence rate – such as increased flood risk and salt water intrusion – poses the increasing population and food production at risk. However, the change in subsidence rate differs between different LU types.

The current study could help in choosing LU types and areas with relatively high or unexpected subsidence rates on which future research should focus to determine the responsible processes. The irrigated rice class with lower subsidence rates than expected is an example of a LU class which requires further study. Focusing on the unexpected rates helps understanding the processes behind the observed differences in subsidence rates between the different LU types. Though groundwater extraction is an important driver for subsidence in the VMD, it has not to be the driving factor behind these *differences*. Hereto, at least further study on the water usage and management per LU type is needed. Besides, a process-based approach could help to determine the importance and timespan of the different time-dependent reactions to past LU changes. This helps to determine the period of past LU which has to be used for the subsidence-rate predictions using the data-mining approach in this study. Hence, this way, research on processes and data-mining can complement each other.

Subsequently, this information could be used by policy makers and locals to mitigate the consequences and to adapt. Though, the current study also showed large variation within subsidence

rates per LU class with overlap between classes. Hence, the differences in the mean subsidence rate should not directly lead to new regulations which promote or oppose certain LU types.

Moreover, the fact that different LU types can be coupled to different subsidence rates is a comprehensive way to show locals their influence on the subsidence rate and especially the related negative consequences. Their influence seems not only to have a short-term, direct effect, but also long-term effects as past LU changes have their impact too. Herewith, awareness could be raised, which is essential to initiate successful adaptations.

The number of remote sensing platforms and corresponding data on the earth surface is quickly growing and the quality is improving. In first instance, remote-sensing data may seem not very useful for subsidence research as this discipline studies the *subsurface*. However, InSAR and LiDAR data proved to be useful for subsidence research as a measurement tool. Additionally, this study showed that other remote-sensing derived parameters such as LU may also have value for subsidence research. Besides, different (remote-sensing) data sources can complement each other. Potentially, other remote-sensing derived parameters can be added to the list.

Next to the above suggestions, further research can focus on improving of the results of the current study for the VMD. Moreover, it can focus on testing to which extent the random forest algorithm can be used in another area or for predicting future subsidence rates. These suggestions are elaborated in the paragraphs below.

Improvements in coupling land-subsidence rates to land-use history

The results of the coupling of subsidence rates to LU history could not easily be compared to existing literature, because similar studies have not been found. As pointed out by Higgins et al. (2013): “Subsidence rates in nonurban, near-shore areas are virtually unknown.” Some studies on specific LU types have been used for comparison, but large differences in other factors related to subsidence (e.g. subsurface composition) complicate comparison. This emphasizes the importance of doing additional subsidence measurements in the VMD as reference to draw more solid, generic conclusions. Performing similar case studies in other deltas will also contribute to this.

In the meanwhile, the results could at first be improved by enhancement of the LU classifications. For example, the LU classification can be ameliorated by combining multiple images of one year – potentially of other remote-sensing platforms due to the limited availability of cloud free images – to decrease the data gaps due to clouds, especially for the map of 2009. This would also improve the classification of the multiple rice cropping systems and other combined LU types over the year. The residual class ‘partly dry-season crop’ could be substituted by a class with a more relevant physical meaning. The choice of relevant LU classes is essential for subsequent coupling to subsidence. Besides, the accuracy and reliability of the classification can be increased by manually increasing the number of samples for each LU class (Huth et al., 2012), because a limited amount of samples for training as well as validation is used in this study. At last, the frequency of the LU maps can be increased by using additional Landsat images with an acceptable cloud cover or images from other satellites. Herewith, it can be checked whether LU did not change in the decades in between. Herewith, the reliability will improve of the results of the mean subsidence rate per LU class and the trends in the mean subsidence rate for areas with a certain LU change at different moments in time.

Secondly, the quality of the results of the current study strongly relies on the quality of the InSAR-based subsidence rates. The subsidence dataset may be improved by including more SAR-images captured at other moments in time or by other satellites as the number of high-resolution radar satellites is increasing. This can reduce the inaccuracies of atmospheric disturbances (pers. com. prof. R. Hanssen). Though, adding images from later or earlier periods will be in conflict with the assumption of a constant land-subsidence rate over the acquisition period of all images. Perhaps, additional data from the same or new satellites could be used to create a more recent InSAR-based

subsidence dataset. Besides, the filter which removes part of the unreliable data could be adjusted to exclude more unreliable data. As long as a sufficient subsidence rates remain for each LU (change) class, the reduction of data is not expected to hinder the predictions.

Improvement and wider applicability of the subsidence predictions

The random forest is consistent and has no bias. However, LU history alone cannot predict the entire subsidence signal. Besides, as indicated earlier, the relation between LU and subsidence may partly change over time due to changes in LU practices over time. This complicates predicting (future) subsidence rates. Hence, a first improvement of the predictions is to use additional input variables to explain the remaining variation in the subsidence rates. These additional data may have 1) a direct link to subsidence processes, such as parameters describing the subsurface composition, 2) a semi-direct link, such as groundwater extraction rates, distance to a pumping well, hydraulic heads and temporal characteristics of the groundwater table, or 3) an indirect link, such as population density. Thematic as well as continuous variables and even incomplete datasets could be used as input for the random forest algorithm. The relevance of the variables can be assessed using the importance output variable of the random forest algorithm. Moreover, even though the currently used InSAR-based subsidence dataset is by far the most extensive and appropriate dataset to be used for the VMD, the improvements of the InSAR-based subsidence rates suggested in the previous paragraph could improve the predictions.

Next to improvements related to changing the input, some technical limitations may be overcome. At first, a main limitation of the predictions is that the R randomForest package cannot handle the large amount of input samples and the large number of LU change classes I intended to use. The r^2 improved if more points were used to train the random forest. So, probably, the predictions further improve if only the number of input points could be larger. Besides, using more classes would enable linking and combining the LU maps into less variables which describe the LU history. Secondly, the calculations in R require much physical memory. A possible solution to these problems could be to use another software package. Other users experienced that the randomForest package in R generally is one of the most inefficient options considering physical memory, input number of thematic classes and computational time. They indicate that Spark, xgboost, Python and H2O are potential better alternatives.

Additionally, future research could test to which extent the random forest algorithm can be used in a broader context in space and time. To test the validity of extrapolation in space, the random forest of a single tile of the dataset used in this study can be used to predict subsidence in the remainder of the delta; the entire dataset can be used for the validation. Extrapolation of the random forest trained on the data of the VMD to another delta is not realistic, because of differences in dominant processes and LU classes present. Though, if a similar dataset of land subsidence and LU data is available or created for another delta, a similar approach can be used. Such a study could be used to test the generality of the trends between LU (changes) and subsidence rates.

To test the quality of forecasting land-subsidence rates based on LU change scenarios, a second subsidence rate dataset of another moment in time and LU changes between the acquisition time of both subsidence datasets are needed. This data can be used as follows: 1. Train the random forest (RF) using the LU changes before the acquisition period of the first dataset, 2. Use this RF to predict the subsidence rates based on the LU changes before the acquisition period of the second dataset, and 3. Validate the results using the second subsidence dataset. Of course, variables next to LU can also be used in these predictions as long as they are used in both the training and application of the RF. If the validation results are as desired, the RF may be applied for real forecasts.

6. Conclusion

Land use (LU) has been classified for 1988, 1996, 2006 and 2009 in the VMD to be able to couple LU history to the InSAR-based subsidence rates of Erban et al. (2014) for the period 2006-2010. The object-based random forest classification resulted in relatively high accuracies compared to previous LU classifications: the overall accuracies ranged between at max. 77% and 94% based on the area of validation samples. The following main trends are observed in the LU maps: 1) natural wasteland was reclaimed and turned into mainly rice fields, 2) mangroves were converted to aquaculture, 3) the urban area expanded: cities grew and more buildings appeared along (new) roads, channels and dikes, 4) agriculture intensified as the areas where a dry-season rice crop is grown expanded, and 5) agricultural areas changed to orchards between 1988 and 1996 along the main river branches.

The first aim of this study was to quantify and compare land-subsidence rates for different LU types and LU changes. Almost all LU classes have a significantly ($\alpha = 0.05$) different mean subsidence rate. This confirms that there is a relation between LU and land subsidence. Urban areas subsided strongest (mean of 2.0 cm/yr based on the entire dataset), followed by agricultural areas with other crops than rice (1.8 cm/yr). Wasteland, fresh-water forests and irrigated double or triple rice cropping fields ('dry-season crop – mainly rice') subsided slowest (0.6, 0.7 and 0.8 cm/yr respectively). The mean subsidence rate for orchards (1.4 cm/yr) was similar to rain-fed rice ('bare field in dry-season') (1.3 cm/yr). The relative differences are largely as expected based on the drivers loading, groundwater extraction and management of the groundwater table. The mean subsidence rate of aquaculture (1.1 cm/yr) and mangrove areas (1.3 cm/yr) were respectively lower and higher than expected. This is probably related to unreliable InSAR values for these water-rich classes. The mean subsidence rate of irrigated rice was lower than expected compared to for example rain-fed rice. This can indicate that 1) less groundwater was extracted for irrigation purposes than expected, and 2) the longer period of inundation resulted in groundwater recharge and significantly less shallow subsidence due oxidation and ripening. The rate of the non-rice crops was higher than expected. This seems partly related to the subsurface: this class is mainly located on top of beach ridges. The compactable layers below these ridges may cause the high subsidence rates as consequence of the strong loading. The relative subsidence rates are considered to be reliable, while absolute rates are not, due to inaccuracies in the InSAR-based subsidence dataset. Based on the relative mean subsidence differences, it can be concluded that in general reclamation, the change from agriculture to orchards and especially urbanization result in stronger subsidence. On the other hand, the intensification of agriculture may reduce subsidence rates. The overlapping within-class spread in subsidence rates of different LU types allows drawing general conclusions, but no conclusions on the impact of a case specific LU change.

The second aim of this study was to determine the importance of time-dependent effects related to LU history on land-subsidence rates. It is concluded that time-dependent effects were important for the subsidence rates in the VMD between 2006 and 2010. Hence, land subsidence should be coupled to LU history rather than to current LU only. This is based on 1) the differences in mean land-subsidence rates for unchanged areas compared to areas with a certain LU change history, and 2) the fact that the subsidence predictions improved if more than one LU period was used for the predictions. It seems that the LU between 1996 and 2006 as well as between 1988 and 1996 is important for the subsidence rates in 2006-2010 in the VMD, but this may depend on the chosen time intervals and it may differ per LU class.

The third aim of this study was to determine to which extent LU history can predict land-subsidence rates. Spatial patterns in the rates predicted with the random forest using two decades of LU history agree well with the patterns in the InSAR-based subsidence rates for the period 2006-2010. More than one sixth (>17%) of the variance in the observed rates could be explained by the predictions of the entire VMD. This percentage is relatively high considering the variation in subsidence rates within the LU classes. This variation is related to InSAR-noise and local variation due to other variables which influence subsidence. The root-mean-squared deviation (RMSD) of the

predictions (0.6 cm/yr) is within the error range of the InSAR-based subsidence rates. Besides, the random forest is promising, because it has no bias and is consistent. Overall, the unexplained variance can be related to the quality and type of input data as well as the type of model. Although LU history can predict a relatively large part of the subsidence signal, more factors should be included to predict the entire signal.

This study helps to choose LU classes with high or unexpected subsidence rates on which research on responsible processes should focus. This could be used by policy makers to mitigate or adapt to consequences. Moreover, the fact that different LU types can be coupled to different subsidence rates is a comprehensive way to create awareness among locals about their influence, which is essential for successful mitigation and adaptation. Lastly, this study also showed that optical remote-sensing derived parameters (LU) could complement more accepted remote-sensing products (InSAR) in land-subsidence research.

List of references

- Amelung, F., Galloway, D. L., Bell, J. W., Zebker, H. A., & Lacznia, R. J. (1999). Sensing the ups and downs of Las Vegas: InSAR reveals structural control of land subsidence and aquifer-system deformation. *Geology*, 27(6), 483–486. [https://doi.org/10.1130/0091-7613\(1999\)027<0483:STUADO>2.3.CO;2](https://doi.org/10.1130/0091-7613(1999)027<0483:STUADO>2.3.CO;2)
- Binh, T. N. K. D., Vromant, N., Hung, N. T., Hens, L., & Boon, E. K. (2005). Land cover changes between 1968 and 2003 in Cai Nuoc, Ca Mau Peninsula, Vietnam. *Environment, Development and Sustainability*, 7(4), 519–536. <https://doi.org/10.1007/s10668-004-6001-z>
- Bouman, B. (2009). How much water does rice use? *Rice Today*, 8(2), 28–29.
- Bouvet, A., & Le Toan, T. (2011). Use of ENVISAT/ASAR wide-swath data for timely rice fields mapping in the Mekong River Delta. *Remote Sensing of Environment*, 115(4), 1090–1101. <https://doi.org/10.1016/j.rse.2010.12.014>
- Breiman, L. (2001). Random Forests. *Machine Learning*, 45, 5–32. <https://doi.org/10.1023/A:1010933404324>
- Breiman, L., & Cutler, A. (2003). Manual - Setting up, using and understanding Random Forests V4.0, pp. 33. Retrieved May 1, 2017, from https://www.stat.berkeley.edu/~breiman/Using_random_forests_v4.0.pdf.
- Buschmann, J., Berg, M., Stengel, C., Winkel, L., Sampson, M. L., Trang, P. T. K., & Viet, P. H. (2008). Contamination of drinking water resources in the Mekong delta floodplains: Arsenic and other trace metals pose serious health risks to population. *Environment International*, 34(6), 756–764. <https://doi.org/10.1016/j.envint.2007.12.025>
- Cahoon, D. R., Lynch, J. C., Perez, B. C., Segura, B., Holland, R. D., Stelly, C., Stephenson, G., Hensel, P. (2002). High-Precision Measurements of Wetland Sediment Elevation: II. The Rod Surface Elevation Table. *Journal of Sedimentary Research*, 72(5), 734–739. <https://doi.org/10.1306/020702720734>
- Chambers, J. M., Cleveland, W. S., Kleiner, B., & Tukey, P. (1983). Comparing data distributions. In *Graphical methods for data analysis* (pp. 60–63). Belmont, California: Wadsworth International Group.
- Chang, K.-W., Shen, Y., & Lo, J.-C. (2005). Predicting Rice Yield Using Canopy Reflectance Measured at Booting Stage. *Agronomy Journal*, 97(3), 872–878. <https://doi.org/10.2134/agronj2004.0162>
- Chen, B., Gong, H., Li, X., Lei, K., Ke, Y., Duan, G., & Zhou, C. (2014). Spatial correlation between land subsidence and urbanization in Beijing, China. *Natural Hazards*, 75(3), 2637–2652. <https://doi.org/10.1007/s11069-014-1451-6>
- Chen, C.-F., Son, N.-T., Chen, C.-R., & Chang, L.-Y. (2011). Wavelet filtering of time-series moderate resolution imaging spectroradiometer data for rice crop mapping using support vector machines and maximum likelihood classifier. *Journal of Applied Remote Sensing*, 5(1), 053525. <https://doi.org/10.1117/1.3595272>
- Chen, C. F., Son, N. T., & Chang, L. Y. (2012). Monitoring of rice cropping intensity in the upper Mekong Delta, Vietnam using time-series MODIS data. *Advances in Space Research*, 49(2), 292–301. <https://doi.org/10.1016/j.asr.2011.09.011>
- Coumou, L. (2016). *The Impact of DEM Quality on Predictions of Inundation Risk due to Sea Level Rise in the Mekong Delta, Vietnam*. pp. 76. Guided MSc. Research Report, Utrecht University.
- Deltares, DeltaAlliance, & DWRPIS (2011). *Mekong Delta water resources assessment studies; Vietnam-Netherlands Mekong Delta Masterplan project*. pp. 62.
- Dijk, V., Hilderink, H., Rooij, W., Rutten, M., Ashton, R., Kartikasari, K., & Lan, V. C. (2013). *Land-use change, food security and climate change in Vietnam; A global-to-local modelling approach*. pp. 122.
- Erban, L. E., Gorelick, S. M., & Zebker, H. A. (2014). Groundwater extraction, land subsidence, and sea-level rise in the Mekong Delta, Vietnam. *Environmental Research Letters*, 9, 1–6. <https://doi.org/10.1088/1748-9326/9/8/084010>

- Erban, L. E., Gorelick, S. M., Zebker, H. a, & Fendorf, S. (2013). Release of arsenic to deep groundwater in the Mekong Delta, Vietnam, linked to pumping-induced land subsidence. *Proceedings of the National Academy of Sciences of the United States of America*, 110(34), 13751-13756. <https://doi.org/10.1073/pnas.1300503110>
- Erkens, G., Bucx, T., Dam, R., De Lange, G., & Lambert, J. (2015). Sinking coastal cities. In *Proceedings of the International Association of Hydrological Sciences* (pp. 189–198). Gottingen: Copernicus GmbH. <https://doi.org/10.5194/piahs-372-189-2015>
- Fujihara, Y., Hoshikawa, K., Fujii, H., Kotera, A., Nagano, T., & Yokoyama, S. (2016). Analysis and attribution of trends in water levels in the Vietnamese Mekong Delta. *Hydrological Processes*, 30(6), 835–845.
- Funkenberg, T., Binh, T. T., Moder, F., & Dech, S. (2014). The Ha Tien Plain – wetland monitoring using remote-sensing techniques. *International Journal of Remote Sensing*, 35(8), 2893–2909. <https://doi.org/10.1080/01431161.2014.890306>
- Galloway, D. L., & Sneed, M. (2013). Analysis and simulation of regional subsidence accompanying groundwater abstraction and compaction of susceptible aquifer systems in the USA. *Boletín de La Sociedad Geológica Mexicana*, 65(1), 123–126.
- Giang, N. V., & Hoa, P. V. (2013). Presentation: Mangrove forest monitoring using multi-temporal satellite images Case Study in Ben Tre and Tra Vinh provinces. In *The Second Annual Coastal Forum Building Coastal Resilience to Climate Change in Coastal Southeast Asia* (pp. 18). 15-18 October 2013, Soc Trang province, Vietnam.
- Giri, C., Defourny, P., & Shrestha, S. (2003). Land cover characterization and mapping of continental Southeast Asia using multi-resolution satellite sensor data. *International Journal of Remote Sensing*, 24(21), 4181–4196. <https://doi.org/10.1080/0143116031000139827>
- Gislason, P. O., Benediktsson, J. A., & Sveinsson, J. R. (2006). Random forests for land cover classification. *Pattern Recognition Letters*, 27(4), 294–300. <https://doi.org/10.1016/j.patrec.2005.08.011>
- Higgins, S. A. (2015). Review: Advances in delta-subsidence research using satellite methods. *Hydrogeology Journal*, 23, 587–600. <https://doi.org/10.1007/s10040-015-1330-6>
- Higgins, S., Overeem, I., Tanaka, A., & Syvitski, J. P. M. (2013). Land subsidence at aquaculture facilities in the Yellow River delta, China. *Geophysical Research Letters*, 40(15), 3898–3902. <https://doi.org/10.1002/grl.50758>
- Hung, N. N., Delgado, J. M., Güntner, A., Merz, B., Bárdossy, A., & Apel, H. (2014). Sedimentation in the floodplains of the Mekong Delta, Vietnam Part II: Deposition and erosion. *Hydrological Processes*, 28(7), 3145–3160. <https://doi.org/10.1002/hyp.9855>
- Huth, J., Kuenzer, C., Wehrmann, T., Gebhardt, S., Tuan, V. Q., & Dech, S. (2012). Land cover and land use classification with TWOPAC: Towards automated processing for pixel- and object-based image classification. *Remote Sensing*, 4(9), 2530–2553. <https://doi.org/10.3390/rs4092530>
- IPCC. (2014). *Climate Change 2014: Synthesis Report*. Contribution of Working Groups I, II and III to the Fifth Assessment Report of the Intergovernmental Panel on Climate Change, pp. 151. The Core Writing Team, R. K. Pachauri, & L. Meyer (Eds.). Geneva, Switzerland: IPCC. <https://doi.org/10.1017/CBO9781107415324>
- Isotton, G., Ferronato, M., Gambolati, G., & Teatini, P. (2015). On the possible contribution of clayey inter-layers to delayed land subsidence above producing aquifers. *Proceedings of the International Association of Hydrological Sciences*, 372, 519–523. <https://doi.org/10.5194/piahs-372-519-2015>
- Karila, K., Nevalainen, O., Krooks, A., Karjalainen, M., & Kaasalainen, S. (2014). Monitoring changes in rice cultivated area from SAR and optical satellite images in Ben Tre and Tra Vinh provinces in Mekong Delta, Vietnam. *Remote Sensing*, 6(5), 4090–4108. <https://doi.org/10.3390/rs6054090>
- Khan, A. S., Khan, S. D., & Kakar, D. M. (2013). Land subsidence and declining water resources in Quetta Valley, Pakistan. *Environmental Earth Sciences*, 70(6), 2719–2727. <https://doi.org/10.1007/s12665-013-2328-9>

- Kono, Y. (2001). Canal Development and Intensification of Rice Cultivation in the Mekong Delta : A Case Study in Cantho Province, Vietnam. *Southeast Asian Studies*, 39(1), 70–85.
- Kuenzer, C., Bluemel, A., Gebhardt, S., Quoc, T. V., & Dech, S. (2011). Remote sensing of mangrove ecosystems: A review. *Remote Sensing*, 3(5), 878-928. <https://doi.org/10.3390/rs3050878>
- Kuenzer, C., & Knauer, K. (2013). Remote sensing of rice crop areas. *International Journal of Remote Sensing*, 34(6), 2101–2139. <https://doi.org/10.1080/01431161.2012.738946>
- Leinenkugel, P., Kuenzer, C., Oppelt, N., & Dech, S. (2013). Characterisation of land surface phenology and land cover based on moderate resolution satellite data in cloud prone areas - A novel product for the Mekong Basin. *Remote Sensing of Environment*, 136, 180–198. <https://doi.org/10.1016/j.rse.2013.05.004>
- Liaw, A., & Wiener, M. (2002). Classification and Regression by randomForest. *R News*, 2/3, 18–22. <https://doi.org/10.1177/154405910408300516>
- Liew, S. C., Kam, S. P., Tuong, T. P., Chen, P., Minh, V. Q., & Lim, H. (1998). Application of multitemporal ERS-2 synthetic aperture radar in delineating rice cropping systems in the Mekong River Delta, Vietnam. In *IEEE Transactions on Geoscience and Remote Sensing* (Vol. 36, pp. 1412–1420). <https://doi.org/10.1109/36.718845>
- Lillesand, T. M., Kiefer, R. W., & Chipman, J. W. (2008). *Remote Sensing and Image Interpretation* (6th edition). John Wiley & Sons, pp. 756.
- Liu, C. W., Zhang, S. W., Lin, K. H., & Lin, W. T. (2010). Comparative analysis of temporal changes of multifunctionality benefit of two major rice paddy plains in Taiwan. *Paddy and Water Environment*, 8(2), 199–205. <https://doi.org/10.1007/s10333-010-0198-2>
- Lovelock, C. E., Cahoon, D. R., Friess, D. A., Guntenspergen, G. R., Krauss, K. W., Reef, R., Rogers, K., Saunders, M. L., Sidik, F., Swales, A., Saintilan, N., Thuyen, L. Q. & Triet, T. (2015). The vulnerability of Indo-Pacific mangrove forests to sea-level rise. *Nature*, 526, 559-563. <https://doi.org/10.1038/nature15538>
- Lu, L., & Liao, M. (2008). Subsidence measurement with PS-INSAR techniques in Shanghai Urban. *The International Archives of the Photogrammetry, Remote Sensing and Spatial Information Sciences*, 37(B7), 173–178.
- Minderhoud, P. S. J., Erkens, G., Pham, V. H., Bui, V. T., Erban, L., Kooi, H., & Stouthamer, E. (2017). Impacts of 25 years of groundwater extraction on subsidence in the Mekong delta, Vietnam. *Environmental Research Letters*, 12(6), pp. 13. <https://doi.org/doi.org/10.1088/1748-9326/aa7146>
- Minderhoud, P. S. J., Erkens, G., Pham, V. H., Vuong, B. T., & Stouthamer, E. (2015). Assessing the potential of the multi-aquifer subsurface of the Mekong Delta (Vietnam) for land subsidence due to groundwater extraction. In *International Association of Hydrological Sciences* (pp. 1–4). Copernicus Publications.
- Miyaji, N., Kohyama, K., Otsuka, H., & Kasubuchi, T. (1995). Surface subsidence of peatland in Bibai, central Hokkaido, Japan. *Japanese Journal of Soil Science and Plant Nutrition*, 66(5), 465–473.
- Nesbitt, H. J. (2005). Water Used for Agriculture in the Lower Mekong Basin, MRC Discussion Paper. Mekong River Commission, Vientiane, Lao PDR, pp. 61.
- Nguyen-Thanh, S., Chi-Farn, C., Cheng-Ru, C., Huynh-Ngoc, D., & Ly-Yu, C. (2014). A phenology-based classification of time-series MODIS data for rice crop monitoring in Mekong Delta, Vietnam. *Remote Sensing*, 6(1), 135–156. <https://doi.org/10.3390/rs6010135>
- Nguyen, L. D., & Viet, P. B. (2013). Presentation: Remote Sensing Applications on Land Use, Land Cover and Air Pollution in South Vietnam. In *International Workshop on “Inventory, Modeling and Climate Impacts of Greenhouse Gas emissions (GHG’s) and Aerosols in the Asian Region.”* (pp. 42). 26-28 June 2013, Tsukuba, Japan.
- Nguyen, L. D., Viet, P. B., Binh, T. T., & Thy, P. T. M. (2013). Presentation: Land use, land cover changes in the Mekong Delta, Vietnam. In *Mekong Environmental Symposium* (pp. 32). 5-7 March 2013, Ho Chi Minh City, Vietnam.

- Nguyen, L. D., Viet, P. B., Minh, N. T., Mai-Thy, P.-T., & Phung, H. P. (2011). Change Detection of Land Use and Riverbank in Mekong Delta, Vietnam Using Time Series Remotely Sensed Data. *Journal of Resources and Ecology*, 2(4), 370–374. <https://doi.org/10.3969/j.issn.1674-764x.2011.04.011>
- Nguyen, T. T. H., De Bie, C. A. J. M., Ali, A., Smaling, E. M. A., & Chu, T. H. (2012). Mapping the irrigated rice cropping patterns of the Mekong delta, Vietnam, through hyper-temporal SPOT NDVI image analysis. *International Journal of Remote Sensing*, 33(2), 415–434. <https://doi.org/10.1080/01431161.2010.532826>
- Nguyen, V., Ta, T., & Tateishi, M. (2000). Late holocene depositional environments and coastal evolution of the Mekong River Delta, Southern Vietnam. *Journal of Asian Earth Sciences*, 18(4), 427–439. [https://doi.org/10.1016/S1367-9120\(99\)00076-0](https://doi.org/10.1016/S1367-9120(99)00076-0)
- Nhan, D. K., Be, N. V., & Trung, N. H. (2007). Water use and competition in the Mekong Delta, Vietnam. In T. T. Be, B. T. Sinh, & F. Miller (Eds.), *Challenges to sustainable development in the Mekong Delta: regional and national policy issues and research needs* (pp. 143–188). Bangkok, Thailand: The Sustainable Mekong Research Network (Sumernet).
- Osmanoglu, B., Dixon, T. H., Wdowinski, S., Cabral-Cano, E., & Jiang, Y. (2011). Mexico City subsidence observed with persistent scatterer InSAR. *International Journal of Applied Earth Observation and Geoinformation*, 13(1), 1–12. <https://doi.org/10.1016/j.jag.2010.05.009>
- Panigrahy, S., & Parihar, J. S. (1992). Role of middle infrared bands of Landsat thematic mapper in determining the classification accuracy of rice. *International Journal of Remote Sensing*, 13(15), 2943–2949. <https://doi.org/10.1080/01431169208904092>
- Paruelo, J. M., Jobbagy, E. G., Sala, O. E., Lauenroth, W. K., Burke, I. C., Applications, E., & Feb, N. (1998). Functional and Structural Convergence of Temperate Grassland and Shrubland Ecosystems, 8(1), 194–206.
- Phuong, N. M., & Catacutan, D. (2014). *Land use change analysis in Dien Bien, Son La and Lai Chau provinces, Northwest Vietnam, for the period 2000-2010*. ICRAF Vietnam, CGIAR Research Program on Integrated Systems for the Humid Tropics, pp. 12.
- Piñeiro, G., Perelman, S., Guerschman, J. P., & Paruelo, J. M. (2008). How to evaluate models: Observed vs. predicted or predicted vs. observed? *Ecological Modelling*, 216(3–4), 316–322. <https://doi.org/10.1016/j.ecolmodel.2008.05.006>
- Renaud, R. G., & Kuenzer, C. (2012). Ch. 1 Introduction. In R. G. Renaud & C. Kuenzer (Eds.), *The Mekong Delta System* (pp. 3–5). Springer Netherlands. <https://doi.org/10.1007/978-94-007-3962-8>
- Rodriguez-Galiano, V. F., Ghimire, B., Rogan, J., Chica-Olmo, M., & Rigol-Sanchez, J. P. (2012). An assessment of the effectiveness of a random forest classifier for land-cover classification. *ISPRS Journal of Photogrammetry and Remote Sensing*, 67(1), 93–104. <https://doi.org/10.1016/j.isprsjprs.2011.11.002>
- Rojstaczer, S., & Deverel, S. J. (1995). Land subsidence in drained histosols and highly organic mineral soils in California. *Soil Science Society of America Journal*, 59(4), 1162–1167.
- Sakamoto, T., Nguyen, N. Van, Ohno, H., Ishitsuka, N., & Yokozawa, M. (2006). Spatio-temporal distribution of rice phenology and cropping systems in the Mekong Delta with special reference to the seasonal water flow of the Mekong and Bassac rivers. *Remote Sensing of Environment*, 100(1), 1–16. <https://doi.org/10.1016/j.rse.2005.09.007>
- Sakamoto, T., Phung, C. Van, Kotera, A., Nguyen, D. K., & Yokozawa, M. (2009a). Detection of yearly change in farming systems in the Vietnamese Mekong Delta from MODIS time-series imagery. *Japan Agricultural Research Quarterly*, 43(3), 173–185. <https://doi.org/10.6090/jarq.43.173>
- Sakamoto, T., Phung, C. Van, Kotera, A., Nguyen, K. D., & Yokozawa, M. (2009b). Analysis of rapid expansion of inland aquaculture and triple rice-cropping areas in a coastal area of the Vietnamese Mekong Delta using MODIS time-series imagery. *Landscape and Urban Planning*, 92(1), 34–46. <https://doi.org/10.1016/j.landurbplan.2009.02.002>

- Smith, L. C. (2002). Emerging Applications of Interferometric Synthetic Aperture Radar (InSAR) in Geomorphology and Hydrology. *Annals of the Association of American Geographers*, 92(3), 385–398. <https://doi.org/10.1111/1467-8306.00295>
- Socialist Republic of Vietnam General Statistics Office. (2015). *Statistical Yearbook of Vietnam*. Statistical Publishing House, pp. 114.
- Son, N. T., & Tu, N. A. (2008). Determinants of Land-Use Change: A Case Study from the Lower Mekong Delta of Southern Vietnam. *Electronic Green Journal*, (27), 1–12.
- Space Technology Institute. (2011). *Land use/land cover change assessment in Mekong river delta from 2004-2005 to 2009-2010*. Department of Remote sensing technology - GIS - GPS; Space Technology Institute – VAST, pp. 23.
- Space Technology Institute. (2014). *Land cover change analysis in Ben Tre and Tra Vinh provinces using multi-temporal SPOT 5 satellite images*. Gland, Switzerland: IUCN, pp. 27.
- Syvitski, J. P. M., Kettner, A. J., Overeem, I., Hutton, E. W. H., Hannon, M. T., Brakenridge, G. R., Day, J., Vörösmarty, C., Saito, Y., Giosan, L., Nicholls, R. J. (2009). Sinking deltas due to human activities. *Nature Geoscience*, 2(10), 681-686. <https://doi.org/10.1038/ngeo629>
- Takagi, H., Thao, N. D., & Anh, L. T. (2016). Sea-level rise and land subsidence: Impacts on flood projections for the Mekong Delta's largest city. *Sustainability*, 8(959), 15. <https://doi.org/10.3390/su8090959>
- Tanaka, K. (1995). Transformation of the rice-based cropping patterns in the Mekong Delta: From Intensification to Diversification. *Southeast Asian Studies*, 33(3), 363–378.
- Tho, N., Vromant, N., Hung, N. T., & Hens, L. (2008). Soil salinity and sodicity in a shrimp farming coastal area of the Mekong Delta, Vietnam. *Environmental Geology*, 54(8), 1739–1746. <https://doi.org/10.1007/s00254-007-0951-z>
- Thu, P. M. (2006). Application of remote sensing and GIS tools for recognizing changes of mangrove forests in Ca Mau Province. In *Proceedings of the International Symposium on Geoinformatics for Spatial Infrastructure Development in Earth and Allied Sciences* (pp. 17). Ho Chi Minh City, Vietnam.
- Thu, P. M., & Populus, J. (2007). Status and changes of mangrove forest in Mekong Delta: Case study in Tra Vinh, Vietnam. *Estuarine, Coastal and Shelf Science*, 71, 98–109. <https://doi.org/10.1016/j.ecss.2006.08.007>
- Tong, P. H. S., Auda, Y., Populus, J., Aizpuru, M., Al Habshi, A., & Blasco, F. (2004). Assessment from space of mangroves evolution in the Mekong Delta, in relation to extensive shrimp farming. *International Journal of Remote Sensing*, 25(21), 4795–4812. <https://doi.org/10.1080/01431160412331270858>
- Toothaker, L. E. (1993). Multiple Comparison Procedures. Sage University Paper series on Quantitative Applications in the Social Sciences, 07-089. Newbury Park, California: SAGE, pp. 96.
- Tosi, L., Teatini, P., Carbognin, L., & Brancolini, G. (2009). Using high resolution data to reveal depth-dependent mechanisms that drive land subsidence: The Venice coast, Italy. *Tectonophysics*, 474(1–2), 271–284. <https://doi.org/10.1016/j.tecto.2009.02.026>
- Tran, H. P., Adams, J., Jeffery, J. A. L., Nguyen, Y. T., Vu, N. S., Kutcher, S. C., Kay, B. H., Ryan, P. A. (2010). Householder perspectives and preferences on water storage and use, with reference to dengue, in the Mekong Delta, southern Vietnam. *International Health*, 2(2), 136–142. <https://doi.org/10.1016/j.inhe.2009.12.007>
- Tran, H., Tran, T., & Kervyn, M. (2015). Dynamics of land cover/land use changes in the Mekong Delta, 1973-2011: A Remote sensing analysis of the Tran Van Thoi District, Ca Mau Province, Vietnam. *Remote Sensing*, 7(3), 2899–2925.
- Tri, V. K. (2012). Ch. 3 Hydrology and Hydraulic Infrastructure Systems in the Mekong Delta, Vietnam. In F. G. Renaud & C. Kuenzer (Eds.), *The Mekong Delta System* (pp. 49–82). Springer Netherlands. <https://doi.org/10.1007/978-94-007-3962-8>
- Trimble. (2015a). *eCognition® Developer 9.1.3. Reference Book*. Trimble Germany GmbH, München, Germany, pp 531.

- Trimble. (2015b). *eCognition*® Developer 9.1.3. User Guide. Trimble Germany GmbH, München, Germany, pp. 265.
- Tuong, T. P., Kam, S. P., Hoanh, C. T., Dung, L. C., Khiem, N. T., Barr, J., & Ben, D. C. (2003). Impact of seawater intrusion control on the environment, land use and household incomes in a coastal area. *Paddy and Water Environment*, 1(2), 65–73. <https://doi.org/10.1007/s10333-003-0015-2>
- USGS (2010). LSDS Science Research and Development (LSRD), bulk order. US Geological Survey, espa.cr.usgs.gov (accessed 14-11-2016).
- USGS (2012). *Landsat Ecosystem Disturbance Adaptive Processing System (LEDAPS) Algorithm Description Document V1.3*. pp. 20.
- USGS (2016a). Frequently Asked Questions about the Landsat missions. US Geological Survey, landsat.usgs.gov/what-are-band-designations-landsat-satellites (accessed 14-03-2017).
- USGS (2016b). LandsatLook Viewer. US Geological Survey, landsatlook.usgs.gov/viewer (accessed 14-11-2016).
- USGS (2016c). Earth Explorer. US Geological Survey, earthexplorer.usgs.gov (accessed 18-11-2016).
- USGS (2017). *Product guide Landsat surface reflectance-derived spectral indices V3.5*. pp. 31. Retrieved from https://landsat.usgs.gov/sites/default/files/documents/si_product_guide.pdf
- van Asselen, S., Stouthamer, E., & van Asch, T. W. J. (2009). Effects of peat compaction on delta evolution: A review on processes, responses, measuring and modeling. *Earth-Science Reviews*, 92(1–2), 35–51. <https://doi.org/10.1016/j.earscirev.2008.11.001>
- Vellinga, P., & Leatherman, S. P. (1989). Sea level rise, consequences and policies. *Climatic Change*, 15(1), 175–189. <https://doi.org/doi:10.1007/BF00138851>
- Vo, Q. T., Oppelt, N., Leinenkugel, P., & Kuenzer, C. (2013). Remote sensing in mapping mangrove ecosystems - an object-based approach. *Remote Sensing*, 5(1), 183–201. <https://doi.org/10.3390/rs5010183>
- Wagner, F., Tran, V. B., & Renaud, F. G. (2012). Ch. 7 Groundwater resources in the Mekong Delta: availability, utilization and risks. In R. G. Renaud & C. Kuenzer (Eds.), *The Mekong Delta System* (pp. 201–220). Springer Netherlands. <https://doi.org/10.1007/978-94-007-3962-8>
- Warner, K., Ehrhart, C., Sherbinin, A. De, Adamo, S., & Chai-Onn, T. (2009). *In Search of Shelter: Mapping the Effects of Climate Change on Human Migration and Displacement*. pp. 36.
- Wen, L. J. (1995). Paddy field, groundwater and land subsidence. In *American Water Resources Association annual summer symposium on water resources and environmental hazards*. Honolulu: American Water Resources Association, Herndon, VA (United States).
- Wilder, M., & Phuong, N. T. (2002). The status of aquaculture in the Mekong Delta region of Vietnam: Sustainable production and combined farming systems (Proceedings of International Commemorative Symposium-70th Anniversary of The Japanese Society of Fisheries Science). *Fisheries Science*, 68(June), 847–850.
- WISDOM (2014). WISDOM information system. WISDOM project, web portal designed and maintained by the German Aerospace Center (DLR), wisdom.eoc.dlr.de/Elvis (accessed 19-09-2016).
- Xiao, X., Boles, S., Frolking, S., Li, C., Babu, J. Y., Salas, W., & Moore, B. (2006). Mapping paddy rice agriculture in South and Southeast Asia using multi-temporal MODIS images. *Remote Sensing of Environment*, 100(1), 95–113. <https://doi.org/10.1016/j.rse.2005.10.004>
- Yan, X. X., Gong, S. L., Zeng, Z. Q., Yu, J. Y., Shen, G. P., & Wang, T. J. (2002). Relationship between building density and land subsidence in Shanghai urban zone. *Hydrogeology and Engineering Geology*, 29(6), 21–25.
- Yuill, B., Lavoie, D., & Reed, D. (2009). Understanding subsidence processes in coastal Louisiana. *Journal of Coastal Research*, SI(54), 23–36. <https://doi.org/10.2112/SI54-012.1.intensity>

APPENDICES


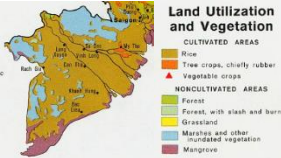

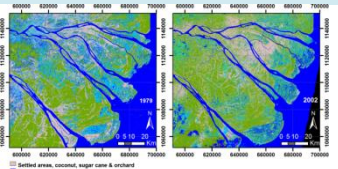

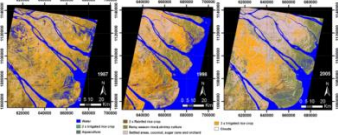
Laura Coumou – 3963942

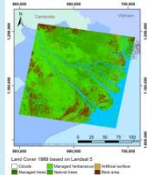
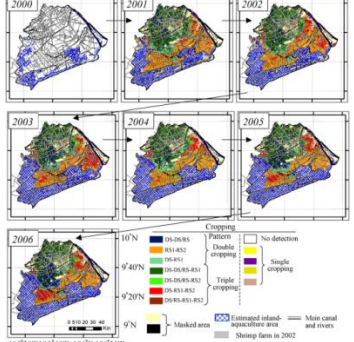
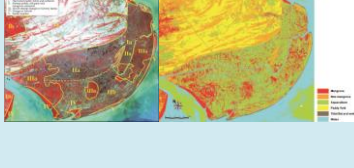
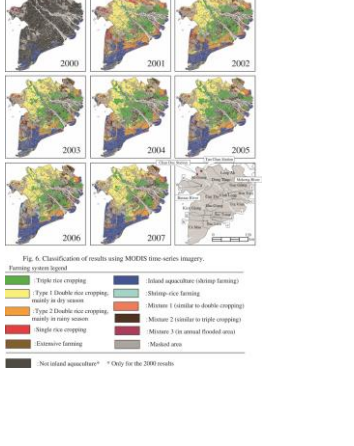
Master Thesis – Final Version July 3, 2017

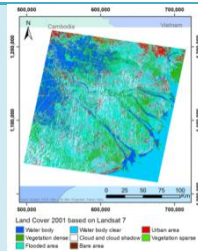
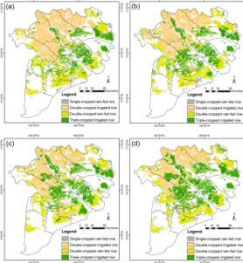
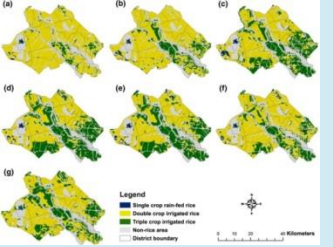
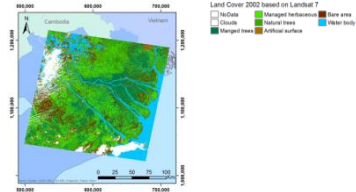
**Relating Land Subsidence to Land Use through Machine
Learning using Remote-Sensing Derived Data**

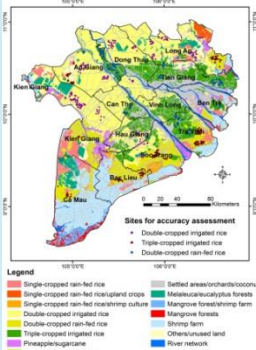

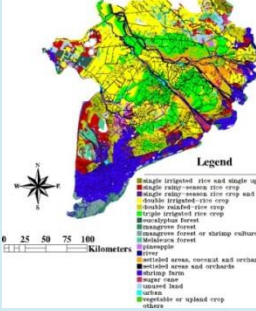
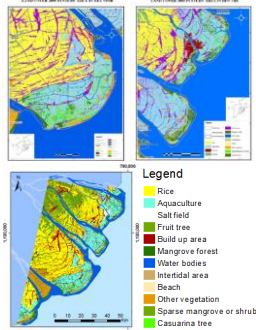
A case study in the Mekong Delta, Vietnam

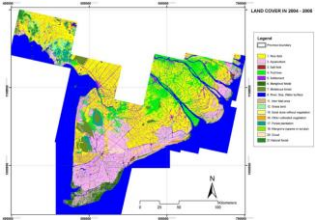
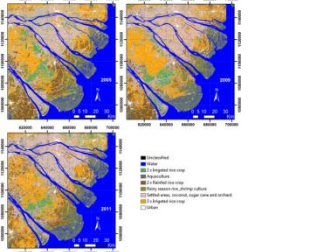
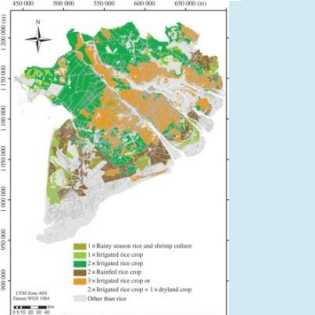
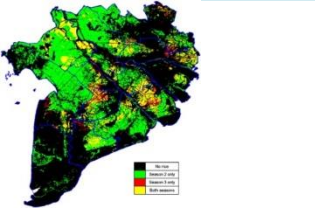
Appendix 1 Overview of pre-existing land-use/cover maps

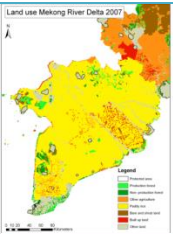
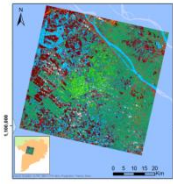
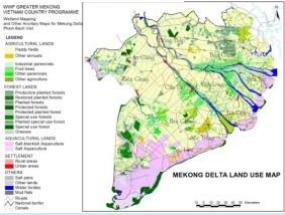
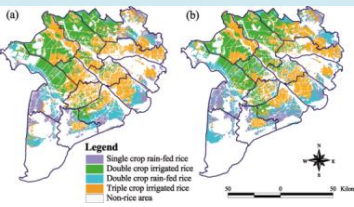
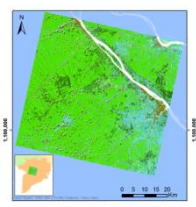
Nr.	Map Title	Year	Extent	Scale	Format	How created?	Source	Quality/Notes	Thumbnail
1	Republic of Vietnam Vegetation Map	1969	Vietnam	1:1.000.000	High res. - scan	-	National Geographic Service Dalat, first edition and printing 1969	- few classes for VMD	
2	Land Utilization and Vegetation	1972	Vietnam	-	Low res. - scan	-	-	- few classes for VMD	
3	Bassin Inferieur du Mekong – Carte de l'occupation du sol (Lower Mekong Basin – Land use map)	1972/1973	Vietnam	1:1.000.000	High res. - scan	-	Committee for coordination of investigations of the Lower Mekong Basin, printed by the French National Geographical Institute.	- few classes for VMD	
4	Figure 4. The land-use classifications from the Landsat imagery	1979/2000	Eastern coast VMD + up-stream	Resp. 60m and 15m	Image in scientific article, geotiff	Pixel-based unsupervised ISODATA classifier Data: Landsat 3 MSS, and 7 ETM	(Karila et al., 2014)	- only 3 land-use classes: all rice, aquaculture and settled areas + coconut + sugar cane + orchard	
5	Hiện trạng sử dụng đất đến năm 1980 (Land use status up to 1980, in Vietnamese)	1980/1981	Vietnam	1:1.000.000	High res. - scan	-	N.T. Vu et al., 1981. General Department of Land Administration	- few classes for VMD - Vietnamese legend	
6	Figure 3. The land-use classifications from the SPOT imagery	1987/1999/2005	Eastern coast VMD	20m	Image in scientific article, geotiff	Pixel-based unsupervised ISODATA classification Data: mosaicked SPOT 1, 2 & 3 images.	(Karila et al., 2014)	- Accuracy 2005 = 88.2% (based on ground truth 7-10 Oct 2013) - multiple rice classes	

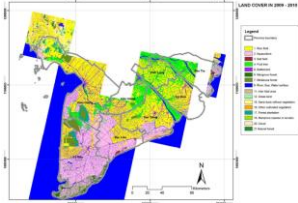
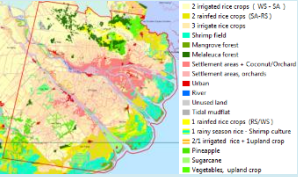

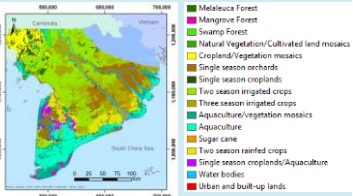

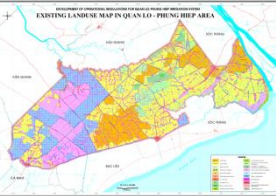
7	Land cover classification for the Mekong Delta from Landsat 5 data from 1989	1989	VMD	Ca. 30m	Geotiff	Pixel-based, semi-automatic, supervised, decision tree classification of a Landsat 5 image	WISDOM Information System (credit: German Remote Sensing Data Center (DFD), German Aerospace Center (DLR)) (Sakamoto et al., 2009b)	<ul style="list-style-type: none"> - unflooded image - vegetation classes based on density, not type - overall accuracy = 94%, individual classes > 85% 	
8	Fig. 9. Annual changes in rice-cropping patterns estimated by the WFCS method from 2001 to 2006, and the inland-aquaculture area estimated by the WFIA method from 2000 to 2006	2000 2001 2002 2003 2004 2005 2006	Hau Giang + Bac Lieu + Soc Trang	250m	Small images in scientific article	Complex classification scheme using 3 wavelet based filters: WFCS, WFFI and WFIA) for which EVI and LSWI are used Data: 7-yr MODIS (MOD09) composite surf. refl. time-series	(Sakamoto et al., 2009b)	<ul style="list-style-type: none"> - small maps - 11 rice cropping system classes + aquaculture - accuracy not included, but district statistics used to get optimal result 	
9	Figure 8. Main land-use classes in Tra Vinh area	2000 22 Jan	Tra Vinh	10 or 20m	Low res. images in scientific article	Thresholding using NDVI, NDWI & SWIR and maximum likelihood classification Data: SPOT4 HRVIR	(Tong et al., 2004)	<ul style="list-style-type: none"> - maps have very low resolution - average accuracy nearly 80% based on ground data & forest map 	
10	Fig. 6 Classification of results using MODIS time-series imagery	2000 2001 2002 2003 2004 2005 2006 2007	VMD	250m	Small images in scientific article	Complex classification flow chart; classification using 4 wavelet filters (WFCS, WFCP, WFFI and WFIA) & a decision tree. Data: MODIS composite surf. refl. time-series	(Sakamoto et al., 2009a)	<ul style="list-style-type: none"> - 10 LU classes, focus on rice and shrimp; other areas masked using Sub-NIAPP LU map of 2002. - area rice, shrimp-rice farming & inland aquac. agreed well with provincial statistics ($R^2 \geq 0.96$). Some prov.: large error margin in estimate. - Mixture classes: pixels have no discriminating EVI feature. 	

11	Land cover classification (LCC) for the Mekong Delta from Landsat 7 ETM+ 2001	2001	VMD except south and NW	Ca. 30m	Geotiff	Unsupervised pixel-based classification with the C5 algorithm using 3000 training data points from image itself. Data: Landsat 7 ETM+	WISDOM Information System (Credit: German Aerospace Center (DLR))	<ul style="list-style-type: none"> - many small clouds - during flooding - 4 land classes; vegetation classes based on density, not type - Overall classification accuracy = 95% 	
12	Figure 8. Spatial distributions of rice cropping systems in the study area.	2001 2002 2003 2004 2005 2006 2007 2008 2009 2010 2011 2012	VMD	500 m	Small images in scientific article	Smooth MODIS EVI time-series for whole period, mask non-rice area based on EVI thresholds, classify rice using timing and number of peaks in EVI Data: MODIS Surf. refl. 8-day L3 time-series (MOD09A1)	(Nguyen-Thanh et al., 2014)	<ul style="list-style-type: none"> - 4 rice only LU classes - overall accuracies & κ: 81.4% & 0.75 for 2002, 80.6% & 0.74 for 2006, 85.5% & 0.81 for 2012 using ground ref. data - relative error in area (REA) between the MODIS-derived rice areas and the government's rice area statistics = 0.9–15.9% 	
13	Fig. 5. Distribution of rice cropping systems for (a) 2001; (b) 2002; (c) 2003; (d) 2004; (e) 2005; (f) 2006; and (g) 2007	2001 2002 2003 2004 2005 2006 2007	An Giang, Dong Thap	250m	Small images in scientific article	Endmember extraction & training in a linear mixture model (LMM) for classification of rice systems, take largest abundance, apply majority filter Data: MODIS NDVI	(Chen et al., 2012)	<ul style="list-style-type: none"> - 4 land-use rice classes - small maps - overall accuracy = 90.1% Kappa coef. = 0.7 - Based on ground-truth (e.g. 2002 Sub-NIAPP LU map) 	
14	Land cover classification for the Mekong Delta from Landsat 7 data from 2002	2002	VMD except south and NW	30m	Geotiff	Semi-automatic, supervised, decision tree classification based on Tasseled Cap of a Landsat 7 ETM+ image	WISDOM Information System (credit: German Remote Sensing Data Center (DFD), German Aerospace Center (DLR))	<ul style="list-style-type: none"> - in S and W large cloud - 5 land classes; vegetation classes based on density, not type 	

15	Figure 1. The 2002 land-cover map of the study area showing different rice cropping systems and the locations of sampling sites used for the accuracy assessment of the classification results	2002	VMD	1:125,000	Image in - scientific article & shapefile	(Nguyen-Thanh et al., 2014) Most probable original source: Sub-NIIAPP	- 14 land-use classes - focus on rice - includes field data points for rice cropping system - image in paper differs slightly from shapefile	
16	Mekong Delta: Land-use	2002	VMD	-	Tiff-file -	Sub-National Institute of Agriculture Planning & Projection (Sub-NIIAPP), Document AA1403 – W ICEM 2014	- 11 land-use classes	
17	Fig. 3. Land-use map for 2002	2002	VMD	30m	Image in scientific article Data sources, i.a. Landsat 7 ETM+ (02-2002), map of agricultural LU 2002 of 12 provinces at 1:50,000 & 1:100,000 scale (Prov. dep. MARD, dep. MONRE), LU map 2000 at 1:250,000 scale (MONRE), 2 field surveys in 2002.	(Sakamoto et al., 2006) Originally from Sub-NIIAPP	- 19 land-use classes	
18	'Land cover 2005 in study area in Tra Vinh' and 'Land cover 2005 in study area in Ben Tre'	2004 1 Dec and 2005 22 Feb	Tra Vinh and Ben Tre	10m	Image in ppt per province & shapefile for entire area Isodata classification and post classification (class combination, LCT assignment, filtering/smoothing) Data: SPOT 5	(Giang & Hoa, 2013) for maps; (Space Technology Institute, 2014) for full report on classification	- 11 land-use classes - legend unreadable in Tra Vinh image in ppt: see shapefile and map of Ben Tre - area outside the study areas less accurately classified	

19	Land cover classification for the Mekong Delta of 13 SPOT 5 scenes from 2004 and 2005	2004 - VMD 2005	10m	Imagine file	Unsupervised ISO-data classification of 13 SPOT 5 scenes. Grouping of the 100 classes for final classes. Ref. data: topographic & LU maps.	Tiff-file: WISDOM Information System Report: (Space Technology Institute, 2011)	- Some cloud remnants - 16 LU classes	
20	Figure 2. The land-use classifications from ENVISAT ASAR imagery	2005 2009 2011 VMD + up-stream	Eastern coast Ca. 74 m	Image in scientific article, geotiff	Unsupervised ISODATA classifier. Data: 9 - 15 ENVISAT ASAR WSM images per year. Accuracy using ground truth 7-10 Oct 2013.	(Karila et al., 2014)	- Incl. rice farming system - Accuracy: 2011 = 80.0%, 2009 = 82.7%, 2005 = 77.3%	
21	Figure 3. 2005 land use map of the Mekong delta with focus on rice areas	2005 VMD	30m?	Image in scientific article	Data: all cloud-free Landsat ETM+ images	(Nguyen et al., 2012) Originally: National Institute Of Agricultural Planning And Projection (NIAPP), 2008 (Ho Chi Minh City, Vietnam: Vien Quy hoach va Thiet ke Nong nghiep (NIAPP) – MARD)	- 7 rice LU classes	
22	Fig. 9. Rice map derived from the STC images for Season 2 and Season 3.	2007 VMD	Probably 92m	Image in scientific article	Radar algorithm & classification thresholds: see paper. Data: ENVISAT ASAR WS	(Bouvet & Le Toan, 2011)	- 4 rice LU classes, for 2 seasons - Overall classification accuracy = 75.8%	

23	Land use Mekong River Delta 2007	2007	VMD	-	Image in report	Unknown (RS & field data according to Dijk et al. (2013))	(Dijk et al., 2013) Originally: FIPI (Forest Inventory Planning Institute)	- 7 land-use classes - very little detail: mainly 'paddy rice'	
24	Combined land cover / land use classification (LC-LUC) for the Mekong Delta from SPOT5 data 2007	2007 Dec	Can Tho	10 m	Geotiff	Unsupervised pixel-based image classification using the C5 classifier based on training points derived from SPOT 5 image itself	WISDOM Information System (credit: German Aerospace Center (DLR))	- small clouds - 6 land classes	
25	Mekong Delta Land Use Map	2008	VMD	-	No	-	(Nguyen et al., 2013) Part of WWF Greater Mekong Vietnam Country Programme, Wetland Mapping and Other Ancillary Maps for Mekong Delta	- 22 land-use classes, many forest classes based on usage - no distinction within rice - some classes difficult to distinguish	
26	-	2008	VMD	250m	Image in scientific paper	Source: MODIS NDVI time-series. Filtering noise with wavelet filter >> parametric & nonparametric class. algorithms: the max. likelihood classifier (MLC) & support vector machines (SVMs)	(Chen et al., 2011)	- 5 land-use classes: rice only - SVMs better than MLC - overall accuracy & Kappa coef. for SVMs = 89.7% & 0.86, for MLC = 76.2% & 0.68	
27	Land cover classification for Can Tho province from SPOT 5 data from 2009	2009 6 Feb	Can Tho	10m	Geotiff	Semi-automatic and supervised decision tree classification approach (using e.g. indices NDVI, GI and MTVI)	WISDOM Information System (credit: German Remote Sensing Data Center (DFD), German Aerospace center (DLR))	- 4 LU classes, 'managed herbaceous cover' dominant, small clouds - Accuracy individual classes > 80% (only lower for 'artificial surface')	

28	Land cover classification for the Mekong Delta of 11 SPOT 5 scenes from 2009 and 2010	2009-2010	VMD	10m	Imagine file	Unsupervised ISO-data classification of 11 SPOT 5 scenes. Grouping of the 100 classes for final classes. Ref. data: topographic & LU maps	Tiff-file: WISDOM Information System Report: (Space Technology Institute, 2011)	- 16 LU classes - Overall accuracy 87.89% - Producer & user accuracy between 0% and 100%	
29	LUT 2010	2010	VMD	-	Yes	-	Received from Dr. V.P.D. Tri at 29 nov. 2016	- many LU classes	
30	Rice paddy mapping using MODIS (2010)	2010	VMD	-	Image in power-point presentation	MODIS data, method unknown	(Nguyen & Viet, 2013) Original source: Pham Duy Tien, AGU	- colors largely undistinguishable - 6 land-use classes	
31	Land use/land cover map of the Mekong Delta, 2010 (MODIS 500)	2010	VMD	500m	Geotiff	Classification of cloud-free MODIS 8-day refl. composites & EVI time-series classification	WISDOM Information System	- 16 land-use classes	
32	Mekong delta: forest cover	2010	VMD	-	Tiff-file	-	Sub-Forest Inventory and Planning Institute (Sub-FIPI), Document AAS1403 – WB ICEM 2014	- forest and its uses cover only	
33	Existing landuse map in Quan Lo - Phung Hiep area - Development of operational regulations for Quan Lo - Phung Hiep Irrigation system	2010	Quan Lo Phung Hiep (a.o. Soc Trang & Bac Lieu)	1:120,000	A0 image with English legend, map-info files	Map of Institute for Agriculture Planning (IAP) (purchased by SIWRP), supplemented with field data & data from local officials	Integrated Coastal Management Programme (ICMP) (received from Mr. Ly Minh Dang)	- Resolution/accuracy up to singly land plot (but no validation available) - For displaying, use layer 'QLPH_Landused_New', field 'loadat'	

34	Land cover classification for parts of the provinces Can Tho, Dong Thap, Vinh Long (Rapid Eye, 2011)	2011 27 Jan	parts of Can Tho, & surroundings	6.5 m	Shapefile	Supervised object-based C5.0 algorithm in TWOPAC (twinned object & pixel-based automated classification chain) using Rapid Eye data	(Huth et al., 2012) & WISDOM information system (credit: German Remote Sensing Center (DFD), German Aerospace Center (DLR))	<ul style="list-style-type: none"> - some small clouds - about 10 land use classes - overall accuracy > 85% - accuracy individual classes >80% 	
35	'Land cover 2012 in study area in Tra Vinh' and 'Land cover 2012 in study area in Ben Tre'	2012 14 Feb and 2012 2 Jan	Tra Vinh and Ben Tre	10m	Image in ppt per province & shapefile for entire area	Isodata classification and post classification (class combination, LCT assignment, filtering/smoothing) Data: SPOT 5	(Giang & Hoa, 2013) for maps; (Space Technology Institute, 2014) for full report on classification	<ul style="list-style-type: none"> - 11 land-use classes - legend unreadable in Tra Vinh image: see shapefile and map of Ben Tre - area outside the study areas less accurately classified - Overall accuracy = 82.7% based on google earth ground control points 	
36	-	2012?	VMD	-	Image in power-point presentation	-	(Nguyen et al., 2013)	<ul style="list-style-type: none"> - 17 land-use classes - no distinction within rice 	
37	Land use/land cover map of the Mekong Delta, 2014 (MODIS 500)	2014	VMD	500m	Geotiff	Classification of cloud-free MODIS 8-day refl. composites & EVI time-series classification	WISDOM Information System	<ul style="list-style-type: none"> - 10 land-use classes; 3 rice classes 	

Appendix 2 Land-use classification: segmentation settings

The first step in object-based image classification is to create the objects to be classified. This step is called segmentation. In this study, multiresolution segmentation in eCognition Developer 9.1.3. has been used. This algorithm adds neighboring pixels together until the user defined homogeneity criterion is exceeded. The **homogeneity criterion** measures how homogeneous the object is within itself, for which it takes both spectral information and the shape of the segments into account (Trimble, 2015b). Areas with little variation result in larger segments. The **scale parameter** determines the maximum allowed heterogeneity for the segments. The larger this parameter, the larger the segments in an image. However, the same scale parameter results in different segments sizes between different images. The relative importance of spectral homogeneity to shape homogeneity determines the total homogeneity criterion. The **spectral homogeneity** is based on the standard deviation of the selected layers and the **shape homogeneity** is based on the deviation from a compact or smooth shape (Trimble, 2015b).

The segmentation settings used for the classification of the clouds for the cloud masks and the classification of LU itself are given in Table 11 and Table 12 respectively. In the case of the classification of the clouds, the different cloud types with different sizes, shapes and thicknesses required different segment sizes to classify all clouds. Hence, three multi-resolution segmentation levels with different scale parameters (100, 200 and 500) were created. In the case of the land-use classification, only one segmentation could be used for the random forest classification. In order to allow for larger variation in the object size and shape, which is needed to optimally represent the areas of each LU class, two subsequent segmentations were performed. At first, a multiresolution segmentation was performed, followed by a spectral difference segmentation. The latter merges segments with similar spectral characteristics.

Table 11 Multiresolution segmentation settings for each classification of clouds (step 2 in Figure 11).

Setting	Value
Scale parameter	100, 200 and 500
Shape parameter	0
Layers	blue, green, red, NIR, SWIR1, SWIR2, TIR, EVI and NDMI

Table 12 Segmentation settings for each land-use classification (step 3 in Figure 11).

Segmentation	Setting	Value
Multiresolution	Scale parameter	200
	Shape parameter	0
Spectral difference	Maximum spectral difference parameter	200 (100 for 2009)
Both	Layers	blue, green red, NIR, SWIR1, SWIR2, EVI and NDMI

Appendix 3 Land-use type code per land-use class

The digital LU maps contain LU type codes (numbers) instead of the full names or acronyms. The names corresponding to each code is given in this appendix.

Table 13 Land-use (LU) classes used in for classification including LU type code.

LU group	LU type/subclass	Acronym	LU type code
Aquaculture	Aquaculture	Aqua	1
	Dry-season crop – mainly rice	Dry-S Rice	2
	Partly dry-season crop – mainly rice	P Dry-S Rice	3
Agriculture	Harvested dry-season crop – mainly rice	H Dry-S Rice	6
	Bare field in dry season	Bare Field	4
	Mixed crops – non-rice	Mix No Rice	5
	Mangrove	Mangr	7
Forest	Melaleuca forest	Mel For	14
	Orchard	Orch	8
	Urban dense	Urb D	9
Urban area	Urban open	Urb O	10
	Urban linear features (dikes, roads with buildings and gardens)	Urb Line	11
	Water body (river/sea)	Water	12
Water	Water: small channels	Water Ch	13
	Wasteland/marsh	Waste	16
Other	Cloud remnants	Cloud	15

Appendix 4 Spectral and spatial characteristics of all LU classes

Aquaculture

The aquaculture group and type mainly consists of shrimp farms, but it also includes fish farms. The man-made ponds are generally concentrated close to the sea. The farms are on average about 5 ha and have a length of a few tens of meters to hundreds of meters. They have a structured geometric pattern: a small dike at the border with more or less rectangular strips of planted rows of mangrove trees inside which are surrounded by the water of the actual shrimp pond (Vo et al., 2013). The cover of mangrove varies strongly. When shrimps are grown, the ponds are filled with water and have a relatively low reflectance in all Landsat 5 TM spectral bands. In case of turbid water or dry ponds, the reflectance is higher.

Agriculture

The reflectance characteristics of crops, among which rice, cyclically vary over the growing season (Figure 20). The first few weeks, the surface characteristics dominate the reflectance, as the (rice) plants are still small (Kuenzer & Knauer, 2013). The values of the vegetation indices EVI and NDVI are still very low (Nguyen-Thanh et al., 2014): the near infrared (NIR) reflectance is only slightly lower than the reflectance in the visible spectrum (VI) (Kuenzer & Knauer, 2013). After about 12 weeks, the NDVI and EVI are maximum as the NIR and VI reflectance reaches their respective maximum and minimum (Kuenzer & Knauer, 2013). After maturity, the plant becomes yellowish and the NIR reflectance decreases (Kuenzer & Knauer, 2013); the EVI and NDVI lower again (Nguyen-Thanh et al., 2014). Hence, the vegetation indices are important for classifying crops among which rice. Though, Panigrahy and Parihar (1992) pointed out that the classification accuracy of rice increases substantially if short-wave infrared (SWIR) bands are also used.

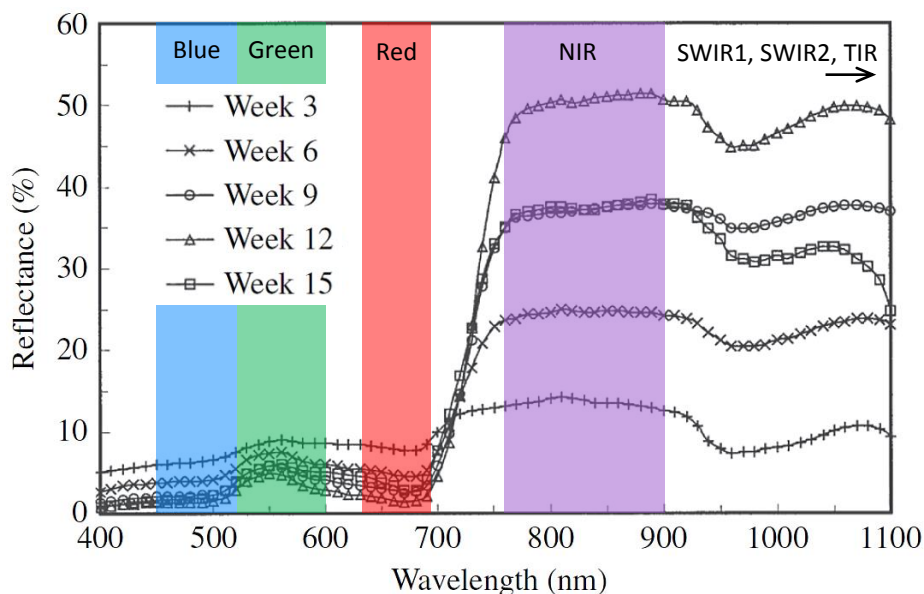


Figure 20 Reflectance signatures of rice plants at different growth stages. The spectral range of the Landsat 5 bands are indicated. After Chang et al. (2005) in Kuenzer & Knauer (2013).

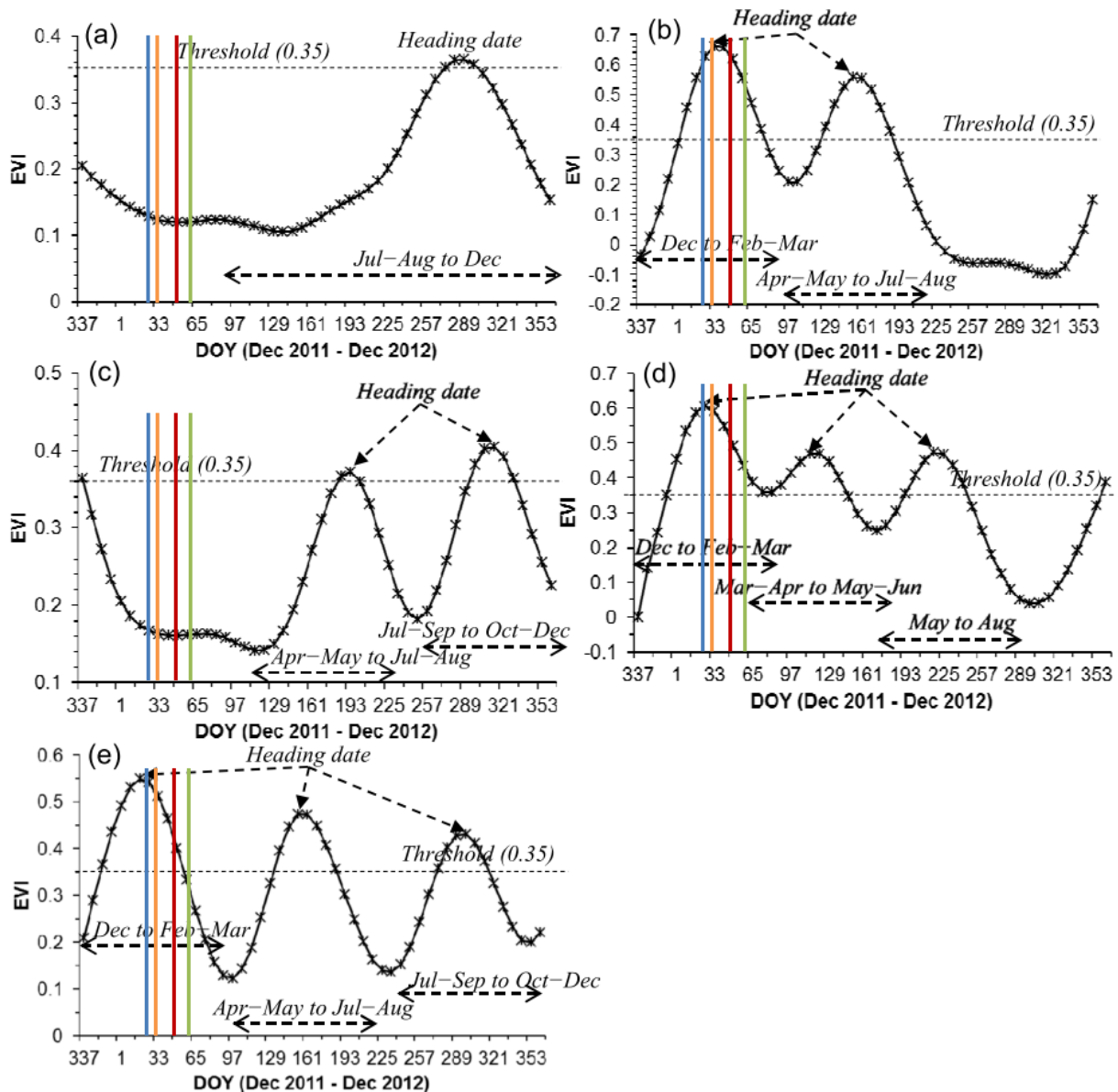


Figure 21 Smoothened EVI (Enhanced Vegetation Index) profiles for (a) single-cropped rain-fed rice, (b) double-cropped irrigated rice, (c) double-cropped rain-fed rice (d) and (e) triple-cropped irrigated rice. DOY = day of the year. Vertical lines correspond to the julian day of the four Landsat 5 TM images used in this study: 1988 = blue, 1996 = red, 2006 = green, 2009 = orange. Note that the profiles are based on data of mainly 2012. After Son et al. (2014).

Nowadays, multiple crops per year are grown in the VMD, but the crop phenology (timing and number of crops) differs over the delta (Table 14). This is reflected in differences in reflectance over space and time. The temporal variation in the EVI vegetation index for different rice systems is shown in Figure 21. It is assumed that these profiles are representative for all years. Hence, all images used in our study roughly overlap with a peak in EVI – and herewith a peak in rice growth – if a dry season crop was grown, as intended.

The dry-season crop class can be distinguished based on the peak in the vegetation indices. This peak is not only a peak over time, but also spatially in comparison to other LU classes. Besides, the shape of the fields surrounded by generally bare dikes is characteristic. Based on pre-existing LU maps of 2000 to 2010, the largest area of this class is covered by rice, but this cannot directly be confirmed from the Landsat images, especially for the images of before 2000. Hence, the subclass(es) have the suffix ‘mainly rice’.

The timing of the dry-season crop peak varies spatially, because the start of the rice cycle depends on the local water distribution scheme (Kuenzer & Knauer, 2013) and herewith on the yearly and spatially varying flood duration and intensity for the flood-prone upper VMD (Sakamoto et al., 2009a). Accordingly, the dry-season crop may just have been harvested in the satellite image to be classified, especially for the relatively late satellite image in 2006. The spectral characteristics change significantly, but based on their dark appearance in a false color image respective to the surrounding unharvested fields, these fields can generally still be classified as dry-season crop. Due to their different characteristics, these fields get a separate class for the LU classification. Afterwards, this class will be merged to the first agriculture class.

The ‘bare fields in dry season’ form another agriculture subclass. Most probably, these fields are covered with rice – or another crop – during the rainy season. The absence of vegetation in the satellite images results in low EVI values, negative NDVI values, a bright appearance in true and false color images and a much higher SWIR1 and SWIR2 reflection than most other classes if the soil is dry. If the soil is wet, the reflectance is significantly lower and the area appears dark. In some cases, a region shows an alternation of fields with and without dry-season crops within small areas. The classification aims at classifying LU at delta scale and therefore, these relatively small scale inter-field alternations are taken together as one class: partly dry-season crop – mainly rice.

The last agriculture subclass is ‘mixed crops – non-rice’, which contains all other crops than rice. Generally, this class has a lower NIR reflection and hence lower vegetation indices than rice. Besides, the fields seem to be smaller and the spectral difference between fields is larger than for rice. For a part, the non-rice crops are grown on the dune ridges parallel to the coast. These patches can be discriminated based on their elongated shape and their relatively high reflection of especially SWIR1 and SWIR2 compared to their surroundings.

Table 14 Rice-cropping seasons and systems. ¹ Son et al. (2014), ² Bouvet & Le Toan (2011).

Season	Vietnamese name ²	From ¹	To ¹	Cropping system ¹	Main location ²
rainy / winter	Mùa	July/Aug.	Dec./Jan.	1x rain-fed rice	Coastal
winter–spring	Đông Xuân	Nov./Dec.	Feb./March	2x irrigated rice 3x irrigated rice	Inland
spring–summer		March/April	May/June	3x irrigated rice	
summer–autumn	Hè Thu	April/May	July/Aug.	2x irrigated rice 2x rain-fed rice 3x irrigated rice	Inland + coastal
autumn–winter	Thu Đông	July/Sept	Oct./Dec.	2x rain-fed rice 3x irrigated rice	Inland

Forest

The forest class is subdivided in three subclasses which contain mainly trees.

The first forest subclass is mangrove. Multiple definitions of mangrove exist (Kuenzer et al., 2011). In this case, the salt-tolerant forest parallel to the coastline is meant, not a specific species growing in such a forest. Generally, the spectral reflectance of mangroves is determined by multiple mangrove species and a tidally varying contribution of water and soil (Kuenzer et al., 2011). In a mangrove in Tra Vinh, the five most abundant groups of mangrove species are *Avicennia* and *Sonneratia*, *Excoecaria agallocha*, *Derris trifoliata*, *Phoenix paludosa* and *Nypa* (Thu & Populus, 2007). Besides, *Rhizophora* and *Laguncularia* can often be found in mangroves in and around the VMD (Kuenzer et al., 2011). Some “mangroves” are actually forestry farms – they are planted by humans for the wood – or mixed low density mangrove with shrimp farms (Thu, 2006).

The spectral signature of each species in the mangrove forest varies over time and space due to changes in biophysical and chemical conditions (Kuenzer et al., 2011). Differences between mangrove species are minimal in the visible part of the spectrum and relatively large in the near-infrared region (Figure 22). However, irrespective of these variations within mangrove forests, Giri et al. (2003) indicate that mangrove forest is easy to discriminate by its specific spectral signature. In the Landsat images, mangrove can be discriminated from other vegetated classes by its lower NIR reflectance than e.g. rice. In addition, its location is crucial: bordering the sea or in between aquacultural ponds.

The second forest subclass is melaleuca forest. *Melaleuca* trees are found in fresh-water flooded conditions and hence mainly occur inland. Their spectral characteristics are similar to mangrove. The main difference between melaleuca forest and mangroves is their spatial distribution: inland versus bordering the coast respectively. Compared to the other inland LU classes, melaleuca forest has relatively low SWIR1 and SWIR2 reflectance values.

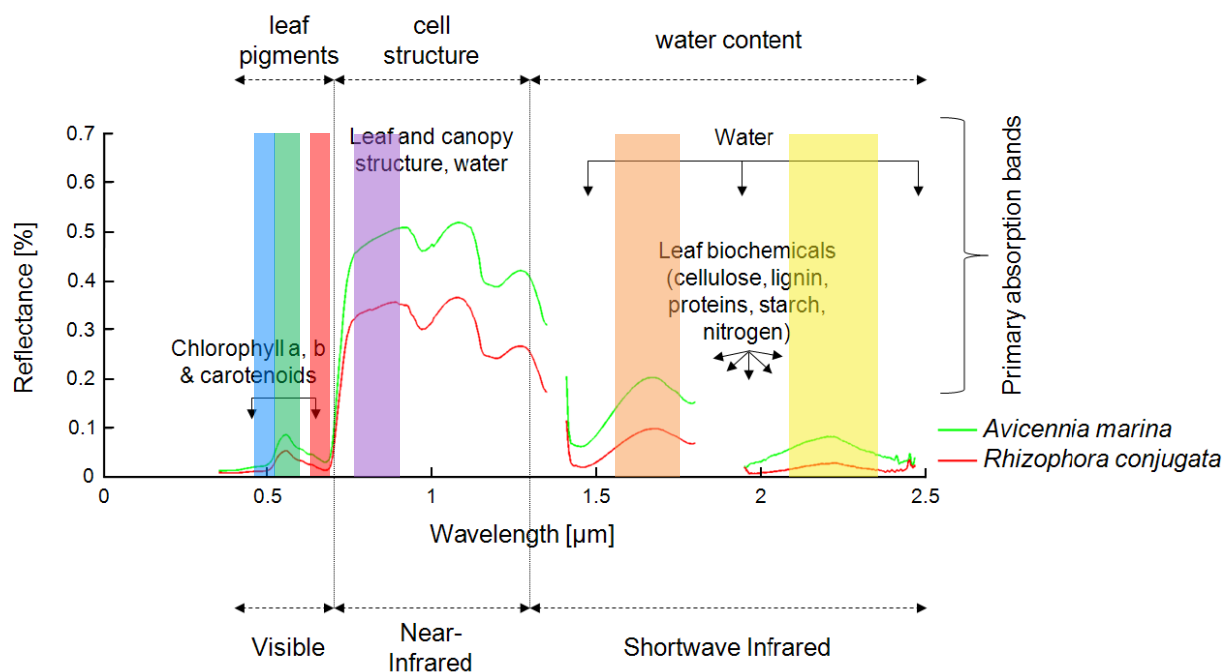


Figure 22 Spectral signature of two mangrove species, measured using a with spectrometer in the province Ca Mau in the the VMD in January 2010. Parameters which influence the signature are indicated. Colored bands correspond to spectral bands of Landsat 5 TM (l-r: blue, green, red, NIR, SWIR1, SWIR2. TIR out of reach at the right). After Kuenzer et al. (2011).

The last forest subclass is orchard. This class comprises the orchards of fruit gardens and pineapple plants, which form the dominant LU close to the main river branches. Examples of fruit trees which are grown are coconut and banana trees (Binh et al., 2005). Generally, the orchards are close to a residential house. If these houses are not part of a clear cluster in the satellite image, these houses are classified as part of the larger scale orchard class. Spectrally, the subclass orchard is similar to the other vegetated classes. However, in this case its NIR reflectance and herewith vegetation indices values are in between those of dry-season rice and melaleuca forest. Additionally, the spectral variation within a patch of this class is slightly larger than for a dry-season rice patch. Spatially, their wide patches close to the main rivers and in strips along canals and roads are characteristic.

Urban areas

The two main subclasses of the urban-areas class are 'urban dense' and 'urban open'. Urban dense corresponds to cities with many buildings close to each other and little vegetation. This class has a high reflection in all bands from VI to SWIR and herewith contrasts to its surroundings, forming local spots. Urban open corresponds to the periphery of cities and other areas with many buildings combined with vegetation. Spectrally, this class is a combination of urban dense and vegetation classes. As a consequence, the spectral variation within a patch of this class is high. Spatially, they form spots along roads and canals and border dense urban areas.

The third urban subclass is 'linear features', which corresponds to dikes and roads with some buildings and gardens along it. These features are spectrally similar to the other urban classes, with high overall reflectance – especially in SWIR – for the roads and bare dikes, which is partly mixed with spectral characteristics of vegetation and water of small channels which are too small to be identified as such.

Water

Water absorbs most of the electromagnetic radiation, resulting in a very low overall reflectance. In the VMD, the water is turbid, resulting in a higher reflection in especially the visible spectrum. Water has the lowest NIR, SWIR1, SWIR2, EVI and NDVI values of all classes except aquaculture. This applies to both water classes: water bodies of rivers and seas, and small channels. The water subclasses can be separated from each other based on their spatial characteristics. The channels – which include man-made straight canals and natural, meandering creeks – are very small and elongated. On the other hand, the water bodies have larger dimensions and are less elongated. The water classes can be separated from aquaculture based on their overlap with the rivers and ocean shapefiles and the fact that aquaculture ponds are alternated with small dikes and mangrove patches.

Other

The other two classes are 'wasteland/marsh' and clouds.

Wasteland refers to areas which are uncultivated or barren; unused by humans. A large part of wasteland in the VMD consists of marshes. Most wasteland/marsh has been reclaimed over the last decades and turned into agricultural fields. Hence, this class is not often found in recent LU maps. In the satellite images, this class lacks many human made patterns and has gradually varying spectral characteristics of wet to dry surfaces and none to some vegetation. The wastelands/marshes are generally located in or at the borders of the flood plain of the main river branches.

Most clouds are masked before classification, but some – especially small – clouds are missed by the masking and are incorporated in the classification. Clouds have very high overall reflectance values. However, if the cloud is thin, a part of the signal from below the cloud can also reach the satellite sensor, and a mixed signal is observed.

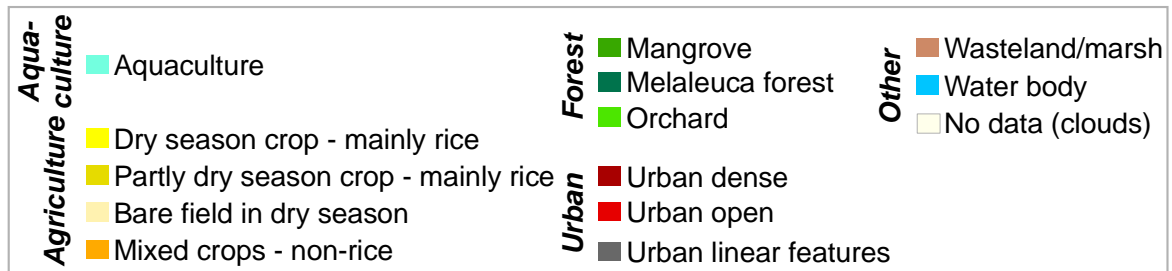
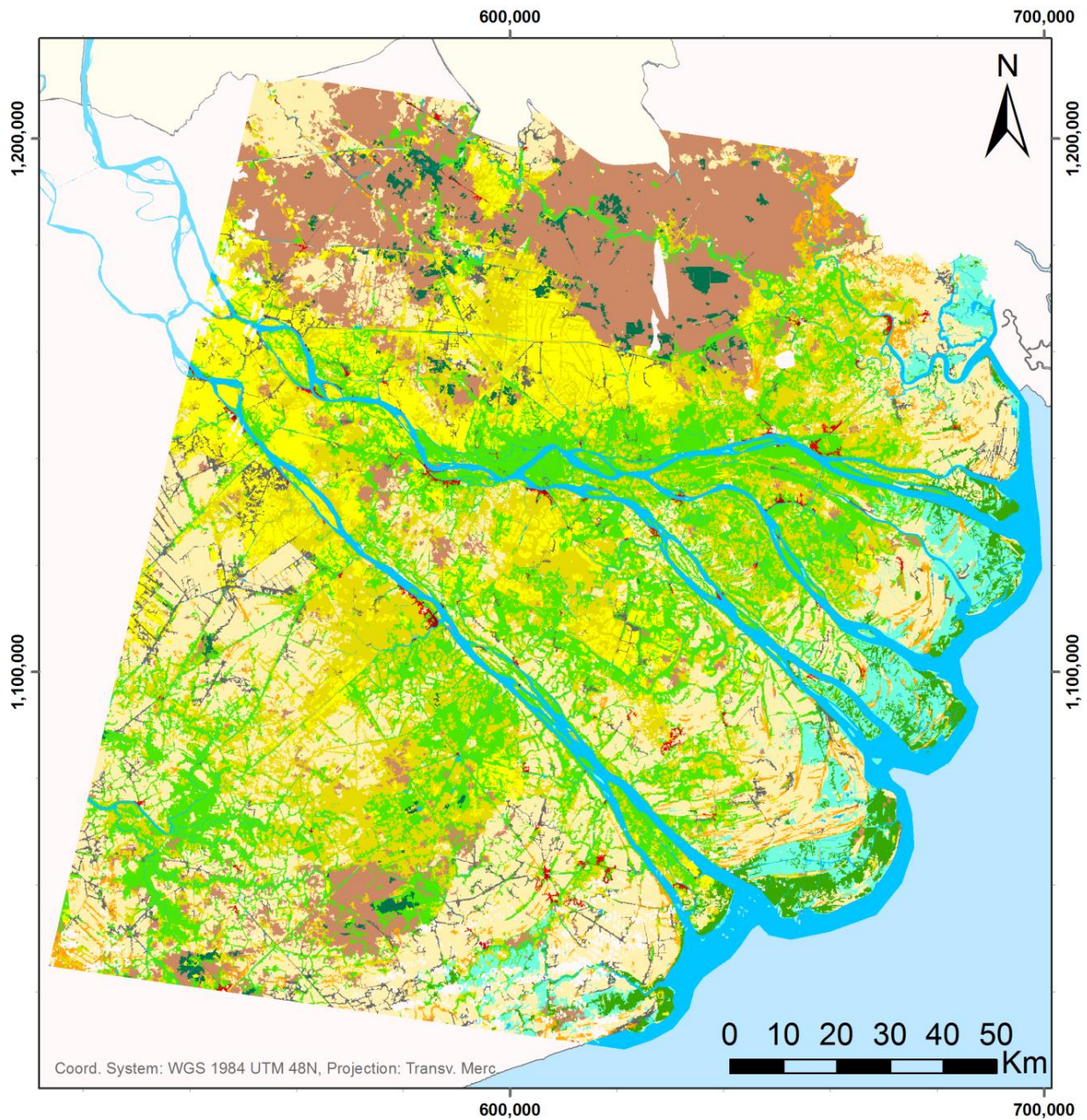
Appendix 5 Spectral and spatial segment features used for land use classification

For explanation on the features, see Trimble (2015a).

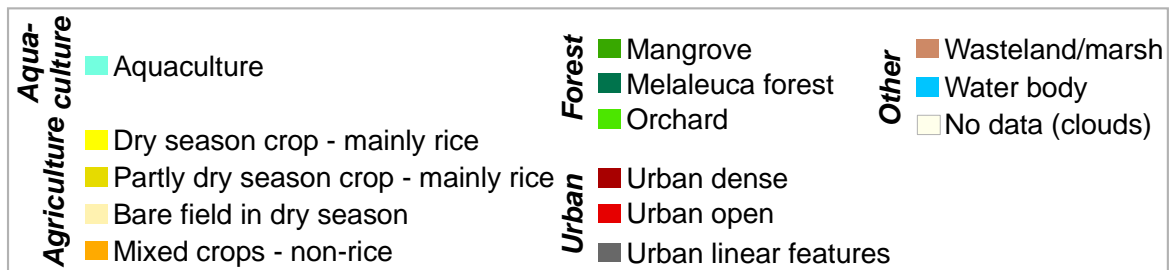
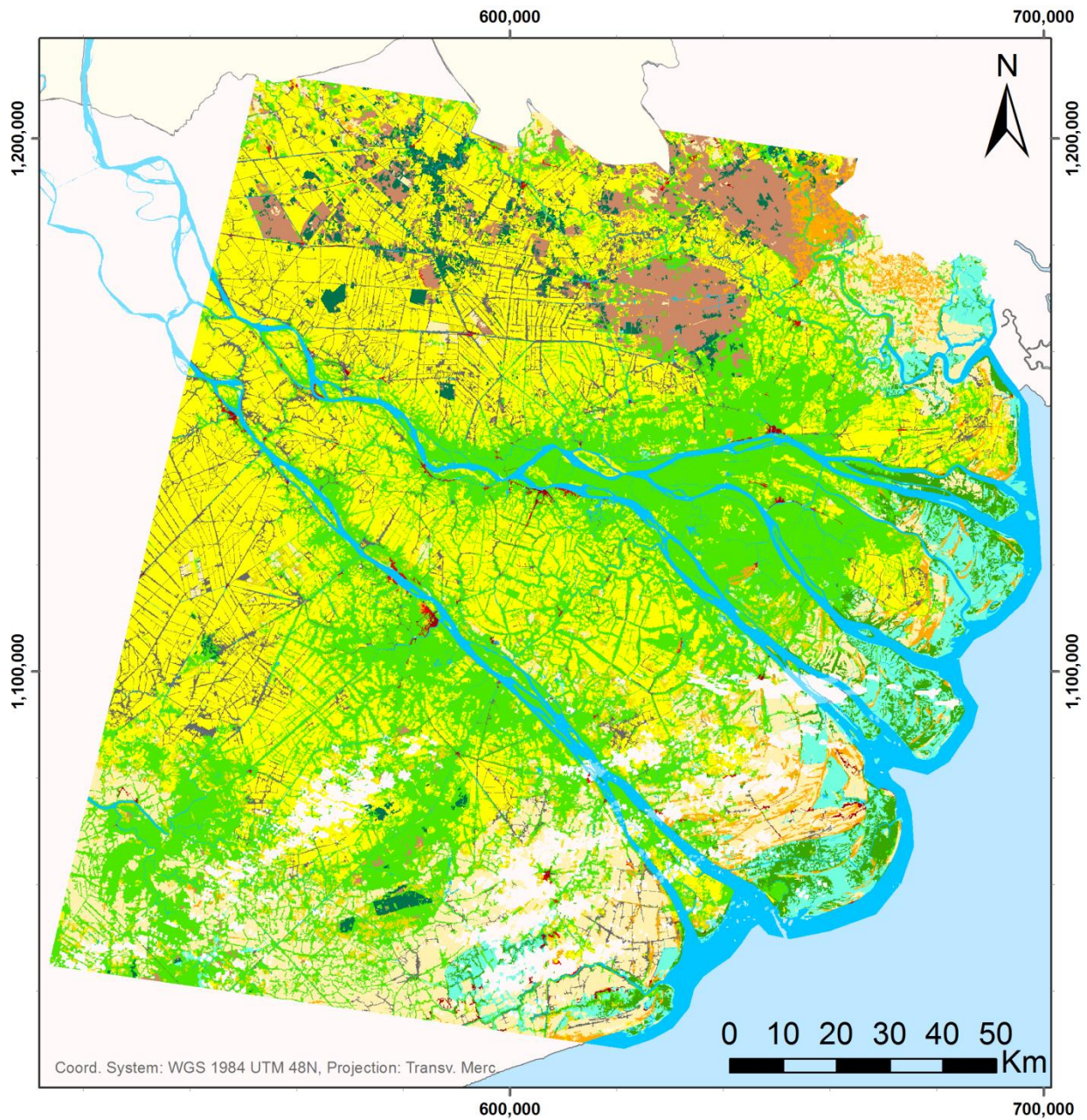
Layer values	<i>Mean</i>	Blue
		Green
		Red
		NIR
		SWIR1
		SWIR2
		TIR
		EVI
	<i>Mode</i>	Blue
		Green
		Red
		EVI
	<i>Standard deviation</i>	NIR
		SWIR1
		EVI
	<i>Quantile</i>	50 th EVI quantile
5 th NDVI quantile		
<i>Pixel-based</i>	Max. red pixel value	
	Max. SWIR1 pixel value	
<i>To neighbors</i>	Mean difference to neighbors: NDVI	
	Mean difference to darker neighbors: NDVI	
	Mean difference to darker neighbors: red	
	Mean difference to brighter neighbors: EVI	
Geometry	<i>Extent</i>	Area (pixels)
		Border length (pixels)
		Length (pixels)
		Length/width (pixels)
		Width (pixels)
	<i>Shape</i>	Asymmetry
		Border index
		Compactness
		Density
		Elliptic fit
		Radius of largest enclosed ellipse
		Radius of smallest enclosing ellipse
		Rectangular fit
	Roundness	
	<i>Based on skeletons</i>	Shape index
		Curvature/length (only main line)
Length of main line (no cycles) (pixels)		
Length/width (only main line)		
Maximum branch length (pixels)		
Standard deviation curvature (only main line)		
Position	<i>Distance to vectors</i>	Distance to Ocean (outline) (pixels)
		Distance to Rivers (centroid) (pixels)
Thematic attributes	<i>Minimum overlap (%) with thematic polygons</i>	Ocean
		Rivers
Customized		$(2 * \text{width} + 2 * \text{length}) / \text{border length}$
		Area/border length
		Mean difference to neighbors: 5% quantile of NDVI
		Mean of neighboring mean NDVI
		Standard deviation EVI divided by mean EVI

Appendix 6 Land-use classification maps

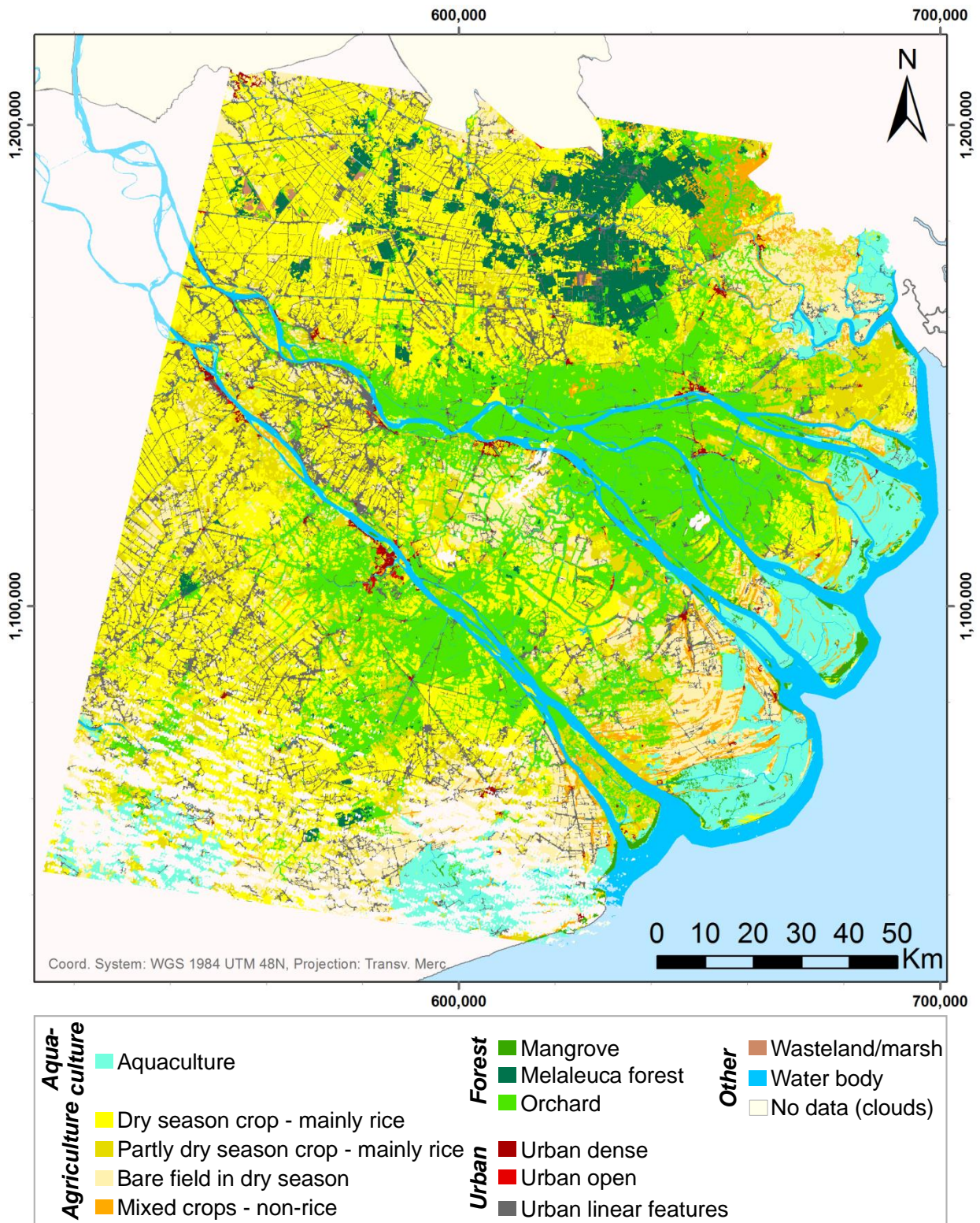
A6.1. Land-use map of 1988



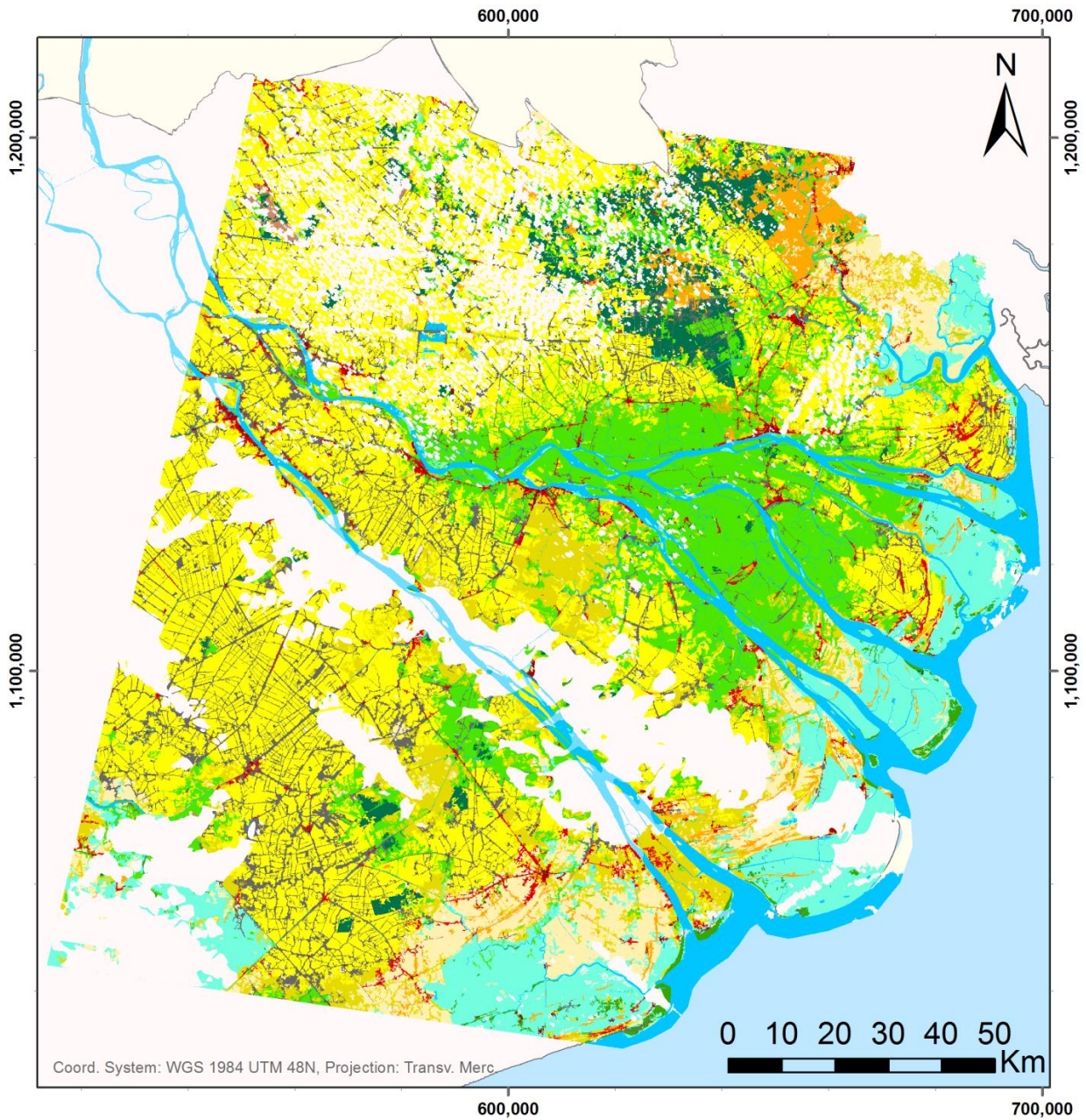
A6.2. Land-use map of 1996



A6.3. Land-use map of 2006



A6.4. Land-use map of 2009



Aqua-culture	Aquaculture	Forest	Mangrove	Other	Wasteland/marsh
	Dry season crop - mainly rice		Melaleuca forest		Water body
	Partly dry season crop - mainly rice		Orchard		No data (clouds)
	Bare field in dry season	Urban	Urban dense		
Mixed crops - non-rice	Urban open				
			Urban linear features		

Appendix 7 Areal statistics of the land-use classification maps

Table 15 Areal statistics of the classified land-use maps. Note that the total area varies as a result of a different area excluded from the statistics due to cloud cover. This also resulted in some differences in area of a certain class between different years.

	Area (km ²)				Area (%)			
	1988	1996	2006	2009	1988	1996	2006	2009
Aquaculture	850	954	1669	1980	3.5%	4.0%	7.3%	10.2%
Dry-S Rice	2002	7296	6514	6558	8.2%	30.8%	28.4%	33.9%
Partly Dry-S Rice	4124	828	2464	1674	16.9%	3.5%	10.7%	8.6%
Bare Field	6147	2768	2498	1415	25.2%	11.7%	10.9%	7.3%
Mix No Rice	429	440	519	532	1.8%	1.9%	2.3%	2.7%
Agriculture	12702	11332	11995	10179	52.2%	47.9%	52.3%	52.6%
Mangrove	524	584	165	124	2.2%	2.5%	0.7%	0.6%
Melaleuca For.	263	422	903	610	1.1%	1.8%	3.9%	3.2%
Orchard	4314	6481	4414	2948	17.7%	27.4%	19.2%	15.2%
Forest	5101	7487	5481	3682	20.9%	31.7%	23.9%	19.0%
Urban Dense	15	48	103	99	0.1%	0.2%	0.5%	0.5%
Urban Open	83	51	14	328	0.3%	0.2%	0.1%	1.7%
Urban Line	533	1019	1982	1560	2.2%	4.3%	8.6%	8.1%
Urban	631	1118	2099	1987	2.6%	4.7%	9.1%	10.3%
Wasteland	3130	957	23	18	12.9%	4.0%	0.1%	0.1%
Water	1935	1805	1676	1521	7.9%	7.6%	7.3%	7.9%
Total	24350	23653	22942	19367	100%	100%	100%	100%

Appendix 8 Confusion matrices land-use maps based on validation segments

All LU maps have been validated using a part of the randomly selected segments similar to those used for the classification itself. Each map has three confusion matrices. The first is calculated internally in the random forest classification using the out-of-bag segment samples, the second and third are based on the separate validation segments. The third confusion matrix is corrected for the varying area of the validation segments. The **accuracy** – or producer’s accuracy or recall – is the percentage of the total number of segments classified as a certain class in the reality which is classified in the same way in the map. The **reliability** – or user’s accuracy or precision – is the percentage of the total number of points classified as a certain class in the map which is classified in the same way in the field.

A8.1. Confusion matrices land-use classification 1988

Table 16 Confusion matrix of the land-use map of 1988 based on the out-of-bag segments in the random forest classification. The numbers indicate the number of segments that have the same class in the ‘ground truth’ validation set as in the classification (green) or the number of deviating segments (red). Overall accuracy in lower right corner, κ coefficient = 0.74. Full class names: see Table 4.

		Reference land-use class																Total	Reliability
		Dry-s Aqua	P dry- rice	H dry- s rice	Bare field	Mix no rice	Mel Mangr	Orch	Urb D	Urb O	Urb Line	Water	Water Ch	Waste	Cloud				
Predicted land-use class	Aqua	42	0	0	0	2	0	0	0	0	0	0	0	0	0	1	0	45	93%
	Dry-s rice	0	83	3	0	0	0	1	0	8	0	0	1	0	1	0	0	97	86%
	P dry-s rich	0	1	61	1	6	4	1	0	11	0	1	3	0	1	3	0	93	66%
	H dry-s rice	1	0	3	3	3	0	0	0	0	0	1	0	0	0	4	0	15	20%
	Bare field	5	0	6	0	197	0	0	0	0	0	0	0	0	0	5	0	213	92%
	Mix no rice	0	0	6	0	4	17	2	0	3	0	0	1	0	0	2	0	35	49%
	Mangr	1	0	2	0	0	0	42	0	2	0	0	0	0	0	0	0	47	89%
	Mel for	0	0	1	0	0	0	0	27	2	0	0	0	0	0	4	0	34	79%
	Orch	0	6	12	0	0	4	3	1	72	0	0	1	0	0	0	0	99	73%
	Urb D	0	0	0	0	14	0	0	0	0	1	1	0	0	0	0	0	16	6%
	Urb O	0	0	2	0	6	0	0	0	0	0	7	0	0	1	0	0	16	44%
	Urb Line	0	1	5	0	2	1	1	0	1	0	0	17	0	2	0	0	30	57%
	Water	2	0	0	0	0	0	0	0	0	0	0	0	12	2	1	0	17	71%
	Water ch	3	0	0	0	0	0	0	0	0	0	0	1	0	49	0	0	53	92%
	Waste	0	0	7	0	7	0	0	6	1	0	0	1	0	0	50	0	72	69%
	Cloud remn	0	0	1	0	7	0	0	0	0	0	0	0	0	0	0	13	21	62%
	Total		54	91	109	4	248	26	50	34	100	1	9	26	12	56	70	13	903
Accuracy		78%	91%	56%	75%	79%	65%	84%	79%	72%	100%	78%	65%	100%	88%	71%	100%		88%

Table 17 Confusion matrix of the land-use map of 1988 based on the separate validation segments. The numbers indicate the number of segments that have the same class in the 'ground truth' validation set as in the classification (green) or the number of deviating segments (red). Overall accuracy in lower right corner, κ coefficient = 0.69. Full class names: see Table 4.

		Reference land-use class																Total	Reliability
		Aqua	Dry-s rice	P dry-s rice	H dry-s rice	Bare field	Mix no rice	Mangr	Mel for	Orch	Urb D	Urb O	Urb Line	Water	Water Ch	Waste	Cloud		
Predicted land-use class	Aqua	22	0	0	0	5	0	1	0	0	0	0	0	0	0	3	0	31	71%
	Dry-s rice	0	34	1	0	0	0	1	0	4	0	0	1	0	0	0	0	41	83%
	P dry-s rich	0	2	24	3	7	0	0	0	1	0	1	1	0	1	3	0	43	56%
	H dry-s rice	0	0	1	0	1	0	0	0	0	0	0	0	0	0	0	0	2	0%
	Bare field	0	0	5	1	89	1	0	0	1	6	2	3	0	1	0	2	111	80%
	Mix no rice	0	0	6	0	0	13	0	0	2	0	0	1	0	0	0	0	22	59%
	Mangr	0	0	0	0	0	0	21	0	1	0	0	0	0	0	0	0	22	95%
	Mel for	0	1	1	1	0	0	0	16	1	0	0	0	0	0	0	4	24	67%
	Orch	0	11	6	0	0	2	0	1	37	0	0	1	0	0	0	0	58	64%
	Urb D	0	0	0	0	0	0	0	0	0	2	0	1	0	0	0	0	3	67%
	Urb O	0	0	1	0	0	0	0	0	0	0	4	0	0	0	0	0	5	80%
	Urb Line	0	0	0	0	1	1	0	0	0	0	0	4	0	1	0	0	7	57%
	Water	0	0	0	0	0	0	0	0	0	0	0	0	2	0	0	2	4	50%
	Water ch	0	0	0	0	0	0	0	0	1	0	0	2	6	23	0	0	32	72%
	Waste	0	0	1	2	3	0	0	0	1	0	0	0	0	0	25	0	32	78%
	Cloud remn	0	0	0	0	0	0	0	0	0	0	0	0	0	0	0	6	6	100%
Total	22	48	46	7	106	17	23	17	49	8	7	14	8	26	35	10	443		
Accuracy	100%	71%	52%	0%	84%	76%	91%	94%	76%	25%	57%	29%	25%	88%	71%	60%		73%	

Table 18 Confusion matrix of the land-use map of 1988 based on the separate validation segments, corrected for the segment area. The numbers indicate the area (ha) of segments that have the same class in the 'ground truth' validation set as in the classification (green) or the number of deviating segments (red). Overall accuracy in lower right corner, κ coefficient = 0.74. Full class names: see Table 4.

		Reference land-use class																Total	Reliability
		Aqua	Dry-s rice	P dry-s rice	H dry-s rice	Bare field	Mix no rice	Mangr	Mel for	Orch	Urb D	Urb O	Urb Line	Water	Water Ch	Waste	Cloud		
Predicted land-use class	Aqua	6174	0	0	0	526	0	63	0	0	0	0	0	0	0	80	0	6843	90%
	Dry-s rice	0	3454	47	0	0	0	42	0	353	0	0	664	0	0	0	0	4560	76%
	P dry-s rich	0	83	13367	153	236	0	0	21	0	13	21	0	101	199	0	0	14194	94%
	H dry-s rice	0	0	47	0	63	0	0	0	0	0	0	0	0	0	0	0	110	0%
	Bare field	0	0	480	24	5294	15	0	0	7	317	100	105	0	11	0	31	6384	83%
	Mix no rice	0	0	298	0	0	1582	0	0	166	0	0	83	0	0	0	0	2129	74%
	Mangr	0	0	0	0	0	0	2566	0	47	0	0	0	0	0	0	0	2613	98%
	Mel for	0	21	103	31	0	0	0	1398	53	0	0	0	0	0	0	274	1880	74%
	Orch	0	1703	621	0	0	79	0	94	5551	0	0	22	0	0	0	0	8070	69%
	Urb D	0	0	0	0	0	0	0	0	0	300	0	15	0	0	0	0	315	95%
	Urb O	0	0	173	0	0	0	0	0	0	0	257	0	0	0	0	0	430	60%
	Urb Line	0	0	0	0	65	165	0	0	0	0	0	748	0	59	0	0	1037	72%
	Water	0	0	0	0	0	0	0	0	0	0	0	0	15229	0	0	27	15256	100%
	Water ch	0	0	0	0	0	0	0	0	19	0	0	45	15283	1300	0	0	16647	8%
	Waste	0	0	66	45	110	0	0	0	97	0	0	0	0	0	21997	0	22315	99%
	Cloud remn	0	0	0	0	0	0	0	0	0	0	0	0	0	0	0	29	29	100%
	Total	6174	5261	15202	253	6294	1841	2671	1492	6314	617	370	1703	30512	1471	22550	87	102812	
Accuracy	100%	66%	88%	0%	84%	86%	96%	94%	88%	49%	69%	44%	50%	88%	98%	33%		77%	

A8.2. Confusion matrices land-use classification 1996

Table 19 Confusion matrix of the land-use map of 1996 based on the out-of-bag segments in the random forest classification. The numbers indicate the number of segments that have the same class in the 'ground truth' validation set as in the classification (green) or the number of deviating segments (red). Overall accuracy in lower right corner, κ coefficient = 0.78. Full class names: see Table 4.

		Reference land-use class																Total	Relia- bility
		Dry-s Aqua	P dry- rice	H dry- s rice	Bare field	Mix no rice	Mel Mangr	Mel for	Orch	Urb D	Urb O	Urb Line	Water Water	Water Ch	Waste	Cloud			
Predicted land-use class	Aqua	48	0	0	0	1	0	0	1	0	0	0	0	0	0	0	1	51	94%
	Dry-s rice	0	170	2	0	0	0	1	8	0	0	1	0	0	0	0	0	182	93%
	P dry-s rich	1	8	32	1	7	3	0	1	12	1	0	1	0	0	0	0	68	47%
	H dry-s rice	2	0	2	9	1	0	0	1	2	0	0	0	0	0	1	0	18	50%
	Bare field	2	0	4	3	107	1	0	0	0	0	0	0	0	0	2	0	119	90%
	Mix no rice	0	0	3	0	1	31	0	0	6	0	0	1	0	0	2	0	44	70%
	Mangr	0	0	0	0	0	1	47	0	3	0	0	0	0	0	0	0	51	92%
	Mel for	0	0	0	0	0	1	0	25	5	0	0	0	0	0	6	0	37	68%
	Orch	1	6	6	0	1	4	5	0	94	0	0	2	0	1	2	0	122	77%
	Urb D	0	0	0	0	3	0	0	0	1	11	1	0	0	0	0	0	16	69%
	Urb O	0	0	4	0	7	0	0	0	2	1	6	1	0	1	0	0	22	27%
	Urb Line	0	3	0	0	3	2	0	0	4	0	0	27	0	0	1	0	40	68%
	Water	1	0	0	0	0	0	0	0	0	0	0	0	20	4	0	1	26	77%
	Water ch	0	0	0	0	0	0	0	0	0	0	0	1	0	50	0	0	51	98%
	Waste	1	0	3	0	3	0	0	0	4	0	0	0	0	0	43	0	54	80%
	Cloud remn	0	0	2	0	1	0	0	0	0	0	0	0	2	0	0	18	23	78%
Total	56	187	58	13	135	43	52	28	142	13	7	34	22	56	57	21	924		
Accuracy	86%	91%	55%	69%	79%	72%	90%	89%	66%	85%	86%	79%	91%	89%	75%	86%		80%	

Table 20 Confusion matrix of the land-use map of 1996 based on the separate validation segments. The numbers indicate the number of segments that have the same class in the 'ground truth' validation set as in the classification (green) or the number of deviating segments (red). Overall accuracy in lower right corner, κ coefficient = 0.77. Full class names: see Table 4.

		Reference land-use class																Total	Relia- bility
		Aqua	Dry-s rice	P dry- s rice	H dry- s rice	Bare field	Mix no rice	Mel Mangr	Mel for	Orch	Urb D	Urb O	Urb Line	Water Water	Water Ch	Waste	Cloud		
Predicted land-use class	Aqua	22	0	1	1	1	0	0	0	0	0	0	0	1	0	0	0	26	85%
	Dry-s rice	0	87	2	0	0	0	0	3	0	0	0	0	0	0	0	0	92	95%
	P dry-s rich	0	2	8	2	2	1	0	2	0	3	0	0	0	0	3	0	23	35%
	H dry-s rice	0	0	2	3	2	0	0	0	0	0	0	0	0	0	1	0	8	38%
	Bare field	0	0	4	1	50	2	0	0	3	1	0	0	0	0	0	2	63	79%
	Mix no rice	0	0	1	0	0	14	0	2	0	0	0	0	0	0	0	0	17	82%
	Mangr	1	0	0	0	0	1	22	2	0	0	0	0	0	0	0	0	26	85%
	Mel for	0	1	4	1	0	1	0	14	1	0	0	0	0	0	1	0	23	61%
	Orch	0	0	10	0	1	2	3	1	51	0	1	2	0	0	2	0	73	70%
	Urb D	0	0	0	0	0	0	0	0	0	5	1	0	0	0	0	0	6	83%
	Urb O	0	0	0	0	0	0	0	0	0	0	4	1	0	0	0	0	5	80%
	Urb Line	0	0	0	0	1	0	0	0	0	0	0	16	0	1	0	0	18	89%
	Water	1	0	0	0	0	0	0	0	0	0	0	0	12	1	0	0	14	86%
	Water ch	0	0	0	0	0	0	0	0	0	0	0	0	0	23	0	0	23	100%
	Waste	0	0	1	1	1	1	0	3	0	0	0	0	0	0	19	0	26	73%
	Cloud remn	1	0	0	0	1	0	0	0	0	0	0	0	0	0	0	9	11	82%
	Total	25	90	33	9	59	22	25	18	61	8	10	19	13	25	26	11	454	
Accuracy	88%	97%	24%	33%	85%	64%	88%	78%	84%	63%	40%	84%	92%	92%	73%	82%		79%	

Table 21 Confusion matrix of the land-use map of 1996 based on the separate validation segments, corrected for the segment area. The numbers indicate the area (ha) of segments that have the same class in the 'ground truth' validation set as in the classification (green) or the number of deviating segments (red). Overall accuracy in lower right corner, κ coefficient = 0.93. Full class names: see Table 4.

		Reference land-use class															Total	Relia- bility	
		Aqua	Dry-s rice	P dry- s rice	H dry- s rice	Bare field	Mix no rice	Mel Mangr	Mel for	Orch	Urb D	Urb O	Urb Line	Water	Water Ch	Waste			Cloud
Predicted land-use class	Aqua	4525	0	87	168	68	0	0	0	0	0	0	0	3	0	0	0	4851	93%
	Dry-s rice	0	14965	32	0	0	0	0	0	54	0	0	0	0	0	0	0	15051	99%
	P dry-s rich	0	36	432	7	121	26	0	0	146	0	152	0	0	0	65	0	985	44%
	H dry-s rice	0	0	153	192	21	0	0	0	0	0	0	0	0	0	3	0	369	52%
	Bare field	0	0	117	41	5980	85	0	0	0	38	16	0	0	0	0	9	6286	95%
	Mix no rice	0	0	37	0	0	2869	0	0	53	0	0	0	0	0	0	0	2959	97%
	Mangr	59	0	0	0	0	47	1507	0	25	0	0	0	0	0	0	0	1638	92%
	Mel for	0	14	297	22	0	55	0	6085	17	0	0	0	0	0	6	0	6496	94%
	Orch	0	0	1344	0	31	125	531	56	14974	0	24	103	0	0	308	0	17496	86%
	Urb D	0	0	0	0	0	0	0	0	0	323	45	0	0	0	0	0	368	88%
	Urb O	0	0	0	0	0	0	0	0	0	0	146	44	0	0	0	0	190	77%
	Urb Line	0	0	0	0	47	0	0	0	0	0	0	12431	0	53	0	0	12531	99%
	Water	96	0	0	0	0	0	0	0	0	0	0	0	2165	62	0	0	2323	93%
	Water ch	0	0	0	0	0	0	0	0	0	0	0	0	0	1920	0	0	1920	100%
	Waste	0	0	20	6	13	9	0	95	0	0	0	0	0	0	9174	0	9317	98%
	Cloud remn	18	0	0	0	12	0	0	0	0	0	0	0	0	0	0	61	91	67%
	Total	4698	15015	2519	436	6293	3216	2038	6236	15269	361	383	12578	2168	2035	9556	70	82871	
Accuracy	96%	100%	17%	44%	95%	89%	74%	98%	98%	89%	38%	99%	100%	94%	96%	87%		94%	

A8.3. Confusion matrices land-use classification 2006

Table 22 Confusion matrix of the land-use map of 2006 based on the out-of-bag segments in the random forest classification. The numbers indicate the number of segments that have the same class in the 'ground truth' validation set as in the classification (green) or the number of deviating segments (red). Overall accuracy in lower right corner, κ coefficient = 0.75. Full class names: see Table 4.

		Reference land-use class																Total	Relia- bility	
		Aqua	Dry-s rice	P dry- s rice	H dry- s rice	Bare field	Mix no rice	Mel Mangr for	Orch	Urb D	Urb O	Urb Line	Water Water	Ch	Waste	Cloud				
Predicted land-use class	Aqua	59	0	0	9	0	0	0	0	0	0	0	0	1	1	0	2	72	82%	
	Dry-s rice	0	114	4	0	0	0	1	0	9	0	0	0	0	0	0	0	2	130	88%
	P dry-s rich	2	2	48	2	9	1	0	0	5	0	0	4	0	0	0	0	2	75	64%
	H dry-s rice	3	0	7	99	5	0	0	0	0	0	0	0	0	0	0	0	0	114	87%
	Bare field	0	0	7	9	112	0	0	0	0	0	0	0	0	0	0	0	1	129	87%
	Mix no rice	0	0	4	4	3	26	0	1	3	0	0	1	0	0	0	0	0	42	62%
	Mangr	1	3	0	1	0	0	21	0	1	0	0	0	0	1	0	0	0	28	75%
	Mel for	0	1	0	0	0	0	0	21	8	0	0	0	1	0	0	0	0	31	68%
	Orch	0	8	6	0	0	1	1	4	41	0	0	3	0	0	0	0	0	64	64%
	Urb D	0	0	1	0	4	0	0	0	0	17	1	1	0	0	0	0	0	24	71%
	Urb O	1	0	7	1	1	0	0	0	0	3	0	1	0	0	0	0	0	14	0%
	Urb Line	3	2	3	1	2	0	0	0	3	1	0	36	0	1	0	1	1	53	68%
	Water	2	0	0	2	0	0	0	0	0	0	0	0	9	1	0	0	0	14	64%
	Water ch	1	0	1	1	0	0	0	0	0	0	0	1	2	29	0	0	0	35	83%
	Waste	0	0	1	0	2	1	0	0	0	0	0	0	0	0	5	0	0	9	56%
	Cloud remn	1	1	1	0	3	0	0	0	0	0	0	0	0	0	0	44	0	50	88%
	Total	73	131	90	129	141	29	23	26	70	21	1	47	13	33	5	52	884		
Accuracy	81%	87%	53%	77%	79%	90%	91%	81%	59%	81%	0%	77%	69%	88%	100%	85%	884	77%		

Table 23 Confusion matrix of the land-use map of 2006 based on the separate validation segments. The numbers indicate the number of segments that have the same class in the 'ground truth' validation set as in the classification (green) or the number of deviating segments (red). Overall accuracy in lower right corner, κ coefficient = 0.77. Full class names: see Table 4.

		Reference land-use class																Total	Reliability
		Aqua	Dry-s rice	P dry-s rice	H dry-s rice	Bare field	Mix no rice	Mangr	Mel for	Orch	Urb D	Urb O	Urb Line	Water	Water Ch	Waste	Cloud		
Predicted land-use class	Aqua	33	0	1	0	0	0	0	0	0	0	0	0	2	1	0	0	37	89%
	Dry-s rice	0	54	3	0	0	1	1	1	4	0	1	2	0	0	0	0	67	81%
	P dry-s rich	0	2	23	0	3	2	0	0	6	0	2	6	0	0	0	0	44	52%
	H dry-s rice	2	0	1	54	2	0	0	0	2	1	1	1	1	0	1	0	66	82%
	Bare field	0	0	4	2	57	0	0	0	0	2	1	1	0	0	0	2	69	83%
	Mix no rice	0	0	0	0	0	13	0	0	1	0	0	0	0	0	0	0	14	93%
	Mangr	0	0	0	0	0	0	13	0	0	0	0	0	0	0	0	0	13	100%
	Mel for	0	0	1	0	0	0	0	13	2	0	0	0	0	0	0	0	16	81%
	Orch	0	7	1	0	0	4	0	1	15	0	0	1	0	0	0	0	29	52%
	Urb D	0	0	0	0	1	0	0	0	0	8	0	0	0	0	0	0	9	89%
	Urb O	0	0	0	0	0	0	0	0	0	0	0	0	0	0	0	0	0	-
	Urb Line	0	1	1	0	0	0	0	0	1	0	2	15	0	1	0	0	21	71%
	Water	0	0	0	0	0	0	0	0	0	0	0	0	3	0	0	0	3	100%
	Water ch	0	0	0	0	0	0	0	0	0	0	0	0	0	15	0	0	15	100%
	Waste	0	0	0	0	0	0	0	0	0	0	0	0	0	0	3	0	3	100%
	Cloud remn	1	0	2	0	1	0	0	0	0	0	0	0	0	0	0	23	27	85%
	Total	36	64	37	56	64	20	14	15	31	11	7	26	6	17	4	25	433	
Accuracy	92%	84%	62%	96%	89%	65%	93%	87%	48%	73%	0%	58%	50%	88%	75%	92%		79%	

Table 24 Confusion matrix of the land-use map of 2006 based on the separate validation segments, corrected for the segment area. The numbers indicate the area (ha) of segments that have the same class in the 'ground truth' validation set as in the classification (green) or the number of deviating segments (red). Overall accuracy in lower right corner, κ coefficient = 0.90. Full class names: see Table 4.

		Reference land-use class															Total	Relia- bility	
		Aqua	Dry-s rice	P dry- s rice	H dry- s rice	Bare field	Mix no rice	Mel Mangr	Mel for	Orch	Urb D	Urb O	Urb Line	Water	Water Ch	Waste			Cloud
Predicted land-use class	Aqua	7406	0	33	0	0	0	0	0	0	0	0	23	8	0	0	7470	99%	
	Dry-s rice	0	7503	214	0	0	16	6	47	191	0	48	18	0	0	0	8043	93%	
	P dry-s rich	0	247	1650	0	65	122	0	0	660	0	36	270	0	0	0	3050	54%	
	H dry-s rice	12	0	27	2581	13	0	0	0	23	8	14	85	5	0	56	2824	91%	
	Bare field	0	0	149	42	3409	0	0	0	0	42	6	28	0	0	0	3728	91%	
	Mix no rice	0	0	0	0	0	2724	0	0	20	0	0	0	0	0	0	2744	99%	
	Mangr	0	0	0	0	0	0	1228	0	0	0	0	0	0	0	0	1228	100%	
	Mel for	0	0	74	0	0	0	0	6345	148	0	0	0	0	0	0	6567	97%	
	Orch	0	4050	68	0	0	592	0	122	6222	0	0	32	0	0	0	11086	56%	
	Urb D	0	0	0	0	88	0	0	0	0	891	0	0	0	0	0	979	91%	
	Urb O	0	0	0	0	0	0	0	0	0	0	0	0	0	0	0	0	-	
	Urb Line	0	3	56	0	0	0	0	0	231	0	41	6664	0	161	0	7156	93%	
	Water	0	0	0	0	0	0	0	0	0	0	0	0	46939	0	0	46939	100%	
	Water ch	0	0	0	0	0	0	0	0	0	0	0	0	0	3496	0	3496	100%	
	Waste	0	0	0	0	0	0	0	0	0	0	0	0	0	0	412	412	100%	
	Cloud remn	23	0	30	0	12	0	0	0	0	0	0	0	0	0	0	293	358	82%
	Total	7441	11803	2301	2623	3587	3454	1234	6514	7495	941	145	7097	46967	3665	468	345	106080	
Accuracy	100%	64%	72%	98%	95%	79%	100%	97%	83%	95%	0%	94%	100%	95%	88%	85%		92%	

A8.4. Confusion matrices land-use classification 2009

Table 25 Confusion matrix of the land-use map of 2009 based on the out-of-bag segments in the random forest classification. The numbers indicate the number of segments that have the same class in the 'ground truth' validation set as in the classification (green) or the number of deviating segments (red). Overall accuracy in lower right corner, κ coefficient = 0.79. Full class names: see Table 4.

		Reference land-use class																Total	Reliability	
		Aqua	Dry-s rice	P dry-s rice	H dry-s rice	Bare field	Mix no rice	Mangr	Mel for	Orch	Urb D	Urb O	Urb Line	Water	Water Ch	Waste	Cloud			
Predicted land-use class	Aqua	58	0	1	0	5	0	1	0	0	0	0	0	2	1	0	1	69	84%	
	Dry-s rice	0	209	1	0	0	0	0	1	4	0	0	2	0	0	0	0	5	222	94%
	P dry-s rich	0	3	44	0	2	4	0	0	0	0	3	2	0	0	0	0	1	59	75%
	H dry-s rice	1	0	0	14	2	0	1	1	0	0	0	0	0	0	0	0	0	19	74%
	Bare field	10	0	4	1	95	0	0	0	0	0	1	0	0	1	0	0	1	113	84%
	Mix no rice	0	0	6	0	3	22	0	0	5	0	1	0	0	0	0	0	0	37	59%
	Mangr	1	1	2	0	0	1	21	0	1	0	0	0	0	0	0	0	0	27	78%
	Mel for	0	0	0	1	0	0	0	38	7	0	0	0	0	0	0	0	0	46	83%
	Orch	1	4	2	0	0	5	0	6	34	0	0	2	0	0	0	0	0	54	63%
	Urb D	2	0	0	0	6	0	0	0	0	21	5	0	0	0	0	0	2	36	58%
	Urb O	0	0	5	0	5	0	0	0	0	6	18	4	0	1	0	0	0	39	46%
	Urb Line	0	5	1	0	3	2	0	0	0	2	2	37	0	0	0	0	0	52	71%
	Water	1	0	0	0	0	0	0	0	0	0	0	0	23	5	0	0	0	29	79%
	Water ch	1	0	0	0	0	0	0	0	0	0	0	0	1	55	0	0	0	57	96%
	Waste	0	0	3	0	0	1	0	0	0	0	0	0	0	0	2	0	0	6	33%
	Cloud remn	2	3	0	0	3	0	0	0	0	0	2	0	0	0	0	0	118	128	92%
Total	77	225	69	16	124	35	23	46	51	29	32	47	26	63	2	128	993			
Accuracy	75%	93%	64%	88%	77%	63%	91%	83%	67%	72%	56%	79%	88%	87%	100%	92%		81%		

Table 26 Confusion matrix of the land-use map of 2009 based on the separate validation segments. The numbers indicate the number of segments that have the same class in the 'ground truth' validation set as in the classification (green) or the number of deviating segments (red). Overall accuracy in lower right corner, κ coefficient = 0.77. Full class names: see Table 4.

		Reference land-use class																Total	Relia- bility
		Aqua	Dry-s rice	P dry- s rice	H dry- s rice	Bare field	Mix no rice	Mangr	Mel for	Orch	Urb D	Urb O	Urb Line	Water Water	Ch	Waste	Cloud		
Predicted land-use class	Aqua	30	0	0	0	5	0	0	0	0	0	0	0	1	0	0	0	36	83%
	Dry-s rice	0	108	0	0	0	0	2	3	0	0	3	0	0	0	0	2	118	92%
	P dry-s rich	0	1	15	0	5	3	0	1	4	0	4	1	0	0	0	1	35	43%
	H dry-s rice	0	0	2	7	3	0	0	0	0	0	0	0	0	0	0	0	12	58%
	Bare field	0	0	4	1	38	2	1	0	0	4	1	1	0	0	0	0	52	73%
	Mix no rice	0	0	1	0	0	12	0	1	2	0	0	0	0	0	0	0	16	75%
	Mangr	0	0	0	0	0	0	9	0	0	0	0	0	0	0	0	0	9	100%
	Mel for	0	0	0	0	1	0	0	18	5	0	0	0	0	0	0	0	24	75%
	Orch	0	2	1	0	0	1	3	0	13	0	0	0	0	0	0	0	20	65%
	Urb D	1	0	0	0	3	0	0	0	0	10	3	0	0	0	0	0	17	59%
	Urb O	0	0	1	0	1	0	0	0	0	4	6	0	0	0	0	1	13	46%
	Urb Line	0	0	3	0	0	0	0	0	0	0	4	21	0	0	0	1	29	72%
	Water	1	0	0	1	0	0	0	0	0	0	0	0	13	0	0	0	15	87%
	Water ch	0	0	0	0	0	0	0	0	0	0	0	0	0	28	0	0	28	100%
	Waste	0	0	0	0	0	0	0	0	0	0	0	0	0	0	3	0	3	100%
	Cloud remn	2	0	2	0	0	0	0	0	0	0	1	0	0	0	0	59	64	92%
	Total	34	111	29	9	56	18	13	22	27	18	19	26	14	28	3	64	491	
Accuracy	88%	97%	52%	78%	68%	67%	69%	82%	48%	56%	32%	81%	93%	100%	100%	92%		79%	

Table 27 Confusion matrix of the land-use map of 2009 based on the separate validation segments, corrected for the segment area. The numbers indicate the area (ha) of segments that have the same class in the 'ground truth' validation set as in the classification (green) or the number of deviating segments (red). Overall accuracy in lower right corner, κ coefficient = 0.88. Full class names: see Table 4.

		Reference land-use class															Total	Relia- bility	
		Aqua	Dry-s rice	P dry- s rice	H dry- s rice	Bare field	Mix no rice	Mel Mangr	Mel for	Orch	Urb D	Urb O	Urb Line	Water Water	Water Ch	Waste			Cloud
Predicted land-use class	Aqua	12471	0	0	0	135	0	0	0	0	0	0	0	24	0	0	0	12630	99%
	Dry-s rice	0	8490	0	0	0	0	47	482	0	0	134	0	0	0	0	26	9179	92%
	P dry-s rich	0	3	3991	0	217	435	0	85	538	0	257	17	0	0	0	26	5569	72%
	H dry-s rice	0	0	73	579	50	0	0	0	0	0	0	0	0	0	0	0	702	82%
	Bare field	0	0	512	19	2873	59	29	0	0	99	11	4	0	0	0	0	3606	80%
	Mix no rice	0	0	23	0	0	2347	0	158	350	0	0	0	0	0	0	0	2878	82%
	Mangr	0	0	0	0	0	0	668	0	0	0	0	0	0	0	0	0	668	100%
	Mel for	0	0	0	0	80	0	0	3168	431	0	0	0	0	0	0	0	3679	86%
	Orch	0	221	64	0	0	71	232	0	3354	0	0	0	0	0	0	0	3942	85%
	Urb D	12	0	0	0	20	0	0	0	0	700	323	0	0	0	0	0	1055	66%
	Urb O	0	0	236	0	247	0	0	0	0	266	654	0	0	0	0	32	1435	46%
	Urb Line	0	0	56	0	0	0	0	0	0	0	488	5216	0	0	0	27	5787	90%
	Water	22	0	0	591	0	0	0	0	0	0	0	0	14433	0	0	0	15046	96%
	Water ch	0	0	0	0	0	0	0	0	0	0	0	0	0	1442	0	0	1442	100%
	Waste	0	0	0	0	0	0	0	0	0	0	0	0	0	0	431	0	431	100%
	Cloud remn	18	0	15	0	0	0	0	0	0	0	49	0	0	0	0	1079	1161	93%
	Total	12523	8714	4970	1189	3622	2912	929	3458	5155	1065	1782	5371	14457	1442	431	1190	69210	
Accuracy	100%	97%	80%	49%	79%	81%	72%	92%	65%	66%	37%	97%	100%	100%	100%	91%		89%	

Appendix 9 Land-use changes

Table 28 Area of land-use (LU) changes between 1988 and 1996 in km². 38% of the total area did not change. Green font color = no change LU class. Orange font color = more than 10% of the area of the class in 1988 shows this change, pink font color = more than 10% of the area of the class in 1996 is a result of this change, blue font color = both the rule for the orange as the pink font color applies. Grey shade = LU change class used for predicting land-subsidence rates for entire InSAR-dataset. Note that some changes with large surface area are not used for the prediction, because they did not pass the criteria based on e.g. class accuracy (see section 2.6.). Total area = study area without all clouds in 1988, 1996 and 2006, without areas classified as water in 1988, 1996 and 2006 and without water in 2006.

		1988													Total
		Aqua	Dry-S Rice	P Dry-S Rice	Bare Field	Mix No Rice	Mangr	Mel For	Orch	Urb D	Urb O	Urb Line	Water	Waste	
1996	Aqua	526	2	13	78	11	129	1	15	0	1	3	55	9	843
	Dry-S Rice	3	1539	1419	1867	31	10	35	837	1	7	153	14	1188	7106
	P Dry-S Rice	4	24	151	317	21	7	3	88	1	6	17	4	96	739
	Bare Field	30	21	139	1597	42	20	3	70	0	7	51	10	113	2102
	Mix No Rice	6	0	35	117	129	9	1	34	0	3	14	2	69	420
	Mangr	130	1	21	57	15	231	0	55	0	0	2	22	3	538
	Mel For	0	8	37	8	3	0	90	59	0	0	2	1	204	413
	Orch	17	264	1675	761	60	41	31	2496	1	30	91	58	355	5880
	Urb D	3	0	4	15	0	0	0	1	5*	4*	2	2	2	40
	Urb O	0	1	12	11	0	0	0	5	3*	6*	3	2	4	47
	Urb Line	3	105	215	174	18	2	14	164	2	2	100	15	153	969
	Water	6	3	21	18	2	4	1	18	0	1	5	108	19	207
	Waste	1	5	38	29	13	0	69	16	0	1	1	1	748	920
	Total		729	1975	3779	5047	348	454	247	3858	14	69	446	294	2965

* These classes will be merged to one urban class for the prediction of land subsidence.

Table 29 Area of land-use (LU) changes between 1988 and 2006 in km². 30% of the total area did not change. Green font color = no change LU class. Orange font color = more than 10% of the area of the class in 1988 shows this change, pink font color = more than 10% of the area of the class in 2006 is a result of this change, blue font color = both the rule for the orange as the pink font color applies. Grey shade = LU change class used for predicting land-subsidence rates for entire InSAR-dataset. Note that some changes with large surface area are not used for the prediction, because they did not pass the criteria based on e.g. class accuracy (see section 2.6.). Total area = study area without all clouds in 1988, 1996 and 2006, without areas classified as water in 1988, 1996 and 2006 and without water in 2006.

		1988													Total
		Aqua	Dry-S Rice	P Dry-S Rice	Bare Field	Mix No Rice	Mangr	Mel For	Orch	Urb D	Urb O	Urb Line	Water	Waste	
2006	Aqua	637	6	45	239	35	313	7	61	0	3	16	103	39	1504
	Dry-S Rice	0	1080	1129	1698	33	11	56	684	1	9	135	33	1444	6313
	P Dry-S Rice	0	240	554	733	75	35	5	479	1	14	68	18	114	2336
	Bare Field	0	174	292	1370	41	8	3	165	1	6	57	5	112	2233
	Mix No Rice	14	8	42	105	95	17	3	74	0	1	12	5	102	478
	Mangr	27	1	4	6	1	52	0	20	0	0	0	44	0	156
	Mel For	1	12	52	10	0	0	118	58	0	0	1	1	623	876
	Orch	29	243	1225	459	32	11	29	1927	0	15	35	46	246	4298
	Urb D	1	6	22	23	2	1	0	17	7*	12*	3	3	2	99
	Urb O	0	1	5	1	0	0	0	4	0*	1*	0	0	0	14
	Urb Line	20	205	409	399	33	7	24	368	3	8	119	37	266	1897
	Water	0	0	0	0	0	0	0	0	0	0	0	0	0	0
	Waste	0	0	1	2	0	0	1	1	0	0	0	0	17	22
	Total		729	1975	3779	5047	348	454	247	3858	14	69	446	294	2965

* These classes will be merged to one urban class for the prediction of land subsidence.

Table 30 Area of land-use (LU) changes between 1996 and 2006 in km². 50% of the total area did not change. Green font color = no change LU class. Orange font color = more than 10% of the area of the class in 1996 shows this change, pink font color = more than 10% of the area of the class in 2006 is a result of this change, blue font color = both the rule for the orange as the pink font color applies. Grey shade = LU change class used for predicting land-subsidence rates for entire InSAR-dataset. Note that some changes with large surface area are not used for the prediction, because they did not pass the criteria based on e.g. class accuracy (see section 2.6.). Total area = study area without all clouds in 1988, 1996 and 2006, without areas classified as water in 1988, 1996 and 2006 and without water in 2006.

		1996													Total
		Aqua	Dry-S Rice	P Dry-S Rice	Bare Field	Mix No Rice	Mangr	Mel For	Orch	Urb D	Urb O	Urb Line	Water	Waste	
2006	Aqua	758	7	20	167	20	322	2	134	8	0	5	58	3	1504
	Dry-S Rice	0	4221	212	359	17	18	122	873	2	3	281	24	182	6313
	P Dry-S Rice	0	844	155	210	86	33	9	841	2	9	114	16	16	2336
	Bare Field	0	645	127	1072	51	14	3	234	5	4	45	5	26	2233
	Mix No Rice	11	14	19	64	159	33	6	88	1	1	8	7	67	478
	Mangr	39	3	2	2	0	70	0	22	0	0	0	19	0	156
	Mel For	0	103	11	14	6	0	169	91	1	2	46	4	428	876
	Orch	21	706	100	79	57	35	55	3017	1	4	83	28	113	4298
	Urb D	0	9	11	10	3	1	0	30	15*	12*	4	4	0	99
	Urb O	0	2	1	0	1	0	0	7	0*	2*	0	0	0	14
	Urb Line	14	553	81	124	19	12	45	542	5	9	382	44	68	1897
	Water	0	0	0	0	0	0	0	0	0	0	0	0	0	0
	Waste	0	0	0	1	0	0	2	1	0	0	1	0	17	22
Total		843	7106	739	2102	420	538	413	5880	40	47	969	207	920	20225

* These classes will be merged to one urban class for the prediction of land subsidence.

Table 31 Area of land-use (LU) changes between 2006 and 2009 in km². 57% of the total area did not change. Green font color = no change LU class. Orange font color = more than 10% of the area of the class in 2006 shows this change, pink font color = more than 10% of the area of the class in 2009 is a result of this change, blue font color = both the rule for the orange as the pink font color applies. Note that this LU change map is not use for correlation with and predictions of the land-subsidence rate, as explained in section 2.5 and 2.6. Total area = study area without all clouds in 2006 and 2009.

		2006													Total
		Aqua	Dry-S Rice	P Dry-S Rice	Bare Field	Mix No Rice	Mangr	Mel For	Orch	Urb D	Urb O	Urb Line	Water	Waste	
2009	Aqua	1243	77	48	61	35	53	2	26	3	0	49	41	0	1638
	Dry-S Rice	3	3453	779	700	16	3	64	748	5	1	503	4	1	6280
	P Dry-S Rice	19	232	381	287	94	5	8	347	6	1	135	11	2	1529
	Bare Field	34	88	85	728	56	2	19	31	7	0	76	1	1	1129
	Mix No Rice	6	29	42	38	164	0	78	112	1	0	31	1	0	503
	Mangr	19	4	5	0	2	66	0	2	0	0	1	3	0	102
	Mel For	0	94	5	2	9	1	356	98	0	0	37	1	0	603
	Orch	11	317	244	77	41	17	84	1952	1	0	129	10	1	2883
	Urb D	3	7	14	13	3	0	1	4	34	3	9	2	0	93
	Urb O	5	15	85	45	25	0	1	33	17	4	67	5	0	302
	Urb Line	4	351	234	76	17	2	46	250	3	1	465	14	1	1463
	Water	44	20	4	1	1	3	1	24	1	0	11	1348	0	1459
	Waste	0	6	1	1	0	0	1	2	0	0	1	0	6	18
	Total		1391	4693	1926	2030	463	153	662	3629	77	11	1515	1441	12

Appendix 10 Land-subsidence rate per land-use class

Table 32 InSAR-based land-subsidence rate statistics per land-use (LU) class based on respectively all points in all tiles and in the Tra Vinh tile for which the LU did not change between 1988 and 2006/2009. Std.dev. is the standard deviation, CV is the coefficient of variation.

LU class	InSAR-based subsidence rate								Nr. of points	
	Mean (cm/yr)		Median (cm/yr)		Std.dev. (cm/yr)		CV (-)			
	All tiles	Tra Vinh	All tiles	Tra Vinh	All tiles	Tra Vinh	All tiles	Tra Vinh	All tiles	Tra Vinh
Aqua	1.11	1.26	1.12	1.24	0.7	0.6	0.6	0.5	59,394	15,795
Dry-S Rice	0.78	1.08	0.78	1.05	0.5	0.5	0.6	0.5	109,013	2,749
P Dry-S Rice	1.35	1.63	1.33	1.57	0.7	0.6	0.5	0.4	6,996	1,232
Bare Field	1.29	1.45	1.26	1.42	0.7	0.6	0.6	0.4	80,210	21,429
Mix No Rice	1.84	1.99	1.82	1.95	0.7	0.7	0.4	0.4	10,450	3,900
Mangr	1.29	1.26	1.31	1.26	0.7	0.6	0.5	0.5	3,018	954
Mel For	0.74	-	0.74	-	0.4	-	0.5	-	11,700	0
Orch	1.35	1.54	1.36	1.54	0.5	0.5	0.4	0.3	264,534	66,032
Urb D	2.04	2.28	2.07	2.2	0.5	0.6	0.2	0.3	1,540	330
Urb O	1.76	2	1.78	2.05	0.5	0.7	0.3	0.3	128	32
Urb Line	0.85	1.46	0.83	1.45	0.5	0.6	0.6	0.4	13,102	462
Waste	0.6	-	0.58	-	0.4	-	0.7	-	2,287	0

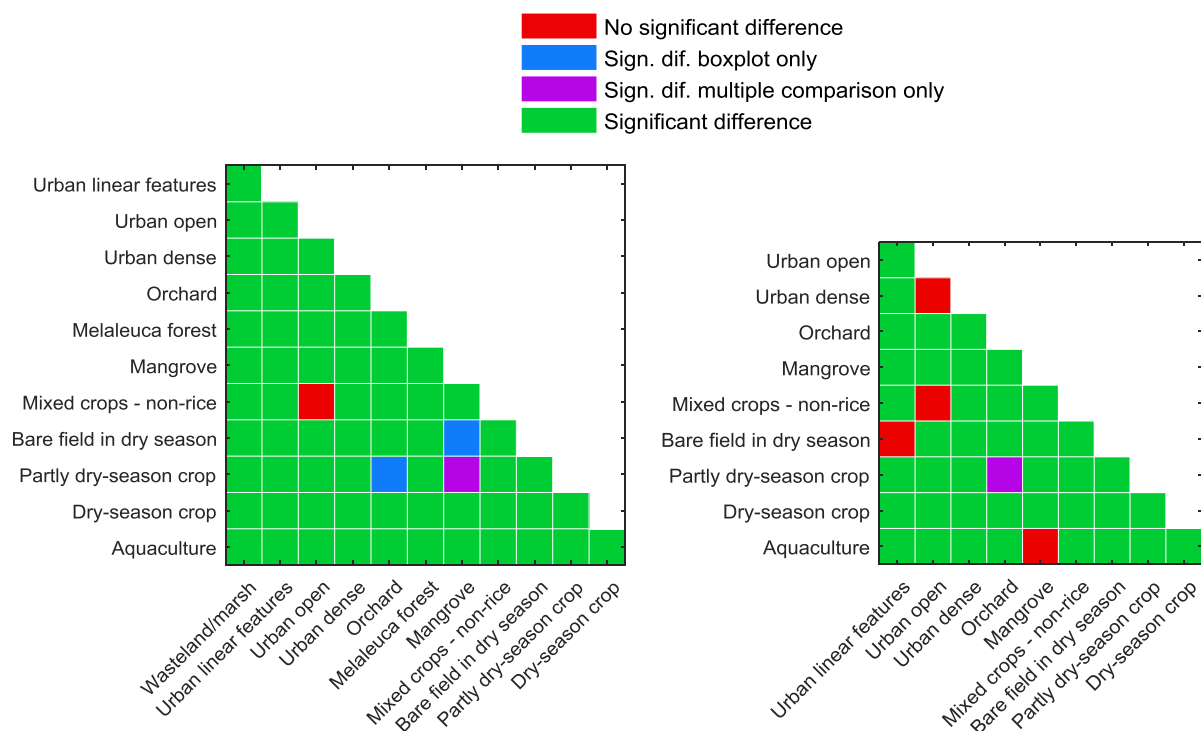


Figure 23 Visualization of which combination of mean or median land-subsidence rates per LU class are significantly different from each other at the 95% confidence level based on boxplot notches and/or multiple comparison. Left: based on all tiles, right: based on Tra Vinh tile only.

Appendix 11 Impact of past land-use changes on subsidence rates

A11.1. Impact land-use change on subsidence based on all InSAR-tiles

Table 33 Impact of past land-use (LU) changes on the average land-subsidence rate based on all InSAR-tiles. A, B, C and D represent respectively arrow 1, 2, 3 and 4 in the legend of Figure 24: A = area with no change in first LU class, B = area with first LU class in 1988 until 1996 and second LU class in 2006/2009, C = area with first LU class in 1988 and second LU class in 1996 until 2006/2009, D = area with no change in LU second class. The significance of the difference between the subsidence rate related to two different timings of a certain LU change is based on the analysis of boxplots notches and a multiple comparison test at the 95% confidence level (y = yes, n = no).

Category	LU change		Subsidence rate (cm/yr) <i>Longer period second class</i>				Significant difference?			Number of points (*10 ³)			
	From	To	A	B	C	D	BC	BD	CD	A	B	C	D
Change to aquaculture	Mangr	Aqua	1.3	1.1	1.1	1.1	n	y	y	3.0	22	15	59
Urbanization	Dry-S Rice	Urb D	0.8	0.9	2.7	2.0	y	y	y	109	0.5	0.02	1.5
	Bare Field	Urb D	1.3	1.6	2.3	2.0	y	y	y	80	0.9	1.1	1.5
	Orchard	Urb D	1.4	1.6	2.0	2.0	y	y	y*	265	2.6	0.2	1.5
	Waste	Urb Line	0.6	0.8	0.8	0.9	y	y	y	2.3	9.6	10	13
Change to and intensification of agriculture	Bare Field	Dry-S Rice	1.3	1.0	0.8	0.8	y	y	y	80	25	112	109
	Waste	Dry-S Rice	0.6	0.8	0.8	0.8	n	n	n	2.3	16	85	109
	Waste	Bare Field	0.6	0.9	1.0	1.3	y	y	y	2.2	1.5	2.8	80
Change to orchards	Dry-S Rice	Orchard	0.8	1.0	1.2	1.4	y	y	y	109	16	18	265
	Waste	Orchard	0.6	0.9	1.1	1.4	y	y	y	2.3	10	8.0	265

* based on boxplot analysis only

A11.2. Impact land-use change on subsidence based on the Tra Vinh InSAR-tile

Table 34 Impact of past land-use (LU) changes on the average land-subsidence rate based on the Tra Vinh InSAR-tile only. A, B, C and D represent respectively arrow 1, 2, 3 and 4 in the legend of Figure 24: A = area with no change in first LU class, B = area with first LU class in 1988 until 1996 and second LU class in 2006/2009, C = area with first LU class in 1988 and second LU class in 1996 until 2006/2009, D = area with no change in LU second class. The significance of the difference between the subsidence rate related to two different timings of a certain LU change is based on the analysis of boxplots notches and a multiple comparison test at the 95% confidence level (y = yes, n = no).

Category	LU change		Subsidence rate (cm/yr) <i>Longer period second class</i>				Significant difference?			Number of points (*10 ³)			
	From	To	A	B	C	D	BC	BD	CD	A	B	C	D
Change to aquaculture	Mangr	Aqua	1.3	1.1	1.1	1.3	y	y	y	1.0	9.6	6.1	16
	Dry-S Rice	Urb D	1.1	1.3	-	2.3	-	y	-	2.7	0	0	0.3
Urbanization	Bare Field	Urb D	1.5	1.7	2.1	2.3	y	y	y	1.2	0.1	0.4	0.3
	Orchard	Urb D	1.5	1.8	1.9	2.3	n	y	y	66	0.4	0	0.3
	Waste	Urb Line	-	-	-	2.3	-	-	-	0	0	0	0.3
Change to and intensification of agriculture	Bare Field	Dry-S Rice	1.5	1.3	1.3	1.1	y	y	y	21	2.9	3.5	2.7
	Waste	Dry-S Rice	-	-	1.2	1.1	-	-	y	0	0	0.5	2.7
	Waste	Bare Field	-	-	1.3	1.5	-	-	n	0	0	0.1	21
Change to orchards	Dry-S Rice	Orchard	1.1	1.3	1.4	1.5	y	y	y	2.7	1.4	1.9	66
	Waste	Orchard	-	-	1.5	1.5	-	-	y*	0	0	0.4	66

* based on multiple comparison test only

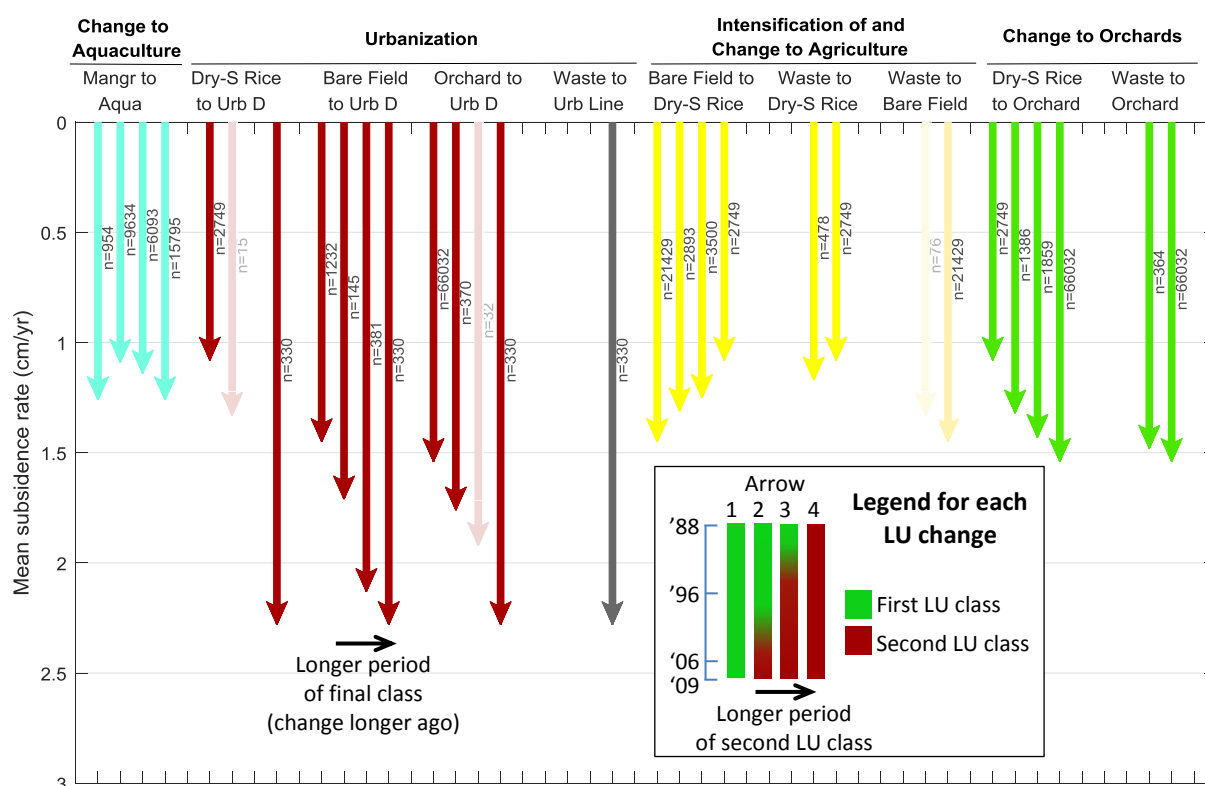


Figure 24 Impact of land-use (LU) changes on the mean land-subsidence rate for the period 2006-2010 based on the Tra Vinh tile only. The first arrow corresponds to the area with no change in the first LU class, the second to the area with the first LU class in 1988 until 1996 and the second LU class in 2006/2009, the third to the area with the first LU class in 1988 and the second LU class in 1996 until 2006/2009 and the last to the area with no change in the second LU class. Note that the changes to orchards are the least important in the VMD over the past decades. n = number of points on which the average is based. The transparent arrow is based on less than 100 data points and is thus less representative. For values and significance of differences between arrows: see Table 33 in this appendix. Full LU class names of the acronyms in the LU changes: see Table 4.

Appendix 12 Importance of the different land-use periods for predicting land-subsidence rates

Table 35 Importance of the different land-use (LU) periods for predicting land-subsidence rates for all tiles and for the Tra Vinh tile based on the increase in mean square error (MSE) importance measure of the random forest regression (see section 2.4). A higher importance value indicates a larger importance of the LU period for the predictions. Different runs are based on different random samples (different seeds) used in the training of the random forest. The run numbers for all tiles are identical to those in Table 9; run 1 - 5 in this table correspond to run 6 - 10 for the Tra Vinh tile in Table 9.

LU period		Increase in MSE (%)									
		Run 1		Run 2		Run 3		Run 4		Run 5	
		Value	Rank	Value	Rank	Value	Rank	Value	Rank	Value	Rank
All tiles	'88-'96	66	1	64	1	61	2	57	2	64	1
	'88-'06	59	2	59	2	64	1	57	1	57	2
	'96-'06	54	3	53	3	53	3	47	4	56	3
	'06(-'09)	47	4	50	4	47	4	48	3	47	4
Tra Vinh tile	'88-'96	53	2	64	1	66	1	68	1	72	1
	'88-'06	54	1	54	3	60	3	62	3	59	3
	'96-'06	51	3	62	2	63	2	63	2	64	2
	'06(-'09)	49	4	44	4	53	4	50	4	50	4

Table 36 Importance of the different land-use (LU) periods for predicting land-subsidence rates for all tiles and for the Tra Vinh tile based on the increase in node-purity importance measure of the random forest regression (see section 2.4). A higher importance value indicates a larger importance of the LU period for the predictions. Different runs are based on different random samples (different seeds) used in the training of the random forest. The run numbers for all tiles are identical to those in Table 9; run 1 - 5 in this table correspond to run 6 - 10 for the Tra Vinh tile in Table 9.

LU period		Increase in node purity									
		Run 1		Run 2		Run 3		Run 4		Run 5	
		Value	Rank	Value	Rank	Value	Rank	Value	Rank	Value	Rank
All tiles	'88-'96	605	2	619	1	601	2	614	1	603	1
	'88-'06	492	3	507	3	474	3	516	3	511	3
	'96-'06	618	1	584	2	632	1	600	2	580	2
	'06(-'09)	393	4	360	4	373	4	385	4	369	4
Tra Vinh tile	'88-'96	389	3	376	3	391	3	382	3	404	3
	'88-'06	425	1	411	1	430	1	424	1	415	2
	'96-'06	400	2	377	2	416	2	411	2	421	1
	'06(-'09)	302	4	297	4	304	4	297	4	274	4